ISBN 978-82-326-0462-3 (printed version)
ISBN 978-82-326-0463-0 (electronic version)
ISSN 1503-8181

Doctoral theses at NTNU, 2014:275

Siri Ann Nyrnes

New ultrasound flow modalities for evaluation of congenital heart defects

NTNU
Norwegian University of
Science and Technology
Faculty of Medicine
Department of Circulation
and Medical Imaging

NTNU – Trondheim
Norwegian University of
Science and Technology

NTNU – Trondheim
Norwegian University of
Science and Technology

Doctoral theses at NTNU, 2014:275

NTNU

Siri Ann Nyrnes

New ultrasound flow modalities for evaluation of congenital heart defects

Thesis for the degree of Philosophiae Doctor

Trondheim, October 2014

Norwegian University of Science and Technology
Faculty of Medicine
Department of Circulation and Medical Imaging

NTNU – Trondheim
Norwegian University of
Science and Technology

NTNU
Norwegian University of Science and Technology

Thesis for the degree of Philosophiae Doctor

Faculty of Medicine
Department of Circulation and Medical Imaging

ISBN 978-82-326-0462-3 (printed version)
ISBN 978-82-326-0463-0 (electronic version)
ISSN 1503-8181

Doctoral theses at NTNU, 2014:275

Printed by Skipnes Kommunikasjon as

Siri Ann Nyrnes

New ultrasound flow modalities for evaluation of congenital heart defects

Illustration photo from the data acquisition with the permission from the parents (Photo: Geir Mogen)

Thanks to the children and their parents who participated in the studies presented in this thesis. We are grateful for your contribution to the field of ultrasound flow imaging research.

Table of Contents

1 PREFACE

1.1 Norsk sammendrag

Nye ultralyd blodstrømsmetoder til undersøkelse av medfødte hjertefeil

Hjertefeil er den vanligste medfødte anomali og også den viktigste årsak til død av medfødte misdannelser. Grunnet bedret behandling og overlevelse er det en voksende populasjon av barn og voksne med medfødte hjertefeil. Det er derfor et stort behov for skånsomme avbildningsteknikker for diagnostikk og oppfølging, og hjerteultralyd har blitt det viktigste verktøyet. Høy diagnostisk treffsikkerhet i hjerteultralyd er nøkkelen til god klinisk oppfølging av pasienter med medfødte hjertefeil. Vi har studert mulige forbedringer av dagens ultralyd blodstrømsavbildning.

Forskningsmiljøet for ultralyd i Trondheim har utviklet nye blodstrømsmetoder for å unngå noen av begrensningene med fargedoppler som er standard metode for å avbilde blodstrøm. Fargedoppler har vært i bruk siden siste halvdel av 1980-tallet og var i sin tid et stort teknisk fremskritt. En av begrensningene med fargedoppler er at metoden kun viser to retninger av blodets bevegelse, til og fra lydhodet, og derfor gir avgrenset informasjon om blodets faktiske bevegelse. Ekkogene punkter som ligner små flekker, såkalte speckler, finnes i større eller mindre grad i alle ultralydopptak. De nye blodstrømsmetodene utviklet i Trondheim baserer seg på sporing av bevegelsene til disse specklene. Først ble Blood Flow Imaging (BFI) utviklet. Metoden viser i tillegg til vanlig fargedoppler dette specklemønsteret og kan fremstille blodets bevegelse også på tvers av ultralydstrålen og dermed gi et mer detaljert bilde av blodstrøm. I samarbeid mellom sivilingeniører og klinikere er metoden tilpasset avbildning av blodstrøm i atrieseptumdefekter (ASD, åpning mellom venstre og høyre forkammer) og lungevener hos barn. I artikkel 1-3 hvor BFI ble testet, har synet vært brukt til å tolke bevegelsene til specklemønsteret.

I løpet av prosjektet har BFI blitt videreutviklet. I dag kan datamaskinen spore specklene og beregne både blodets bevegelse og hastighet. Slik får man fremstilt nye detaljer i blodets bevegelse. Dette har man klart ved å ta opp ultralydbilder på en alternativ måte ved å kombinere såkalt planbølgeavbilding og parallelt strålemottak. I tradisjonell hjerteultralyd bruker man fokuserte lydbølger hvor bildene bygges opp en linje av gangen. En ulempe med denne opptaksmetoden er at et bilde må bygges opp av et stort antall sendestråler, noe som gjør at antall bilder en kan lage pr sekund (billedraten) synker. Dette kan gjøre det problematisk å følge hurtige bevegelser i blodstrøm. Dette er

spesielt en begrensning for fargedoppler, hvor datamengden som tas opp for å danne hvert bilde av blodstrømshastigheter kan være svært høy. Ved å sende ut bredere ufokuserte lydpulser kan man bygge opp et bilde med få sendestråler. Denne modaliteten kalles planbølgeavbilding. Ved at det samtidig dannes flere mottakerstråler for hver utsendte lydpuls (parallelt strålemottak), økes billedraten betraktelig. Dette kan utnyttes til å skaffe ny informasjon om hvordan blodet strømmer. Ved sporing av speckler (såkalt «speckle tracking») kan datamaskinen følge en unik signatur i blodstrøms-ekkoet over tid. Ved å måle hvor ekkosignaturen flytter seg mellom to enkeltbilder, kan maskinen beregne blodstrømmens hastighet og retning. Figuren under viser et eksempel hvor denne teknikken er brukt.

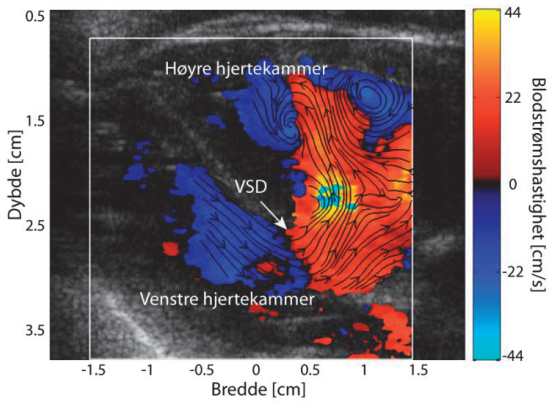

Speckle tracking av blod: Figuren viser et ultralydbilde av hjertet til en nyfødt med VSD (ventrikkel septum defekt = åpning i skilleveggen mellom hjertekamre). Her ser vi blodstrømmens detaljer ved hjelp av speckle tracking som er vist med piler oppå eksisterende fargebilder (fargedoppler). Blått viser blodstrøm bort fra ultralydhodet, mens rødt viser blodstrøm mot ultralydhodet. Pilene (speckle tracking av blod) viser tilleggsinformasjon som ikke fremkommer i fargebildene. Man ser hvordan blodet strømmer gjennom åpningen i skilleveggen og at dette fører til at det dannes blodstrøms-virvler i høyre hjertekammer.

Det pågår nå en klinisk pilotstudie hvor verdien av speckle tracking av blod skal testes. Artikkel 4 er en teknisk artikkel basert på tilleggsopptak med et ultralydapparat utviklet for forskningsformål fra to pasienter i denne studien.

Artikkel 1

I en pilotstudie ble tradisjonell fargedoppler og den nye metoden BFI sammenlignet. 13 barn med ASD ble prospektivt undersøkt. Fire eksperter (kardiologer og barnekardiologer) fikk presentert umerkede videoer fra undersøkelsene og rangerte blodstrømsbilder med to ulike mengder fargeforsterkning på en visuell analog skala (1-100) med tanke på hvor sikre de var på om det var blodstrøm over forkammerskilleveggen. Fargedoppler og BFI-rangeringene ble sammenlignet. Henholdsvis to og tre

observatører rangerte BFI som signifikant bedre enn fargedoppler ved vanlig og økt fargeforsterkning. Studien konkluderte med at BFI kan gi bedret blodstrøms-avbildning i atrieseptumdefekter.

Artikkel 2

Lungevener er blant de anatomiske segmenter som er involvert i flest diagnostiske feil innen barnehjerteultralyd, og det er behov for bedret avbildning. Standard hjerteultralyd med fargedoppler og BFI av lungevener ble prospektivt utført på 26 nyfødte henvist med spørsmål om medfødt hjertefeil. Fire eksperter fikk presentert umerkede videoer fra undersøkelsene i tilfeldig rekkefølge. Ekspertene rangerte konsekvent BFI som bedre enn fargedoppler, og studien konkluderte med at BFI kan forbedre avbildningen av lungeveneblodstrøm hos nyfødte.

Artikkel 3

I en oppfølgingsstudie i samarbeid med barnehjertemiljøet på Rikshospitalet ble BFI testet i forbindelse med propplukning av atrieseptumdefekter. Under narkose legges rutinemessig en ultralydsonde ned i spiserøret til barna for å rettlede propplukningen og vi koblet blodstrøms-undersøkelser med BFI til denne undersøkelsen. Det ble gjort BFI blodstrøms-undersøkelse av atrieseptumdefekter og lungevener hos 28 barn som ble inkludert prospektivt. BFI ble sammenlignet med gjeldende, men mer invasive referansemetoder. BFI viste godt samsvar med lungeangiografi og hadde som forventet noe lavere estimat for ASD-større enn ballongstrukket diameter. Repeterbarheten av BFI-målingene var god, tilsvarende måleusikkerheten som oppgis i dagens ultralydsystemer.

Artikkel 4

I en studie basert på to pasienteksempler ble ultralyd speckle tracking av blod med høy billedrate brukt til å beregne blodstrøms-hastigheter i en atrieseptumdefekt (ASD) og en ventrikkelseptumdefekt (VSD). Det ble benyttet et ultralydapparat utviklet for forskningsformål hvor plane bølger og parallelt strålemottak ble utnyttet for å oppnå blodstrømsbilder i en bred sektor med høy kvalitet, og samtidig høy billedrate. Ved hjelp av speckle tracking av blod kunne det beregnes blodstrøms-hastigheter gjennom VSDen og ASDen i hele hjertesyklus. Det ble oppdaget en virveldannelse i høyre hjertekammer nær VSDen som ikke var mulig å se med standard fargedoppler ved hjelp av vektor plot. Metoden ble også validert *in vitro*. Forsøkene tyder på at metoden har potensiale til gode hastighetsmålinger av blodstrøm og er et godt utgangspunkt for videre metodeutvikling. Metoden bør testes på flere pasienter for å evaluere robusthet og klinisk nytte.

Navn kandidat: Siri Ann Nyrnes

Institutt: Institutt for sirkulasjon og bildediagnostikk, DMF, NTNU

Hovedveileder: Førsteamanuensis Bjørn Olav Haugen, Institutt for sirkulasjon og bildediagnostikk, DMF, NTNU

Biveiledere: Professor Hans Torp, Institutt for sirkulasjon og bildediagnostikk, DMF, NTNU og Førsteamanuensis Lasse Løvstakken, Institutt for sirkulasjon og bildediagnostikk, DMF, NTNU

Finansieringskilder: Samarbeidsorganet mellom Helse Midt-Norge og NTNU. MI-Lab – Senter for medisinsk avbildning (Medical Imaging Laboratory).

Ovennevnte avhandling er funnet verdig til å forsvares offentlig
for graden PhD i medisinsk teknologi
Disputas finner sted i auditorium MTA i medisinsk teknisk forskningssenter, St.Olav's Hospital/NTNU
Fredag 24.10.14 kl 10.15 og 12.15

1. 2 Acknowledgements

This work was carried out at the Department of Circulation and Medical Imaging, Norwegian University of Science and Technology in parallel to clinical work as a consultant in Pediatric Cardiology in the Department of Pediatrics, St.Olavs University Hospital. The research has been funded by the Medical Imaging Laboratory (MI Lab) and the Liaison Committee between the Central Norway Regional Health Authority (RHA) and the Norwegian University of Science and Technology (NTNU).

This research project would not have been possible without the support of many people to whom I owe my sincerest gratitude: The work was initiated by my principal supervisor Bjørn Olav Haugen. At that time he was working as Associate Professor in the Department of Circulation and Medical Imaging, NTNU and as a consultant in the Department of Cardiology, St. Olav's University Hospital. His excellent combination of research and clinical work during the project period has inspired me to try out the same mixture. Bjørn Olav has been an eminent scientific supervisor and has become a good friend. His trademark is quick and wise feedback, mixed with a nice sense of humor, and these qualities have made the cooperation with him both instructive and fun. At the same time, he has been supportive and tolerant and given me the freedom to carry out own ideas. I am very thankful for the technical expertise and help from my co-supervisors Hans Torp and Lasse Løvstakken. Hans Torp is the leader of the Ultrasound research group at the Department of Circulation and Medical Imaging, NTNU. He developed the method Blood Flow Imaging and guided us in the clinical testing of this method. Hans is a brilliant mentor and researcher and made me feel welcome in his department from day one. Lasse Løvstakken, now Associate Professor and senior engineer in the Department of Circulation and Medical Imaging, has worked with further development of the method and adapted the method for imaging neonates and children. He created the advanced computer programs for presentation of the echocardiographic images to the observers. Lasse has been a great support. He has been together with me at the patient's bedside and seen the clinical challenges with his own eyes. This has been important in order to gather experience and ideas to further development of the flow imaging technique.

Thank you also to engineer Solveig Fadnes for your interest in congenital heart disease and nice cooperation on further development of the flow technique in study 4. I am very pleased you will continue with this work also after your planned dissertation later this year.

Eirik Skogvoll has been an invaluable collaborator throughout the work, guiding us through all the statistical challenges. He has a broad experience being a specialist in both pediatrics and anesthesiology, in addition to being an expert in statistics! Thank you for your excellent help with interpretation and analysis of the data.

I want to express my sincere gratitude to Erik Thaulow (section head), Gaute Døhlen (consultant and interventionist) and Kjetil Lenes (echo-technician) for the generous hospitality and help during patient inclusion in paper 3 at Oslo University Hospital, Rikshospitalet. A special thanks to Gaute for organizing ASD-closures to one period monthly so that I was able to participate in all the closures for just over a year. I really admire your expertise and handiness in the cath-lab!

Thanks to Finn Høivik, Hans Kristian Langsetmo, Brage Amundsen, Stein Samstad, Terje Skjerpe, Thomas Renhult Skaug Skaug and Anders Thorstensen for contributions as observers in papers 1 and 2. I am also very thankful to the senior cardiologists Gunnar Norgård, Terje Skjærpe, Torbjørn Graven and Stein Samstad for valuable help with measurements and co-authorship in paper 3.

Thank you to Olav Haraldset, professor and head of MI-lab, for believing in the project and giving us start help with funding. Thanks also for adding your invaluable experience and golden pen to the research protocol which resulted in funding for the whole the project period.

During the research period, I worked as a clinician in the department of pediatrics. I want to thank all my good colleagues in the department! Particularly thanks to Wendy Williams for taking care of me from the start and teaching me cardiac ultrasound with enthusiasm and educational skill. She also offered invaluable help with proof reading of my thesis. Thanks to Hans Kristian Langsetmo for flexibility during a long period of short-handedness where the two off us had to share on-call duties 50/50 for a long time. I would also like to thank Elisabeth Selvåg, Kari Risnes and Torstein Røe for seeing the value of research in the department.

Thank you to all my nice office colleagues throughout the years at the department. Especially thanks to Anders Thorstensen, Håvard Dalen and Thomas Renhult Skaug for support, cooperation and stimulating discussions. Thanks also to Trine Moholdt, Charlotte Bjørk Ingul and Kirsti Kron Garnæs for inviting me into new projects in cooperation with the Cardiac Exercise Research Group (CERG).

I am also grateful to my friends who regularly contribute to social activities outside of work. Thanks to Hanne, Kitty, Ellen, Marianne, Lisbeth, Eli and Gunhild for amusing trips and tough training hours, usually accompanied by nice talks….Thanks also to Kristin for many treasured conversations which reminds me what is important in life.

Finally and most off all I would like to thank my family. Thanks to my parents Elsa and Hans, for teaching me that working hard for a goal in fact makes you happy, but most off all for your love. Thanks to my parents-in-law Liv and Arne for encouragement and support. Thank you, Pål, Oda and Anders for bringing so much joy and laughter to my life.☺ Lastly, but most importantly I am grateful to my husband and soul mate Petter, who is everything to me ♥.

Trondheim, May 2014,

Siri Ann Nyrnes

1.3 List of papers

Paper 1

Nyrnes SA, Løvstakken L, Torp H, Haugen BO. Blood Flow Imaging - A new angle-independent ultrasound modality for the visualization of flow in atrial septal defects in children. Echocardiography. 2007;24(9):975-981.

Paper 2

Nyrnes SA, Løvstakken L, Skogvoll E, Torp H, Haugen BO. Does a new ultrasound flow modality improve visualization of neonatal pulmonary veins? Echocardiography. 2010;27(9):1113-1119.

Paper 3

Nyrnes SA, Løvstakken, Døhlen G, Skogvoll E,Torp H, Skjærpe T, Norgård G,

Samstad S, Graven T, Haugen BO. Transesophageal echocardiography with Blood Flow Imaging during atrial septal defect closure: A comparison with the current references. Echocardiography. 2014; Apr 5. Epub ahead of print.

Paper 4

Fadnes S, Nyrnes SA, Torp H, Løvstakken L. Shunt flow evaluation in congenital heart disease based on Two-Dimensional Speckle tracking. Ultrasound Med Biol. 2014;40(10):2379-2391.

1.4 Abbreviations

ASD = Atrial septal defect

BFI = Blood flow imaging

B-mode = Brightness mode

BSD = Balloon stretched diameter

CDI = Color Doppler imaging

CHD = Congenital heart disease

CMR = Cardiovascular magnetic resonance

CT = Computed tomography

M-Mode = Motion mode

2D = two-dimensional

3D = three-dimensional

FDA = US Food and Drug Administration

LA = Left atrium

LLPV = Left lower pulmonary vein

LUPV = Left upper pulmonary vein

LV = Left ventricle

LVOT = Left ventricular outflow tract

MI = mechanical index

PRF = Pulse repetition frequency

Qp/Qs = The ratio of pulmonary (Qp) to systemic (Qs) blood flow

RA = Right atrium

RLPV = Right lower pulmonary vein

RUPV = Right upper pulmonary vein

RV = Right ventricle

SD = Standard deviation

TEE = Transesophageal echocardiography

TTE = Transthoracic echocardiography

TI = Thermal index

2 INTRODUCTION

Congenital heart disease (CHD) is among the most prevalent malformation occurring in approximately 1% of neonates in Norway, and is the leading cause of death from congenital malformations (1). Due to improvements in care and survival, there is a growing population of children and adults with congenital heart disease (2). There is a need for non-invasive tools for visualization of CDH and their functional consequence, and echocardiography has become the most important non-invasive diagnostic tool. Echocardiography alone may be sufficient to map a congenital heart defect before heart surgery, even if the defect is complex (3). Correct treatment depends therefore on the echocardiographic examination, combined with a thorough clinical examination. A high degree of diagnostic accuracy in echocardiographic imaging is the key to clinical management of patients with CHD (4). However, diagnostic imaging requires specific skills and knowledge and in some cases the diagnostic imaging can be difficult. Delayed or inaccurate diagnosis places children with CHD at risk for complications.

Diagnostic errors in pediatric echocardiography have decreased in parallel with improved ultrasound technology. Pediatric studies in the early 1980s found errors in 15-19% of diagnoses, but with improved Doppler technology in the mid-1980s, the errors decreased to 5-6% of diagnoses (5). In 1992, Sharma et al reported a diagnostic accuracy of echocardiography of 95% compared to findings at surgery (6). However, other centers report much higher error rates: In 1999 Stranger et al reported a nearly 20 fold greater error rate than in the mentioned 1992-study when pediatric echocardiograms were performed in adult laboratories (5). Recent publications from the high quality Echocardiography Laboratory at Boston Children's Hospital found an overall error rate of 0.17% (7, 8). However, the majority of the congenital echocardiography errors affected clinical management or resulted in an adverse event (7, 8). In addition to cognitive errors, both technical and patient specific factors are reported as common contributors to diagnostic errors (7, 9). Technical factors constitute one third of the errors, including poor acoustic windows, modality limitations or imaging artefacts. Also, the overall image quality may not be good enough. Pulmonary vein imaging and atrial septal defects are among the top anatomic segments involved in diagnostic errors in pediatric cardiology (7). In the imaging of these defects, the visualization of blood flow is essential.

Today, Color Doppler Imaging (CDI) is used to detect and visualize blood flow. However, CDI has limitations that might lessen its diagnostic value. CDI is angle dependent, which

means that it can only measure velocities along the ultrasound beam. Further, when the Nyquist limit for blood velocity is reached, aliasing artefacts will occur, obscuring the true velocity and the direction of flow (10, 11).

In the ultrasound research environment in Trondheim a new flow modality called Blood Flow Imaging (BFI) has been developed to overcome the limitations most often encountered in CDI (12, 13). BFI is a qualitative method aimed to visualize the blood flow in more detail than today's Doppler techniques. Since limitations in the technology can make echocardiographic imaging of the pulmonary veins and ASDs difficult, the main purpose of the present project was an attempt to limit some of these challenges.

The research was performed in close collaboration with the engineers that developed the new method and the clinical experience enabled further refinement of the technology in an interactive approach. The BFI technique was therefore continuously being improved throughout the project period. Flow speckle tracking was a result of this development, as illustrated in article 4. This method requires some post processing of the data to yield quantitative measurement of the blood speckle movement. However, the goal is to generate live data, and the latest development is live ultrasound-based particle visualization. A closer description of this development will be presented in chapter 9.

3 BACKGROUND

3.1 Echocardiography

The word ultrasound refers to all sound with a frequency humans cannot hear. Ultrasound is characterized by intensity, frequency and wavelength. The frequency in diagnostic echocardiography (ultrasound examination of the heart) is usually between 2-12 MHz. Higher frequencies provide better image resolution (i.e. ability to image small structures), but cannot penetrate as deep as lower frequencies because of increased attenuation. Therefore low frequencies are used in adults and high frequencies are preferred in babies and small children. The sound wave moves straight, but can be focused and/or bent. The scattered sound, or echo, is what gives the ultrasound image its features. In the B-mode image, varying shades of grey reflect different tissue scattering characteristics.

An ultrasound wave consists of oscillating pressure variations caused by vibration of the ultrasound transducer against the skin surface: The piezoelectric crystal in the transducer probe induces a local compression of the tissue with which the crystal is in contact. This local tissue compression propagates away from the piezoelectric crystal (acoustic wave). Spatial heterogeneities in tissue density result in a scattering or reflection of the propagating wave. Reflection describes the interaction of ultrasound with large and smooth surfaces, while scattering refers to the interaction of ultrasound with small structures like red blood cells. Reflection and scattering produces echoes that propagate back towards the piezoelectric crystal. The crystal deforms and produces an electric field which can be detected. This pulse-echo is processed and results in a single line in the ultrasound image. An ultrasound image is built up by many lines. When a pulse is emitted, the transducer has to wait for the returning echoes, before a new pulse can be emitted to generate the next line in the image. With the present technology, images in echocardiography can be generated at about 50 frames per second (FPS). The human visual perception has a temporal resolution of about 25-50 frames per second. However, off-line replay may be done at reduced frame rate, thus enabling the visualization at higher temporal resolutions. For example, if moving blood is captured with a high frame rate and then played back in slow motion, the movement of the blood speckle pattern can be seen by the human eye.

In cardiac ultrasound, or echocardiography, there are various imaging modalities, which mainly differ by how the reflected ultrasound wave is analyzed and visualized.

3.1.1 Selected history of echocardiography

The history of cardiac ultrasound started at the University of Lund, Sweden, in 1953 when the physician Inge Edler and engineer Carl Hellmuth Hertz used a sonar machine to conduct the first human echocardiogram. Their first publication subsequently occurred in 1954 (14). Hertz and Edler used M-mode to evaluate Mitral stenosis and their collaboration is commonly accepted as the beginning of clinical echocardiography. In the United States of America, Feigenbaum and his colleagues started echocardiographic imaging of the ventricles in the early 1960s (15). In 1967, Herz and Asberg presented the first demonstration of real-time-two- dimensional cardiac images. Commercially available scanners were available from the latter part of the 1970's.

In 2001, Terje Skjærpe and Liv Hatle described the Norwegian story of cardiac ultrasound with emphasis on the development in Trondheim (16). The background for the development of Doppler ultrasound techniques in Trondheim was a close cooperation between engineers working at NTNU and clinicians from the Department of cardiology in St Olav's University hospital which was established in 1969. Angelsen and colleagues developed PEDOF, a pulsed echo Doppler Flow velocity meter. Rune Åslid brought one of these prototypes to Rikshospitalet, where the cooperation with Jarle Holen led to further development of non-invasive assessment of pressure gradients (17). Rikshospitalet still has a strong research group in echocardiography, most renowned for their contribution to measurements of left ventricular function (18-20).

Liv Hatle and Bjørn Angelsen made important contributions in validating the Doppler method as a tool for diagnosis and follow up of cardiac diseases (21, 22). Their famous book: "Doppler Ultrasound in Cardiology. Physical principles and clinical applications" came out in 1982 and is listed as number one in the Norwegian cardiology's top 10 list (Listed in the book: "Det norske Hjerte"). At the same time Vingmed first combined the Doppler modality with the two-dimensional echocardiography, which represented the breakthrough for clinical use of Doppler. Subsequently, the color Doppler technology was pioneered by Japanese investigators, and introduced in 1984 by Omoto and then in 1986 by Vingmed(16). Since then Trondheim has been in the forefront of cardiac ultrasound research for many years (23-26), and many of the new applications developed by this research group are now used routinely in hospitals throughout the world. The cooperation between engineers and clinicians expanded later to other fields, as for example fetal medicine (27).

The history of pediatric echocardiography has developed in parallel with the field of adult echocardiography (28). In the late 1950's, Effert et al reported the results of echocardiography in

patients with congenital heart disease. However, the technology available at that time restricted further work until approximately one decade later. Again, Lund in Sweden was a central contributor, and Nils Rune Lundström presented data from various forms of congenital heart diseases (29). At Rikshospitalet in Oslo, Norway, echocardiographic examination of children was first used by Per Bjørnstad in 1979. The first two dimensional scanner was purchased in the pediatric department in 1979, approximately two years after Rikshospitalet bought their first M-mode ultrasound machine for the adult department (16). In Trondheim, the first pediatric cardiologist to practice echocardiography was David Linker, who started in 1985.

3.1.2 Grey scale echocardiography

In M-mode (Motion-mode), the ultrasound waves are emitted along a single line and the returning ultrasound wave is displayed as a depth-time-plot with depth information on the y-axis and temporal information on the x-axis. The intensity of each returning echo determines the shade of grey on the M-mode image. The method yields excellent time resolution (sampling rate 1000/second).

The B-mode (Brightness-mode or two dimensional imaging) is constructed using multiple lines which are produced as for the M-mode-display. The transducer is then aimed at a different angle, and a new line of information is formed. This is the standard image in echocardiographic imaging, and is an important mode to visualize cardiac anatomy, cardiac function and is further used as an underlying tool for other modalities, i. e the position of the line in M-mode.

3.1.3 Doppler echocardiography

When an acoustic source moves relative to an observer, the frequencies of the transmitted and the observed waves are different. This is known as the Doppler shift, named after Christian Doppler, who first described this phenomenon in 1843. One example of the Doppler shift is when an ambulance passes a static observer. The received frequency is higher than the emitted frequency during the ambulance's approach and lowered when it moves away. This change in the wave's frequency also occurs from the motion of reflectors in the body, such as red blood cells. The backscattered ultrasound pulses are shifted in frequency compared with the emitted pulse, and this shift is related to the velocity and direction of blood flow, the angle between the ultrasound beam and the blood flow, and the speed of sound in tissue. The Doppler equation describes this relationship:

$$f_d \approx 2 * f_o * v * \cos(\theta) / c$$

$$\Downarrow$$

$$v \approx f_d * c / (2 * f_o * \cos(\theta))$$

f_d = Doppler shift, f_o = transmitted frequency, v = target velocity (i. e blood flow velocity), θ = insonation angle (between ultrasound beam and velocity vector) and c = velocity of sound in tissue (≈1540 m/s).

Based on the Doppler equation, the Doppler shift is utilized in echocardiography to measure blood velocities. Typical blood velocities cause a Doppler shift in the sonic range (20 Hz-20 kHz) and can also be made audible to the user. A high pitch (large Doppler shift) corresponds to a high velocity and a low pitch (small Doppler shift) corresponds to a low velocity. In this way, the echocardiographer acquires both visual and audible information.

To determine the location of blow flow abnormalities, one can use pulsed wave (PW) Doppler imaging. Combined with two dimensional imaging, the sample volume can be placed in the area of interest, and the blood flow velocity can be measured in this specific site (30). When the echo machine is set in the PW modality, a single crystal intermittently emits and then receives ultrasound waves. The next pulse cannot be transmitted before the last signal has returned. This prevents PW Doppler from measuring velocities beyond a given threshold, called the Nyquist limit, defined as the pulse repetition frequency (PRF)/2. The inability to measure high velocities is a major limitation with this modality. If the depth is increased from 5 cm to 10 cm, the emitted pulse must travel twice as far before the next pulse can be emitted, and the PRF is approximately halved. The Doppler shift is moreover inversely proportional to the frequency of the transducer. At the same depth, a 2,5 MHz transducer may display velocities of twice the magnitude as a 5 MHz transducer. If the Nyquist limit is exceeded, the scanner cut off the true signal and displays the signal in the opposite direction. This phenomenon is called frequency aliasing.

To measure high velocity flow, the echo machine is set on continuous wave (CW) Doppler. In this case, the transducer uses two crystals, one constantly emitting ultrasound waves and the other constantly receiving the reflected waves (31). The frequency shift (Doppler shift) is continuously measured and displayed in a spectrogram to illustrate the different velocities within the ultrasound beam. A major limitation of this technique is the inability to locate the position of the highest flow

velocity. The ultrasound signal weakens with depth due to attenuation, and velocities close to the transducer will contribute more than the ones further away.

3.1.4 Color Doppler Imaging

Color Doppler imaging creates a real-time two-dimensional image where Doppler shift information is coded in color and laid over the grey scale image (11). The blood velocity measurements are obtained in the same manner as with pulsed wave Doppler, with multiple sample volumes interrogated sequentially and displayed in a 2 D region of interest. Movement away from the transducer is commonly encoded in blue and movement towards the transducer is commonly encoded as red. The intensity of the color relates to the mean velocity of flow: The higher the velocity, the brighter the color signal, with aliasing above the threshold velocity (the Nyquist limit). Color Doppler Imaging currently does not permit precise quantitative velocity measurements. On the other hand, the color image provides spatial information about blood flow that is unavailable with other techniques. Color Doppler allows a rapid flow overview and is therefore ideal for assessing areas of disturbed flow, and the technique has become very valuable in pediatric cardiology. The method is used to detect and locate shunts, to map jet orientation and to detect valvular regurgitation.

Figure 1 demonstrates a color Doppler image from a superficial vein of the upper limb. The color displayed at each point of the image depends on both the blood velocity and the Doppler angle at that point.

Figure 1: Color Doppler Imaging

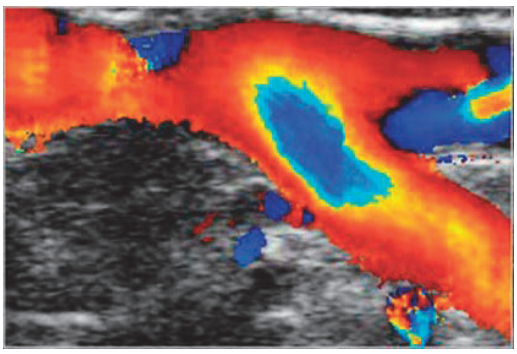

3.1.5 Color Doppler limitations

Color Doppler is an important diagnostic tool in pediatric cardiology. However, the method has significant inherent limitations (10).

- The method is **angle dependent**, which means that only the velocity component along the ultrasound beam is measured and displayed. In Figure 1, the angle of isonation relative to the axis of flow approaches 90 degrees in some parts of the image, for example in the right upper corner of the image. Here the Doppler shifts decrease and may fall beneath the threshold for detection. Therefore an adjacent area in the same vessel is encoded with both red and blue falsely mimicking disorganized flow. Furthermore the angle estimated from the Color Doppler Images represent a two dimensional estimate of a three dimensional vector and the true angle of blood flow may not lie in the plane of the image.

- As with PW Doppler, **aliasing** may occur with color Doppler imaging because of a restricted Nyquist limit. Aliasing means the production of false frequency estimates due to under sampling. In the color Doppler display, Doppler shifts greater than PRF/2 are “wrapped around” and give the false impression that blood flows in the opposite direction to real flow (i. e. blue instead of red). With most color Doppler schemes, aliasing is depicted in pale red or blue, which usually can be distinguished from flow separation with more deep shades of color as in angle insonation. In Figure 1 aliasing is visualized at the point where the branch coming from below meets the branch which is perpendicular to the ultrasound beam. Many disturbed jets in restricted orifices will exceed the Nyquist limit and result in aliasing and an ambiguous display. This problem can be somewhat reduced by increasing the pulse repetition rate (PRF) allowing less time for motion between the two acquisitions. Decreasing the transducer frequency also provides a higher Nyquist limit, but at the expense of the resolution in the B-mode image.

- The display represents the mean velocity and not the peak velocity. The accuracy of this estimate has not been validated, and there is reason to assume an underestimation of velocities.

- The **spatial and temporal resolution** of the superimposed color Doppler image is likely to be less than the resolution in the underlying B-mode image. The insufficient spatial resolution leads to so called “color blooming artefacts”, which means that the color is bleeding into the surrounding tissues. This phenomenon is also demonstrated in figure 1. Acquisition of the Doppler information requires much more time than the structural image, since several pulse transmissions per scan line is required to obtain flow information. To achieve higher frame rates, the image can be made up of fewer scan

lines with interpolating algorithms to fill in the lost information. Thereby the image can be completed faster, but some spatial information is lost. Compromises need to be made in order to produce a color image with an adequate frame rate and image quality. The frame rate may also be improved by limiting the area (depth and with) of the flow sector.

3.1.6 Blood Flow Imaging

The ultrasound research environment in Trondheim has developed a new real-time ultrasound flow modality called blood flow imaging – BFI (12, 13). This was done in collaboration with GE Vingmed Ultrasound which has a Research & Development department working closely with the ultrasound research group.

BFI is able to visualize blood flow in any direction of the image by supplementing Color Doppler Imaging (CDI) with qualitative information of flow by visualizing an additional angle independent speckle movement not affected by velocity aliasing. Thereby the method avoids two of the limitations most often encountered in conventional CDI. BFI is commercially available for vascular imaging. The method is now also adapted to evaluate flow in pulmonary veins and atrial septum defects in children, and the present project is a clinical evaluation of this method. The method is more thoroughly described in the methods section.

3.1.7 The safe use of ultrasound in pediatric cardiology

Ultrasound has an excellent safety record. However, to ensure the safe use of ultrasound, it is important for clinical users to have some understanding of this subject. As a result of absorption processes, energy from ultrasound is deposited in the tissue. This absorption causes two main bio-effects of ultrasound: heating and cavitation. Current regulations refer to the safety indices that relate to these two effects: the thermal index (TI) and the mechanical index (MI).

The thermal index gives an indication of the temperature rise in tissue due to absorption of ultrasound. The most likely tissues to experience heating are bone and adjacent soft tissues. Thermal effects are best predicted from the knowledge of energy flow over time (32). For neonatal cardiac imaging, recommended exposure time should be restricted when TI is >1 (33). Maximum TI-values declared by producers of ultrasound scanners are low compared to the US Food and Drug Administration's (FDA) normal maximum permitted value of 6,0. Values are highest in the pulsed Doppler mode and least in B-mode- imaging.

The mechanical index indicates the probability of occurrence of cavitation. Cavitation is the formation and subsequent collapse of gas bubbles which arises from shear forces and free radical formation. The most likely tissues to experience mechanical damage are those adjacent to gas, i.e. at the surface of the lung, the intestine and with contrast agents. Mechanical effects can be best predicted from knowledge of individual pulses (peak negative pressure) (32). FDAs maximum permitted MI is 1.9.

The TI and MI values are available on the screen of the ultrasound scanner. Where low values cannot be achieved, examination time should be kept short and at least be within the recommendations.

Developments in ultrasound technology have resulted in vast improvements in image quality, but also some increases in acoustic output levels(34). However, diagnostic ultrasound imaging is safe as long as one remain within the recommended limits.

3.2 Congenital heart disease

The incidence of congenital cardiac disease is stable, but longevity has improved and hospitalizations for infants and adults with congenital heart disease are increasing (2). Further research to optimize health care for this patient group is therefore necessary, and improved echocardiographic diagnostics is essential in this context. The most common congenital heart defects are persistent ductus arteriosus (PDA) and isolated septal defects (ASD alone or VSD alone) according to Liu et al (35).

3.3 Atrial septal defects

Defects of the atrial septum account for 7-12 % of congenital heart disorders (36, 37), and atrial septal defects (ASD) are thereby one of the most common congenital cardiac anomalies. The functional consequences of the defect are related to the anatomical location, its size, and the presence or absence of other cardiac anomalies. Approximately 70 % of all ASDs are secundum defects, which may close spontaneously, remain unchanged or enlarge as the child grows (38-40). When ASDs are clinically significant, follow up with echocardiography is mandatory to select those requiring either surgical or interventional closure. It is also helpful confirming spontaneous closure.

3.3.1 Atrial septal defect imaging

Transthoracic echocardiography (TTE) combined with conventional color-Doppler imaging (CDI) is diagnostic in the majority of children with ASD. However, due to a false coloring of the interatrial septum from overlapping color and B-mode images (i.e. color blooming artifacts), the flow through

atrial septal defects is not always easy to detect, especially when 2D images are suboptimal and when defects are small. Also Doppler shift techniques are only able to measure velocities along the ultrasound beam, and are thus angle dependent. Often a prior knowledge of the anatomy and ultrasound beam angle is required to interpret the information presented. Further, when the Nyquist limit for blood velocity is reached, aliasing artifacts will occur, obscuring the true velocity and the direction of flow (11).

In the apical four-chamber view, the parallel angle of the echo beam, the limited lateral resolution and the thinness of the fossa ovalis can cause artifactual echo dropouts of the septum and thereby lead to an inaccurate diagnosis (41). Subcostal imaging minimizes the dropout of the atrial septal echoes, but some defects may be missed. The subcostal image view may further be suboptimal for obese patients (42).

Transesophageal echocardiography (TEE) provides better images of the interatrial septum (43, 44). But since TEE applicability is limited by the need for general anesthesia in children, the method is predominantly used to guide catheter closure.

Studies have presented real-time 3-D echocardiography (45, 46), and magnetic resonance imaging (MR) as useful ASD imaging modalities (47, 48). But the need for sedation and/or the fact that these modalities are time consuming limits the use of these methods in daily clinical practice. In spite of all new modalities for ASD-visualization, 2D-TTE still is the most commonly used technique for ASD imaging in children.

3.3.2 Atrial septal defect imaging during thanscatheter closure

High-quality imaging of ASD size and morphology is essential for successful transcatheter closure. This is done by transthoracal echocardiography (TTE) before the procedure and further transoesophageal echocardiography (TEE) throughout the closing procedure (49, 50).

Balloon sized diameter (BSD) is regarded as the reference method for measuring ASD maximum diameter and is used to select the appropriate size of the device (51). To measure BSD, a compliant balloon is filled with dilute contrast, placed across the ASD and inflated until a waist in the balloon is visible on fluoroscopic imaging. In this way, BSD provides information of physical stretch, which cannot be predicted by echocardiography (52). However, if there are multiple defects, echocardiography may be better in the estimation of size (46).

Color Doppler imaging (CDI) measurement of the ASD size correlates well with BSD and surgical measurements (53, 54). However, there are sources of error in determining the size of the jet, including CDI gain, examination depth and transducer frequency. CDI may also underestimate an irregular defect.

3.4 Pulmonary vein imaging

Echocardiography with conventional Doppler techniques has become the most important imaging modality to detect anomalies of the pulmonary veins (55, 56). Although high frequency transducers in combination with CDI have improved the sensitivity, visualization of totally anomalous pulmonary venous connections may be difficult. Partial anomalous pulmonary venous connections are often not recognized in standard echocardiography (57). Because this anomaly is associated with an ASD, the pulmonary veins must be carefully assessed before transcatheter closure (36, 58). At Oslo University Hospital, Rikshospitalet, echocardiography was routinely supplemented by angiography at the time this study was performed. However, angiography is an invasive procedure which also leads to radiation and hopefully may be avoided with improved ultrasound visualization. Stenosis of normally connecting pulmonary veins may be difficult to detect (59), and even if all four pulmonary veins are normally connected, they may not necessarily be imaged using CDI. The low velocities in the pulmonary veins are best recorded when the flow is parallel to the sound beam. In views where the venous structures are perpendicular to the sound beam, the low velocity blood flow may be difficult to visualize.

4 AIMS

4.1 General aims

Our aim was to study whether the new method blood flow imaging (BFI) may improve the ultrasound visualization of atrial septal defects and pulmonary veins in children and thus improve the diagnostic information in congenital heart defects.

The evaluation of BFI in atrial septal defects and pulmonary veins was focused on assessing the extent to which the new method could produce better information about the flow conditions, the defect size and the venous drainage sites as this is important details for the medical doctors in deciding if, when and how to perform intervention. We also wanted to evaluate the method using different probes and for a wide spectrum of patient size from neonate to adult.

Last but not least, an aim of this study was further improvement of the ultrasound flow technology in order to provide more information about flow conditions in congenial heart defects.

4.2 Specific aims

1) To study if Blood flow imaging (BFI) provided improved visualization of the blood flow in atrial septal defects compared to conventional color Doppler imaging (CDI) in transthoracal echocardiography in children.

2) To study if BFI provided improved visualization of pulmonary veins compared to conventional color Doppler imaging (CDI) in transthoracal echocardiography in neonates.

3) To compare ASD-sizing using the new method BFI in transoesohageal echocardiography with the current and more invasive reference in ASD sizing, Balloon stretched diameter (BSD).

4) To find out if BFI used in transesophageal echocardiography of the pulmonary veins was equally good as the more invasive reference pulmonary angiography in the visualization of the pulmonary veins.

5) To find out if angle-independent vector flow velocity estimation in an ASD and VSD was conceivable in neonates.

6) To explore if high frame rate flow-visualization revealed new information of blood flow patterns in congenital heart defects.

5 MATERIALS AND METHODS

5.1 Study overview and design

The host institution of this project was Norwegian University of Science and Technology (NTNU)/St. Olav's University Hospital, Trondheim, Norway. Cardiologist Bjørn Olav Haugen and pediatric cardiologist Siri Ann Nyrnes planned study 1, 2 and 3. BFI was developed by the engineers Hans Torp and Lasse Løvstakken, who provided their technological expertise during the whole project period.

Study 4 is a technical sub-project of a clinical feasibility study on flow speckle tracing. This project has its own study protocol drafted by Siri Ann Nyrnes and critically reviewed by Lasse Løvstakken. Patient inclusion still continues in this project called "High frame rate flow visualization in neonates and children with congenital heart defects". Lasse Løvstakken had the idea and initiated the technological sub-project presented in this thesis (study 4). Engineer and PhD-student Solveig Fadnes worked with post processing of the data in study 4 performed the in-vitro flow phantom validation, and is the first author of paper 4 (study 4).

In this research project, there was a close collaboration between the engineers that developed Blood Flow Imaging and flow speckle tracking and the clinicians, with the objective of using the clinical experience for further refinement of the technology in an interactive approach. The data in all studies was collected in a prospective design by the author. Study 3 was a collaboration project with the Department of Pediatric Medicine, Section for Pediatric Cardiology, Oslo University Hospital, Rikshospitalet.

5.2 Study population characteristics

5.2.1 Materials - Study 1

This feasibility study was performed at the Department of Pediatrics, St Olav's University Hospital, in Trondheim, Norway. A total of 13 children with ASD were evaluated between March and August 2006. The age ranged from neonates to 9 years, with a median age of 12 months. The inclusion criterion was ASD sized 4 mm or more at the time of diagnosis. Patients were recruited in the outpatient clinic and from the hospital ward, and both newly diagnosed and previously diagnosed patients were included. The reason for referral to a pediatric cardiologist in most of the patients was the presence of a heart murmur. In one patient, hemiparesis and cerebral infarction led to further investigation with

echocardiography. One patient with a previously diagnosed ASD was excluded due to spontaneously closure of the defect discovered at the time of study inclusion.

The patient characteristics are described in Table 1. One patient had a primum ASD and the others had secundum defects. The ASD size ranged from 2-9 mm. All defects were 4 mm or larger at time of diagnosis. Because of the natural history of secundum ASD`s, some of the defects were smaller at the study examination. Two of the patients had two defects. One neonate had raised vascular pulmonary resistance and bidirectional shunting. The others had left to right shunting across the ASD. Both patients with pulmonary stenosis had small shunts and mild stenosis. Eight of the patients were girls. Seven patients had additional cardiac anomalies. One of the patients had total atrioventricular (AV) block, while the others had sinus rhythm. Three patients had significant right ventricular volume overload and required intervention. The 12 month old girl who presented with stroke had a 5 mm secundum ASD which closed spontaneously during follow up.

TABLE 1

Study 1 – ASD feasibility study - Patient characteristics

Age	Diagnosis	ASD size	Other cardiac anomalies
9 years	Secundum	7 mm	Small patent ductus arteriosus
12 months	Secundum	5 mm	
22 months	Secundum	4 mm and 2 mm	Broncopulmonary dysplasia and mild pulmonary hypertension
4 months	Primum	6 mm	
1 month	Secundum	4 mm	Muscular ventricular septum defect (VSD)
13 months	Secundum	3 mm	Pulmonary valve stenosis
19 months	Secundum	4 mm	Pulmonary valve stenosis
2 weeks	Secundum	4 mm	Perimembranous VSD
2 months	Secundum	3 mm	
3 years	Secundum	9 mm	
21 months	Secundum	6 mm and 3 mm	
5 days	Secundum	4 mm	Grade III atrioventricular (AV)-block
6 weeks	Secundum	4 mm	

5.2.2 Materials - Study 2

The study was performed at the Department of Pediatrics, St. Olav's University Hospital,Trondheim, Norway. A total of 26 neonates referred to a pediatric cardiologist because of suspected congenital heart disease were included prospectively from February to April 2008. Patients were recruited from the hospital ward. The reasons for referral to a pediatric cardiologist were either the presence of a

heart murmur, other congenital defects, asphyxia or arrhythmias. The patient characteristics are described in table 2.

TABLE 2

Study 2 – Pulmonary veins in neonates - Patient characteristics

Patient	Age/days	Echocardiography findings	Supplementary information
1	4	Normal	Intrauterine supraventricular tachycardia
2	10	Tetralogy of Fallot	Di George syndrome, Inguinal hernia, Supraventricular tachycardia
3	0	Pulmonary hypertension PDA	Duodenal atresia, infantile myofibromatosis
4	0	Muscular VSD and PDA	
5	5	Pericardial effusion, Pulmonary hypertension PDA	Diaphragmatic hernia Primary intestinal lymphangiectasia
6	21	Peripheral pulmonary stenosis	Prematurity (31 weeks + 2 days)
7	2	Muscular VSD Reduced left ventricular contractility	Prematurity (34 weeks), asphyxia, RDS
8	6	Secundum ASD Peripheral pulmonary stenosis	
9	0	Atrial septal aneurysm	
10	2	Muscular VSD Secundum ASD	
11	6	Normal	Prader Willi syndrome Hip dysplasia
12	2	PDA, Frequent premature atrial contractions	
13	1	PDA	Esophageal atresia
14	3	Normal	Hypospadia
15	0	Secundum ASD, PDA	Asphyxia
16	4	PDA	Prematurity (28 weeks + 5 days)
17	33	Peripheral pulmonary stenosis	
18	1	PDA	
19	0	Transposition of the great Arteries, PDA	
20	13	2 muscular VSDs and a secundum ASD	
21	3	Secundum ASD	Bilateral radial aplasia
22	0	PDA	Did not pass pulse oximetry screening (saturation 94%)
23	0	PDA, Atrial septal aneurysm	Oesophageal atresia
24	20	Normal	Tachypnea
25	5	Muscular VSD and secundum ASD	
26	12	AVSD	Down`s syndrome NEC in newborn period, colonic strictures

The median age of the patients was 5.9 days and there were 17 boys and 9 girls. The patients' conditions varied from critically ill to healthy. Five patients received ventilation support during

echocardiography; 2 patients with conventional mechanical ventilation, 2 patients with high frequency ventilation and one patient with continuous positive airway pressure. Two patients had pulmonary hypertension and 18 patients had shunts at inclusion. All patients had normal venous connections.

5.2.3 Materials and methods - Study 3

This study was a collaboration project between the Department of Pediatric Medicine, Section for Pediatric Cardiology, Oslo University Hospital, Rikshospitalet, Norway and the Norwegian University of Science and Technology (NTNU)/St. Olav's University Hospital, Trondheim, Norway. Patient inclusion took place at Rikshospitalet, where all interventional pediatric ASD-closures in Norway are centralized. NTNU/St Olav's University hospital contributed with the new technology BFI, echocardiography and data collection.

The inclusion criteria in the study were children aged 0-16 years with isolated secundum ASD accepted for interventional ASD-closure. To be accepted for interventional closure, the secundum ASD had to be hemodynamically significant, i.e. signs of pulmonary hyperflow with qualitative evidence of right ventricular and/or right atrial dilatation on echocardiography. A total of 28 children scheduled to interventional ASD-closure were included prospectively from February 2008 to February 2009. The patients were recruited from hospitals all over Norway.

The ratio of pulmonary to systemic blood flow (Qp/Qs) was calculated from saturations obtained from superior and inferior vena cava, pulmonary vein and artery and systemic saturation. ASD closure device was chosen based on balloon sizing using the stop flow technique.

The patient characteristics including the BSD values and the Qp/Qs values are described in table 3. The age of the patients ranged from 8.5 months to 16 years. There were 19 girls and 9 boys. Nine patients had more than one atrial septal defect. The BSD ranged from 9.5 to 20.5 mm and the ratio of pulmonary (Qp) to systemic (Qs) blood flow ranged from 1.2 to 4. Four patients had Qp/Qs <1.5. However, closure was considered reasonable because these patients had echocardiographic evidence of right atrium and right ventricular dilatation. Furthermore, they had a rather large ASD and/or more than one defect. None of the patients had pulmonary hypertension, 19 patients had a systolic murmur and 18 patients had a fixed split second sound.

TABLE 3

Study 3 - ASD closure - Patient characteristics

Patient	Age/years	BSD (in mm)	Qp/Qs
1	1.2	16.0	3.0
2	1.9	16.0	2.0
3	2.2	11.0	1.3
4	3.8	20.5	2.0
5	16.3	18.0	1.2
6	3.6	16.0	2.4
7	1.6	9.5	4.0
8	14.2	13.0	2.0
9	3.6	16.0	3.0
10	2.1	20.0	4.0
11	5.6	11.5	2.0
12	1.1	16.0	2.5
13	2.1	17.5	2.0
14	1.3	14.0	1.8
15	4.1	14.0	1.6
16	0.7	11.0	2.2
17	3.0	17.5	2.9
18	3.4	18.5	1.7
19	2.9	14.6	1.8
20	2.3	14.0	1.2
21	0.8	14.0	1.5
22	5.5	14.0	1.6
23	4.3	21.0	1.7
24	7.6	18.0	3.0
25	4.6	19.0	1.3
26	11.2	20.0	2.0
27	7.2	19.0	2.5
28	4.2	15.0	2.5

The patient characteristics are described in table 3. Twenty-seven patients underwent successful ASD Amplatzer closure, two of these patients required two devices. In one patient, the attempt at closure was unsuccessful because of insufficient attachment of the Amplatzer device to the atrial septal rims.

By June 2012 (3-4 years after closure), there were no registered complications among the patients. In two patients, the Amplatzer device was touching the mitral valve, but there were no mitral obstruction or insufficiency. One patient had a large device related to septal size. In this patient, there was a temporary increased flow velocity in the upper left pulmonary vein. This had resolved by one year after closure.

5.2.4 Materials - Study 4

This technical study was based on additional ultrasound acquisitions with a research scanner in connection with an ongoing feasibility study on flow speckle tracking. Data collection was carried out at the Department of Pediatrics, St Olav's University Hospital, in Trondheim, Norway. Two neonates from these data collections were chosen to describe the method. Patient 1 was an 8 day old boy who was 3340 g at the time of the ultrasound recordings. He had a perimembranous VSD which was the focus of the study. He was also born with a secundum ASD, a pulmonary artery sling (the left pulmonary artery anomalously originating from the right pulmonary artery) and anal atresia. Patient 2 was a girl who was born prematurely (31 weeks and 4 days). She has a secundum ASD and no other congenital malformations.

5.3 Blood Flow Imaging

The real-time ultrasound flow modality called Blood Flow Imaging (BFI) supplements Color Doppler Imaging with additional angle-independent information of flow direction. This is done by visualizing the blood speckle movement superimposed on the Color Doppler Images.

In all ultrasound imaging, there is a speckle pattern which is recognized as an irregular pattern where homogenous tissue is expected. The ultrasound speckle pattern from blood is present inside the vessel lumens and heart chambers, but is normally not visible in the B-mode (B=brightness) image due to the weak strength of the echoes from blood compared to the surrounding tissue structures. However, this blood speckle pattern can be visualized by first filtering out the stronger tissue echoes (wall filtering). The movement of the blood speckle pattern between image acquisitions corresponds to the actual blood cell movement, but can only be captured by acquiring images with a frame rate in the kHz range. In an image acquisition scheme termed beam interleaved acquisition (60), such high frame rates can be achieved for separately acquired sub regions of the total image sector. On display, speckle images acquired for different sub regions are shown at a rate equal to the total image sector frame rate, leading to a slow motion display of the speckle movement, which can be tracked by the human eye. In Blood Flow Imaging, this speckle pattern technique is combined with regular Color Doppler Imaging. The speckle pattern in BFI is angle independent and has no upper aliasing velocity scale limitation.

Figure 2 demonstrates flow in a superficial vein of the upper limb with blood flow imaging. The color Doppler information corresponds to Figure 1, but in Figure 2 there is an additional speckle pattern superimposed in the images. The additional information from this speckle pattern is

best appreciated in movie clips where you can see the movement of the speckle pattern precisely, also in areas with ambiguity in the underlying color images.

Figure 2: Blood Flow Imaging

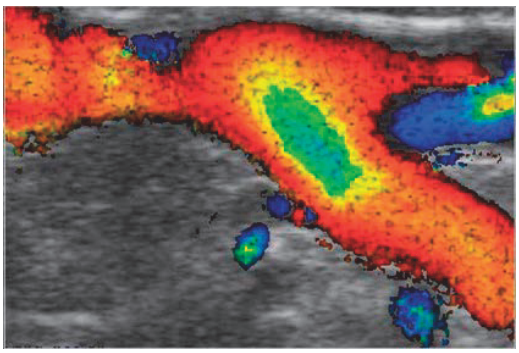

The data acquisition and processing scheme used in BFI is schematically shown in figure 3. As illustrated, both color-Doppler and speckle images are produced from the same data recording. In parallel to conventional color-Doppler processing, speckle images from blood are produced by wall filtering followed by conventional B-mode-processing. Wall filtering means removing low-frequency Doppler shifts from soft tissues such as myocardium and vessel walls, which are lower than the Doppler shifts from moving blood. Further, an amplitude normalization procedure is applied to avoid flashing artifacts due to discontinuities in the blood signal power for different image regions. Finally CDI and speckle images are combined by adding the speckle variation to the Doppler power estimates. A two-dimensional color scale including both the mean Doppler frequency and power is displayed on the screen. Based on the 8-12 temporal image samples typically acquired in CDI, one color image and 4-8 speckle images can be produced.

Figure 3: BFI acquisition and processing

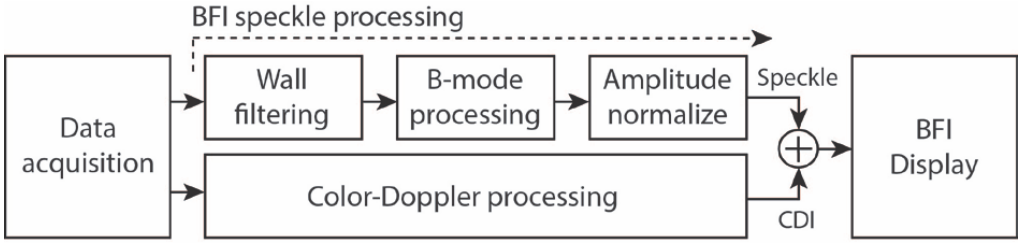

Figure 3: Reproduced from Paper 2, with permission from Jon Wiley and Sons.

A block diagram illustrating the data acquisition and processing scheme utilized in BFI. The general data acquisition is identical for CDI and BFI. In parallel to conventional CDI processing, speckle images from blood are produced by wall filtering and conventional B-mode processing. A normalization procedure is applied to avoid flashing artifacts in the speckle images due to discontinuities in signal power from different regions in the image. In the end, the speckle image variation is added to the Doppler power estimates in CDI and displayed using a two-dimensional color map including both Doppler power and mean frequency. BFI = Blood Flow Imaging; B-mode = "Brightness" mode; CDI = Color Doppler Imaging

The BFI technique is commercially available for vascular imaging on GE systems, but was not freely available for cardiac probes or transesophageal probes during this project. The GE M4S probe was specially adapted to make the BFI technique available for study 1. The same adaptions were made for the GE 7S probe for study 2, and the GE 9T & 6T TEE probes in study 3. In study 3, the lateral image resolution of the setup was approximately 1.0-1.3 mm for the 6T probe and 1.0-1.4 mm for the 9T probe. The axial image resolution was approximately 0.4-0.5 mm for both probes.

5.4 Blood flow imaging limitations and potentials

The BFI technique is based on the same data acquisition scheme as CDI, but some trade-offs regarding optimal CDI setup are often needed to ensure suitable blood speckle visualization. The pulse repetition frequency (PRF) often needs to be reduced which may increase aliasing artefacts in CDI. Further, the image resolution and line density needs to be increased to ensure sufficient quality of speckle images, something which may lead to a reduced penetration and color-Doppler frame rate.

In its current implementation, BFI is limited to imaging shallow depths (< 10 cm), making it suitable for vascular imaging and imaging in pediatric cardiology (61-63). However, getting closer to the heart through the esophagus implies that the method should also have potential for cardiac imaging in adults using TEE.

Figure 4 demonstrates an ASD imaged with both a transthoracal probe (M4s) and a transesophageal probe (6T). The example is from patient no 5 in study 3 who was 16 years old with height 175 cm and weight 67.6 kg. He had one ASD and the measured BSD was 18 mm. In the TTE examination to the left, the speckle pattern in BFI is much coarser than in the transesohageal examination to the right. The speckle pattern degrades and has lower quality when the depth is in this order of magnitude. TEE reduces imaging depth, in this case from 10 to 3 cm, and the speckle quality is therefore better, thus making this technique also applicable in adults.

Figure 4: Comparison of transthoracic and transesophageal BFI visualization of ASD

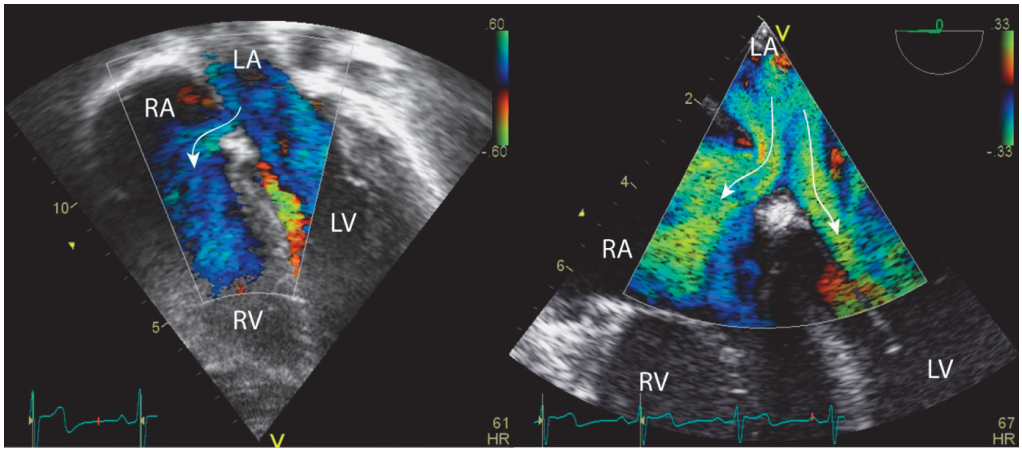

Figure 4: Transthoracal (left) and Transoesophageal (right) four chamber views with Blood Flow Imaging; Visualization of an atrial septal defect, the left atrium (LA), left ventricle (LV), right atrium (RA) and right ventricle (RV). The arrows show the direction of the speckle pattern.

In the neonate, the depths are shallow and the speckle pattern movement in BFI is clearer than in older children.

5.5 Parallel receive beam forming, plane wave imaging and flow speckle tracking

Parallel receive beam forming means to receive multiple image lines for each emitted ultrasound pulse. This technique has been used to increase the frame rate in Color Doppler Imaging. However, the method gives rise to visible image artefacts using conventional focused ultrasound beams. By using a linear imaging probe where plane unfocused beams can be emitted (plane wave imaging), it is possible to reduce these image artefacts and to increase the frame rate further.

Figure 5 demonstrates the conventional ultrasound acquisition with a phased array transducer (left) compared with parallel receive beam forming with a linear transducer (right). To the left, one focused transmit line and one focused received line is acquired. Each pulse requires time to travel forward and back through the tissue, and in this setup a high number of transmit beams is needed to construct the ultrasound image, which limits the frame rate. To the right, a broad unfocused wave is transmitted and multiple image lines are received simultaneously. In this way the acquisition time is lowered and higher frame rates are achieved. In theory the frame rate increases with a factor equal to the number of parallel receive beams. In practice there may also be limits on the amount of data that can be processed in real-time by the ultrasound system which lowers this theoretical limit.

Figure 5: Parallel receive imaging beam forming and plane wave imaging

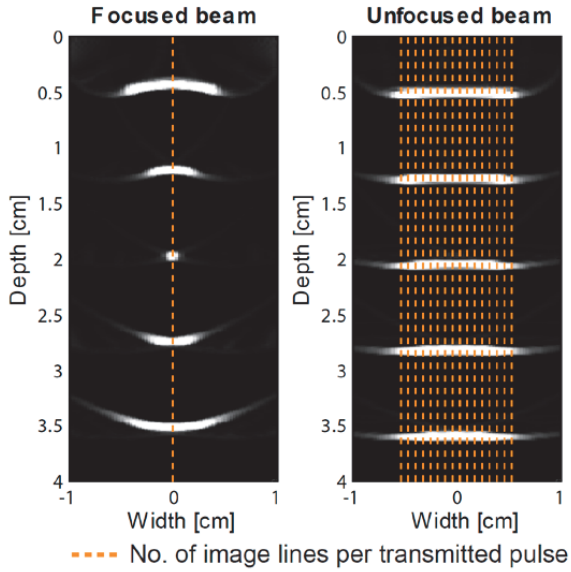

Using pattern-matching techniques, the movement of blood speckle can be quantified in 2-D images. The 2-D velocity information can be visualized as arrows or streamlines overlaid color-Doppler images that help to highlight areas of complex flow patterns such as vortex formation in congenital heart disease. Figure 6 demonstrates the speckle pattern tracking principle. A kernel is defined in a first acquisition and the best match of this kernel is searched for in the next acquisition.

Figure 6: The speckle tracking principle

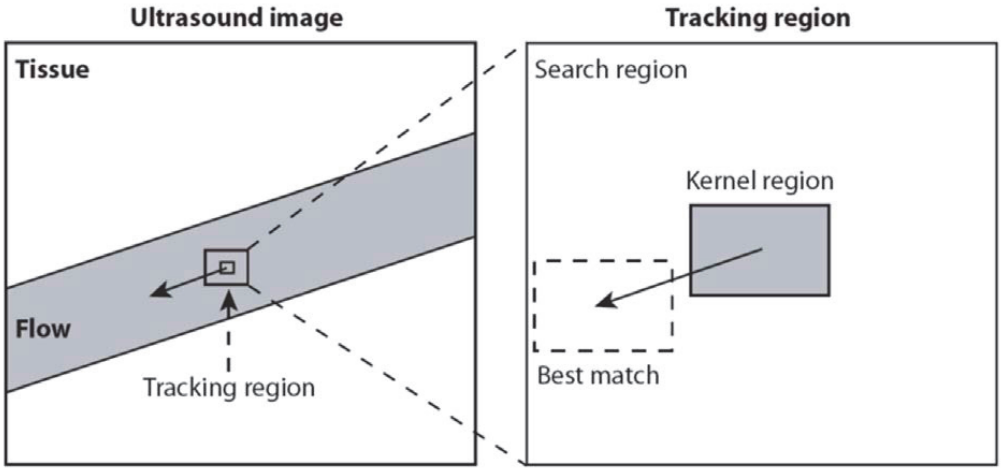

Figure 6: Reproduced from paper 4, with permission from Elsevier. A kernel is defined in an acquisition and the best match of this kernel is searched for in the next acquisition.

5.6 Ultrasound Equipment and setup

The echocardiographic examinations in study 1-3 were performed using a GE Vingmed Vivid 7 (GE Vingmed, Horten, Norway) ultrasound machine. We used different probes in the three sub-studies. In study 1, the transthoracic echocardiography examinations were performed with a GE M4S cardiac probe (GE Healthcare, USA) and in study 2 a GE 7S cardiac probe (GE Healthcare, USA) was used. In study 3, the transesophageal echocardiography examinations were performed using a 9T or 6T-probe. (GE Healthcare,USA). Imaging with BFI has safety measurements in the same range as CDI, and satisfy the requirements from the American Food and Drug Administration.

In study 4, a SonixMDP ultrasound scanner (Ultrasonics Richmond, BC, Canada) with a 4-9MHz linear transducer and a Sonix DAQ for channel data acquisition was used for both in vivo and in vitro recordings. Prior acoustic measurements satisfied the requirements from American Food and Drug Administration. Table 4 demonstrates the values from the acoustic report from the SonixMDP scanner. Scanning with the Vingmed Vivid E9 (GE Vingmed, Horten, Norway) with 9L-D og 11L-D (GE Healthcare, USA) was done in advance.

Table 4 – Safety measurements in the SonixMDP-scanner

Setting		1	2	3	4	5	
TxFrequency	[MHz]	5.0	5.0	5.0	6.7	6.7	
Aperture	[elements]	128	128	128	128	26	
TxNumberOfHalfPeriods	[ ]	3	5+3+5	5	3	2	
Focal depth	[mm]	∞	∞	∞	∞	19	
PRF	[kHz]	15	12	12	15	12.6	
Acoustic measurements	[V]	68	56	56	68	83	Limit
MI (inv)	[ ]	0.5	0.5	0.4	0.3	0.8	1.9
TIS (inv)	[ ]	1.3	1.3	1.4	0.9	0.05	3.0
TIB (inv)	[ ]	1.5	1.5	1.6	1.3	0.25	3.0
TIC (inv)	[ ]	1.3	1.2	1.3	1.3	0.25	3.0
$I_{spta.3}$ (inv)	[mW/cm^2]	121	115	124	63	451	720
Temperature (inv/non-inv)	[V]	48/68	48/56	45/56	48/68	56/56	Limit
ΔT_{air} (inv/non-inv)	[°C]	—/19.0	—/24.2	—/23.0	—/18.3	1.8/1.8	27/27
$\Delta T_{phantom}$ (inv/non-inv)	[°C]	4.5/7.3	4.7/6.6	4.3/6.5	4.3/9.1	0.8/0.8	6/10

Table 4: Reproduced from the REP014: Safety measurements (2011-12-13). A set of safety measurement have been done on a 5MHz L9–4/38 linear array ultrasound probe connected to a SonixMDP ultrasound scanner. Author Øyvind K.-V. Standal, Department of Circulation and Medical Imaging, Norwegian University of Science and Technology

Abbreviations: TIS = Soft tissue thermal index, TIB = Bone thermal index, TIC = Cranial thermal index, Ispta.3 (attenuated spatial peak time average intensity)

Study 4 was part of a flow speckle tracking feasibility study. First we used a Vingmed Vivid E9 scanner with a custom color flow imaging acquisition based on plane wave imaging (unfocused) with 16 image lines generated in parallel for each emitted pulse. These data will be presented in a separate paper. In addition, we used the SonixMDP-scanner to generate data to study 4 in order to increase the number of image lines generated. With the SonixcMDP scanner, 256 image lines are generated for each emitted pulse, which further increases the frame rate. Data from this research scanner is useful in the further development of future scanners for use in daily clinical practice.

5.7 Image acquisition and processing

5.7.1 Echocardiography

In study 1, the blood flow through the atrial septal defects was first studied with a conventional TTE examination using CDI. BFI was used to supplement the examination. In study 2, a full standard echocardiography examination was performed on all the patients, and BFI scanning of the pulmonary veins was supplementary to the examination. Flow in the pulmonary veins was examined from the suprasternal short axis view, as well as the apical, subcostal and long axis views. In study 3, a full standard transesophageal echocardiography examination was performed on all the patients before the transcatheter closure, and BFI scanning of the ASD and the pulmonary veins was supplementary. The echo examinations with BFI in the project were performed by the author. The first examinations of each study were performed in conjunction with engineer Lasse Løvstakken in order to adjust and optimize the technical settings for Blood Flow Imaging in each probe and study. The echo examinations in study 3 were performed in cooperation with Kjetil Lenes, who at that time worked as an echo technician in Department of Pediatric Medicine, Section for Pediatric Cardiology, Oslo University Hospital, Rikshospitalet

Figure 7: The cath lab at Rikshospitalet

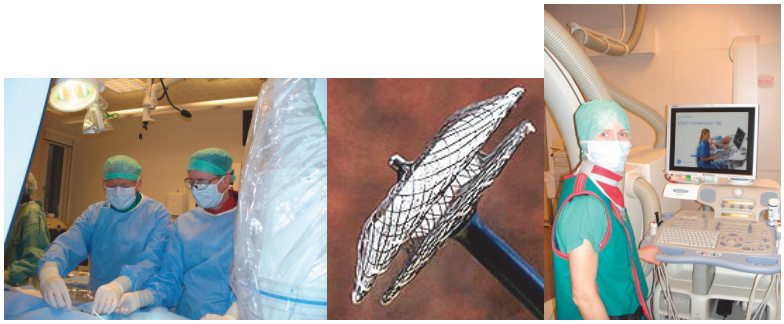

Figure 7: The picture to the left and right is from the cath-lab in Rikshospitalet during inclusion of patients. The picture in the middle shows an Amplazer device which closes the defect in the atrial septum.

In study 4 extra image acquisitions with the research scanner (SonixMDP ultrasound scanner) were done in addition to scanning with the Vingmed Vivid E9 (GE Vingmed, Horten, Norge) as part of an ongoing study called: “Flow speckle tracking for detailed visualization of flow patterns in neonates with congenital heart defects”.(64) Image acquisition with the SonixMDP scanner was done in

cooperation with engineer Solveig Fadnes after gaining an overview with the Vivid 9 scanner. Imaging with the SonixMDP scanner only took a few seconds, but the transfer of data after scanning took nearly 10 minutes with the setup used.

5.7.2 Data processing and analysis

Although offline analysis is not required in daily practice, CDI and BFI images in studies1-3 were prepared and analyzed in GcMat for comparison by observers. GcMat is a semiautomatic software (GcMat; GE Vingmed Ultrasound Horten, Norway), which runs on a MATLAB platform (The MathWorks, Inc., Natick, MA, USA). From the examinations in study 1-3, representative movie clips were chosen to be analyzed. When all patient data in each study was collected, a presentation program containing these selected movie clips was prepared and presented to independent observers for analysis. In all studies, the color image information presented was identical in both modalities (CDI and BFI), i.e. in the BFI movie clips speckle movement images were added to the ordinary color images. This means that the adjustments to the color information presented were always identical in paired CDI and BFI movie clips. The presented CDI and BFI images were not labelled in any way, nor were they numbered with respect to the patients. However, since there is a visible difference between the methods, the observers were able to recognize the flow method presented.

The observers were not otherwise involved in the project and had no information about the patients. Four observers evaluated the images in each study, and a total of nine different observers were involved in studies 1-3.

Study 1

Two different movie clips demonstrating ASD flow from the subcostal view were prepared for CDI and BFI. In one movie clip, the color images were optimized for best possible visualization of the flow through the ASD. In a second movie clip, the amount of color-gain was slightly increased to simulate the color blooming artefact which may arise in CDI. This was introduced in order to evaluate the potential of BFI when CDI images are suboptimal.

The echocardiograms were independently reviewed by four observers: Two pediatric cardiologists, one adult cardiologist, and one physician with ultrasound experience from research. The two pediatric cardiologists had no previous experience with BFI, but were introduced to the concept prior to the evaluation. The other observers were familiar with the technique from vascular applications. The images from the two modalities were presented to the observers in random order.

The observers were then asked to range from 0-100 on a visual analogue scale (VAS) how certain they were that there was blood flow across the atrial septum.

The observers were also asked to rank the general quality of the images on a visual analogue scale from 0-100, where 100 was the best possible image quality. They were asked to rank the general ultrasound quality for each clip, and the presentation of the anatomy.

Study 2

Movie clips with BFI and CDI of the pulmonary veins from the suprasternal short axis view and one additional view were presented in random order to four independent observers (pediatric cardiologist/adult cardiologists) for evaluation. The same movie clips were also presented with slightly increased color gain (color blooming artifacts) in both modalities. All observers were experienced echocardiographers without previous experience with BFI. They were introduced to the method through a short presentation prior to the evaluation. The observers evaluated the quality of the diagnostic imaging using a visual analogue scale (VAS), with score 0% (worst) to 100% (best).

They were asked 3 questions:

1. Clinical: On a scale from 0-100%, how certain are you that there are normal pulmonary venous connections? (90% certainty means 10% chance of anomalous venous connections) Figure 8 is an example from the presentation program.

Figure 8: Illustration of the presentation program for observers

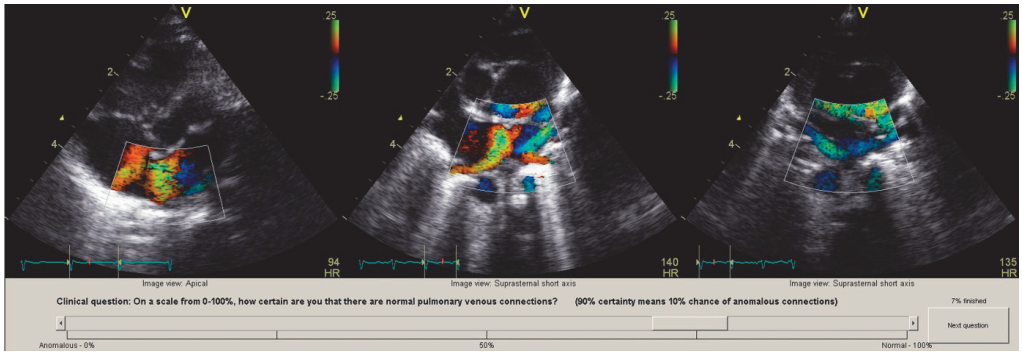

Figure 8: An example from the screen in the presentation program demonstrated to observers. The percentage marker could be moved to the left and to the right with 50% as starting position in the program. After choosing percentage on one screen, the observer clicked on next question and the percentage chosen was stored.

2. Technical: On a scale from 0-100%, how well can you determine the direction of flow in the pulmonary veins?

3. General: Please rank the general quality of the ultrasound images for the assessment of pulmonary veins with complete evaluation including image view, image quality, color blooming, flow direction. A 100% score on the VAS scale corresponds to best possible image quality (“good”), 50% corresponds to satisfactory image quality (”fair”) and 0% corresponds to ”poor” image quality.

Study 3

ASD sizing: Four observers were asked to measure the ASD size in the presented BFI and CDI images. If there was more than one ASD present in one movie clip, they were asked to measure the largest defect.

The process of measurements of the BFI and CDI movie clips is described in Figure 9: In each patient, a screen with two movie clips showing the ASD in the two widest planes (Clip 1 and Clip 2) was presented with BFI. The same BFI screen was repeated again later during the measurement process. Identical screens showing the ASD visualized with CDI from the same patient were presented in the same manner. This means that every observer made eight ASD measurements for each patient (four measurements with BFI and four measurements with CDI). The BFI and CDI screens and replications were presented to the observers in a random order.

Figure 9: Illustration of process of ASD – measurements by observers

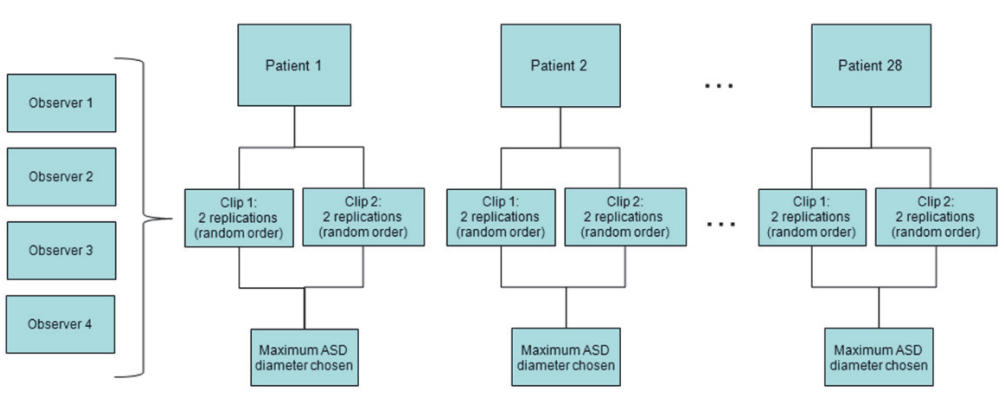

Figure 9: Reproduced from paper 3 with permission from Jon Wiley and Sons.

To reflect the clinical reality, we chose the maximum ASD-diameter measured with BFI (BFImax, later referred to as "BFI" only) in each observer for comparison with BSD- and CDI-measurements.

The four observers in study 3 were experienced echocardiographers (consultant cardiologists) without previous experience with BFI. They were given a short introduction to the BFI method prior to the evaluation. Since the observer job in this study was quite comprehensive, they were also co-authors in the study and contributed to the final evaluation of the manuscript.

Pulmonary veins: The pulmonary veins were evaluated during the examination by an echo technician in cooperation with a pediatric cardiologist using BFI. The results were recorded as one of the following: Normal pulmonary veins, one anomalous pulmonary vein, two anomalous pulmonary veins, or pulmonary vein stenosis. The BFI investigations were finished and documented before the pulmonary veins eventually were examined by routine angiography by the interventionist.

Image analysis was done in a custom software package (GcMat), while statistical analysis was done using IBM SPSS version 19 and package lme4 of the software R version 2.15

Study 4

Figure 10 schematically shows the data acquisition and post processing in this study. A separate acquisition setup was used for B-mode and flow imaging to ensure a sufficient image quality for both modalities. The channel data is acquired and beam forming is done offline. The plane wave data is clutter filtered (a high pass clutter filter was applied to separate the blood signal from the strong tissue signal) before blood velocity estimation is done using the autocorrelation approach and speckle tracking. One transmit beam covered a region equal to the transducer width and full parallel receive beamforming was utilized. To achieve high quality B-mode images it is beneficial to interleave two different acquisition setups in a duplex modality, one for color-Doppler and one for B-mode. The duplex modality frame rate will then be given by the time to acquire both B-mode and color-Doppler images. When using focused B-mode images and plane wave color-Doppler images, the total acquisition time will be dominated by the B-mode image which limits the frame rate. Still we were able to achieve full field-of-view color-Doppler and high quality B-mode imaging at 107 fps.

The research scanner is able to store and process the channel radio frequency data from all the channels in the transducer (128 channels). When the channel data is available, one can beamform any number of receive lines simultaneously in the software as illustrated in figure 10.

Figure 10: Flow speckle tracking acquisition and post processing

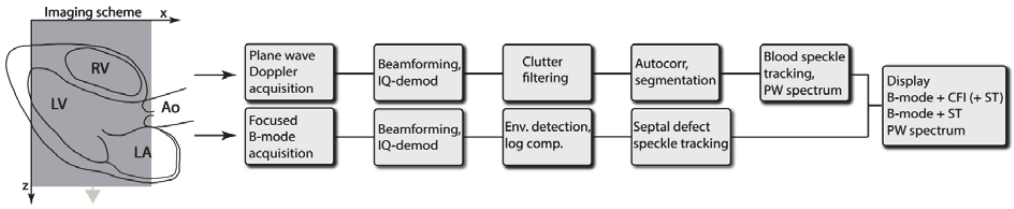

Figure 10: Reproduced from paper 4.

With this acquisition scheme, high frame rate flow images are aquired where color doppler imaging, blood flow speckle tracking and PW-Doppler estimation can be performed using the same dataset. An in vitro flow phantom was used to test the acquisition setup and speckle tracking algoritm. For further details regarding the method, see the full description in the technical article, paper 4.

5.9 Statistical methods

5.8.1 Statistics - Study 1

The null hypothesis was that there is no difference between BFI and CDI in the visualization of interatrial blood flow, versus the alternative hypothesis that BFI improves the ASD visualization.

The degree of certainty (VAS scale 0-100) was compared within each observer using the exact two tailed Wilcoxon signed-rank test for paired samples (65). Ratings of the optimal and suboptimal cineloops were analyzed separately. The difference between CDI and BFI ratings were considered significant when the p-value were less than 0.05. The statistical analysis and plotting were done in the numerical MATLAB software with the statistics toolbox (The MathWorks Inc., Natick, USA).

5.8.2 Sample size in study 2 and 3

We used the feasibility study (study 1) as background for choosing sample size in study 2 and 3. In study 1, an absolute difference between the methods of 19% on the VAS scale was observed, a difference considered to be of clinical interest. With an observed standard deviation of 31% (absolute), a two-sided paired-samples t-test requires 24 observations to have a power of 80% at the 5%

significance level (65). This number was rounded upwards to accommodate deviations from normality and the use of a non-parametric test.

5.8.3 Statistics - Study 2

The null hypothesis in this study corresponds to no difference between BFI and CDI in the visualization of flow in the pulmonary veins, and the alternative hypothesis that BFI improves the visualization.

The methods (BFI vs. CDI) were compared within each observer using Wilcoxon's exact signed-rank test for paired samples (65). The variability of this evaluation of quality between observers and methods was investigated using Bartlett's test of homogeneity of variance (66). Ratings of the optimal cine loops and the cine loops with too much color gain were analyzed separately. P-values less than 0.05 were considered to be statistically significant. The statistical analysis and plotting was done in the numerical MATLAB software with the statistics toolbox (The MathWorks Inc., Natick, USA), and the statistical software R (67).

5.8.4 Statistics - Study 3

ASD-sizing: The mean difference between the BFI and BSD measurements and the BFI and CDI measurements were analyzed using a paired samples t-test. Furthermore, the BFI- and BSD-measurements and the BFI- and CDI-measurements were plotted against the other. Finally, agreement between the BFI and BSD measurements and the BFI and CDI measurement were evaluated using Bland-Altman plots, in which the difference between BSD and BFI measurements and BFI and CDI measurements were plotted against their respective means (68).

To assess repeatability, a linear mixed effects model with BFI as the outcome variable was employed in a variance components model. We treated observers and patients as crossed random factors (Figure 9), whose net effects are assumed to be zero. The residual error of this model yields a measure of repeatability, i.e. the remaining variation when different observers do measure identical movie clips in the same patient. Estimation was done with restricted maximum likelihood using the *lmer* command of R version 2.15 (67).

Pulmonary veins: By visualizing the pulmonary veins with BFI and compare with the reference method angiography, one can calculate sensitivity and specificity for the new method. Point estimates with exact 95 % confidence intervals (CI) were calculated based on the binomial distribution.

5.9 Ethics

Written informed consent for participation was obtained from children older than 12 years of age and the parents of all study subjects. All the sub-studies are approved by the Norwegian regional Committee for medical and health research ethics (REK, Midt-Norge). Patient safety measurements were within the guidelines from the US Food and Drug Administration (FDA). All the clinical studies was performed according to the national and international laws, regulations and conventions for research on humans and patients.

6 SUMMARY OF RESULTS

6.1 Results - Study 1

All four observers ranked BFI high. When the presented color images were technically optimized, two observers ranked BFI as significantly better than CDI in the visualization of interatrial blood flow (figure 11, left). The two other observers also ranked CDI very high (near 100 percent), with the result that no significant difference could be measured. When the images had slightly increased color gain, three of the observers rated BFI as being significantly better (figure 11, right). The physician with ultrasound research experience (observer number 4) regarded the two methods as equal in both scenarios. All ASDs visualized with CDI were confirmed using BFI. In one patient the recordings with BFI revealed two ASDs and not one as first suspected in the prior CDI recording.

Figure 11: Dot-plots – Transthoracic ASD visualization

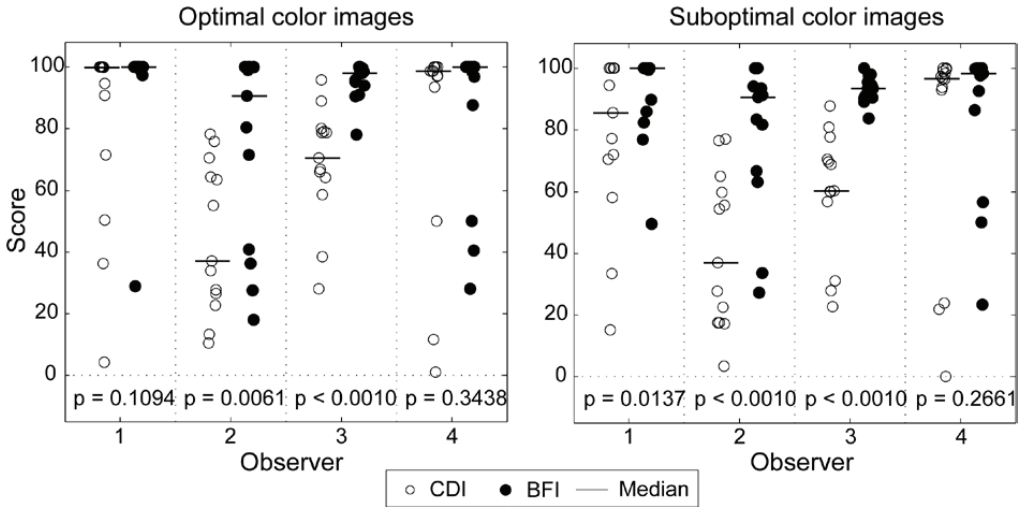

Figure 11: *The observers were asked to range from 0-100 on a VAS how certain they were of interatrial flow. The dot plots show the observers assessments of CDI versus BFI when the color images were optimal to the left and suboptimal (i.e. slightly increased color gain) to the right.*

Examples of ASD flow imaging with BFI and CDI in two patients are shown in figure 12.

Figure 12: Illustration of transthoracic ASD imaging with CDI and BFI side-by side

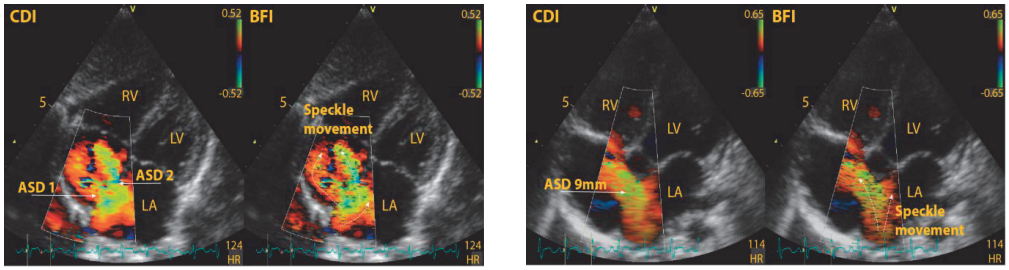

Figure 12: Images to the left: CDI and BFI images of two separate ASDs with flow jets in different directions

Images to the right: CDI and BFI images of one 9 mm ASD. ASD = atrial septal defect; CDI = color doppler imaging; BFI = blood flow imaging; LA = left atrium; LV = left ventricle; RV = right ventricle.

6.2 Results - Study 2

Blood Flow Imaging was consistently ranked as better than Color Doppler Imaging in the visualization of the pulmonary veins (figure 13). Median differences on the VAS scale in favor of Blood Flow Imaging among the observers regarding pulmonary venous connections ranged from 0-8%, direction of flow ranged from 6-48% and overall pulmonary vein imaging quality ranged from 4-34%. (All p-values<0.01).

Figure 13: Dot-plots – Pulmonary vein imaging in neonates

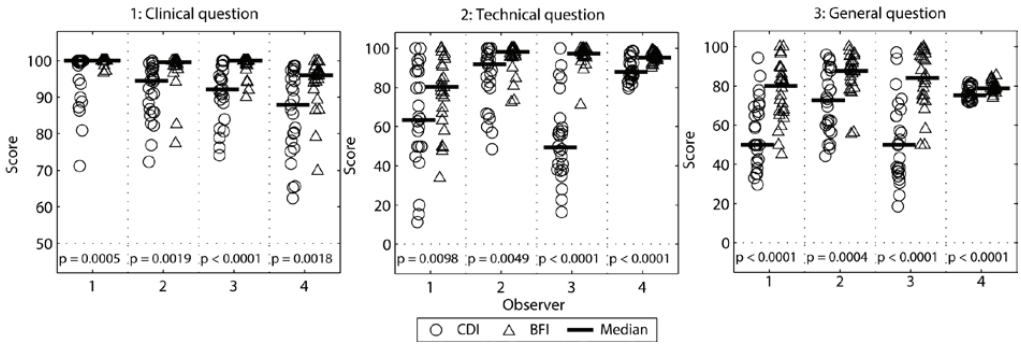

The variance of assessment differed significantly among the observers and methods (p<0,001). The difference between the methods was not altered when the color gain was increased (i.e. color blooming artifacts created).

Examples of BFI visualization of pulmonary veins in two patients from the study are shown in figure 14.

Figure 14: Illustration of pulmonary vein BFI in neonates

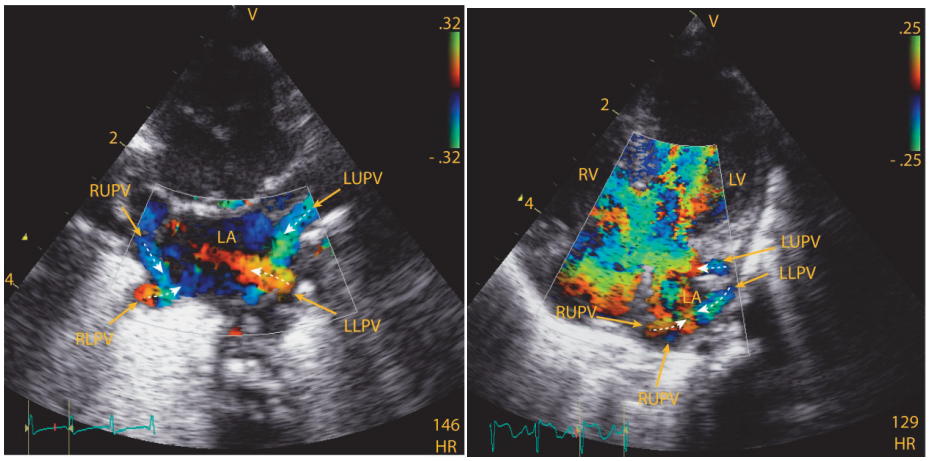

Figure 14: BFI in the visualization of the pulmonary veins: Suprasternal short axis view to the left and the apical view to the right. The image to the right is from a neonate with an atriovetricular septal defect.

LUPV= left upper pulmonary vein; LLPV= left lower pulmonary vein; RUPV= right upper pulmonary vein; RLPV= right lower pulmonary vein.; LA = left atrium; LV = left ventricle; RV = right ventricle.

6.3 Results - Study 3

ASD-sizing

The mean maximum diameter measured by BSD was 15.9 mm (±SD 3.0 mm), and the mean maximum diameter measured by BFI was 12.1 mm (±SD 2.4 mm); yielding a mean difference between the measurements of 3.8 mm (±SD 2.2 mm), with a 95% confidence interval from 3.4 to 4.2 mm. The 95% limits of agreement extended from -0.7 to 8.3 mm with no obvious trend in the data.

Figure 15 shows the scatter plot of the BSD measurements vs. the BFI ASD diameter measurements to the left and the Bland-Altman plot with 95% limits of agreement for the difference between the BSD and BFI measurements to the right.

Figure 15: ASD-sizing with BFI and BSD

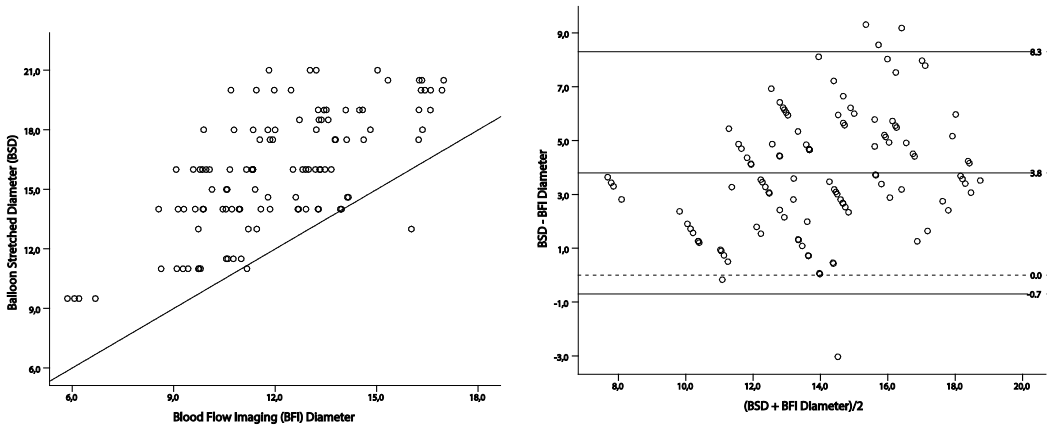

Figure 15: Two methods of measuring atrial septal defect (ASD) size, in mm: The maximum ASD diameter measured by Blood Flow Imaging (BFI) and Balloon stretched diameter (BSD) in 28 patients measured by 4 observers. The Bland-Altman plot to the right shows differences against the mean and 95% limits of agreement. The figure demonstrates that almost all BSD measurements were larger than BFI measurements.

The corresponding ASD diameter measured by CDI was 11.8 mm (±SD 2.5 mm); yielding a mean difference between the CDI- and BFI- measurements of -0.3 mm (±SD 1.3 mm) with a 95% confidence interval from -0.6 to -0.1 mm. The 95% limits of agreement extended from -3.0 to 2.3 with no obvious trend in the data.

Figure 16 shows the scatter plot of the CDI measurements vs. the corresponding BFI-measurements to the left and the Bland-Altman plot with 95% limits of agreement for the difference between the BFI and CDI measurements to the right. There were two outliers labelled A and B in Figure 16. The outlier A measurements were CDI 8.6 mm, BFI 13.3 mm and corresponding BSD 16 mm. The outlier B measurements were CDI 10.4 mm, BFI 16.3 and corresponding BSD 20.5 mm. Since we couldn't identify obvious errors regarding these outliers, we kept them in the material.

Figure 16: ASD-sizing with BFI and CDI

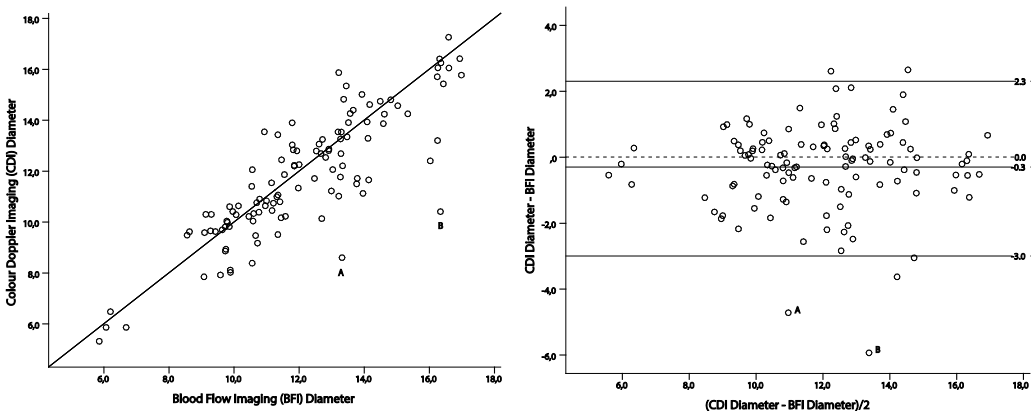

Figure 16: Two methods of measuring atrial septal defect (ASD) size, in mm: The maximum ASD diameter measured by Blood Flow Imaging (BFI) and the paired Color Doppler Imaging (CDI) measurements in 28 patients measured by 4 observers. The Bland-Altman plot to the right shows differences against the mean and 95% limits of agreement. There were two outliers labelled A and B. The corresponding BSD-measurements for A and B were 16 mm and 20.5 mm, respectively.

Figure 17 demonstrates ASD flow-visualization with BFI from the transesophageal examination (6T probe) from patient no 5, who was 16 years old with height 175 cm and weight 67.6 kg. He had one ASD and a measured BSD of 18 mm.

Figure 17: BFI visualizing an ASD in transesophageal echocardiography

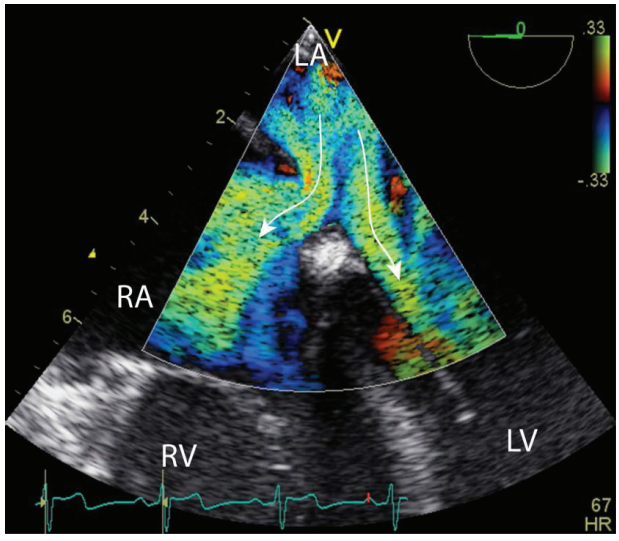

Figure 17: Transesophageal long-axis-view of the atrial septum: Blood Flow Imaging in the visualization of two atrial septal defects (ASD), the left atrium (LA) and the right atrium (RA). The arrows show the direction of the speckle pattern.

The repeatability of the BFI measurements

The linear mixed effects model (Illustrated in figure 9) yielded the following standard deviation estimates; patient 2.1 mm, observer 0.4 mm and residual (i.e. the movie clips presented) 1.2 mm. Given a mean BFI-value of 12.1 mm, this corresponds to coefficients of variation (CV) of 18%, 4% and 9.6% respectively. The latter may be taken as a measure of repeatability, the remaining variation when different observers perform measurements on identical movie clips from the same patient.

The pulmonary veins

Pulmonary angiography demonstrated normal pulmonary connections for all pulmonary veins in the 28 patients. Visualization of the upper left and the upper and lower right pulmonary veins using transesophageal examination with BFI was successful in all patients. The site of drainage of the left lower pulmonary vein was identified in 27 of the 28 patients studied. In one patient the left lower pulmonary vein was difficult to visualize using BFI and CDI in TEE. Pulmonary angiography visualized the lower left pulmonary artery in this patient, and the drainage was normal – as were the other pulmonary veins in this patient. Pulmonary angiography corresponded with the BFI visualization of the pulmonary vein connections in all patients except in this one case. This leads to a sensitivity of BFI in detecting the correct entry of the pulmonary veins of 0.96 (95% CI: 0.82-1.0)

An example of transoesophageal BFI visualization of the left sided pulmonary veins is shown in Figure 18. This image is from patient 23, who was 4 years and three months old, 102 cm high and 14.5 kg. We used the 9T-probe for this examination.

Figure 18: BFI visualizing the left upper pulmonary vein with transoesohageal echocardiography

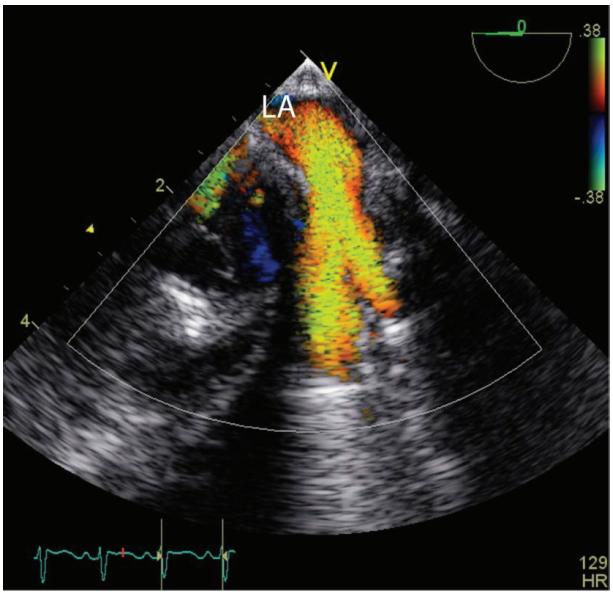

Figure 19: Blood flow Imaging in the visualization of the left upper pulmonary vein entering the left atrium (LA).

6.4 Results - Study 4

In vitro flow phantom tube

The speckle tracking velocity estimate for the 26 independent measurements had a low standard deviation (1-3 cm/s) and were in good agreement with the reference velocities, demonstrated in figure 19. For a 1 mm x 1 mm area in the middle of the tube, the mean axial velocity was 0.5 m/s ± 0.02 m/s for CDI (termed autocorrelation method in the article) and 0.51 ± 0.01 m/s for speckle tracking. The mean lateral velocity was 0.88 ± 0.03 m/s for speckle tracking. The resulting absolute velocity was 0.99 ± 0.04 m/s for the angle corrected CDI (autocorrelation method, ACM) and 1.02 ± 0.02 m/s for speckle tracking. The reference velocity in the same region was 0.98 m/s.

Figure 19: Stationary flow in an in vitro flow phantom

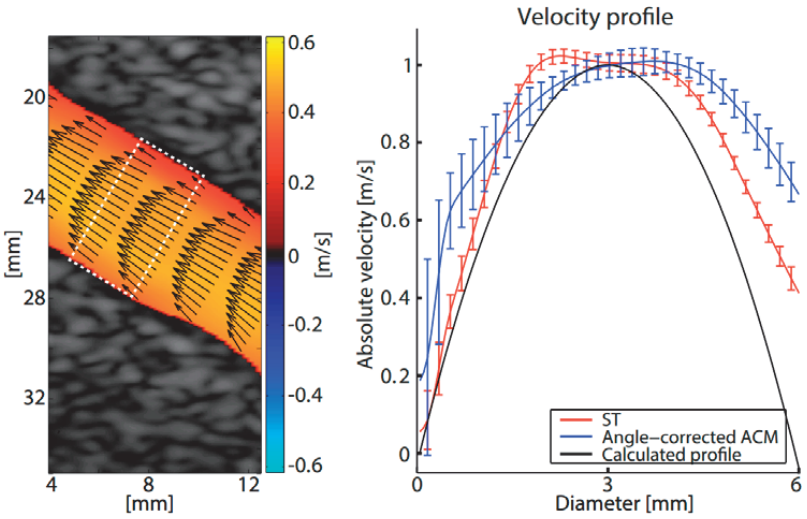

Figure 19: Reproduced from paper 4, with permission from Elsevier. Stationary flow in an in vitro straight tube phantom with a beam-to-flow angle of 60 degrees. To the left, a color flow image with speckle tracking estimates overlaid as arrows. To the right, the mean speckle tracing and angle corrected autocorrelation method (ACM) velocity profiles with standard deviations from 26 measurements are compared with the calculated reference velocity profile.

In vivo (two neonates)

In vivo results demonstrate that speckle tracking may provide flow velocity estimates in a VSD and ASD throughout the cardiac cycle in two neonates. This is demonstrated in figure 20 and 21 where the corresponding CDI image is presented to the left.

Figure 20: Color Doppler and Flow speckle tracing in a VSD

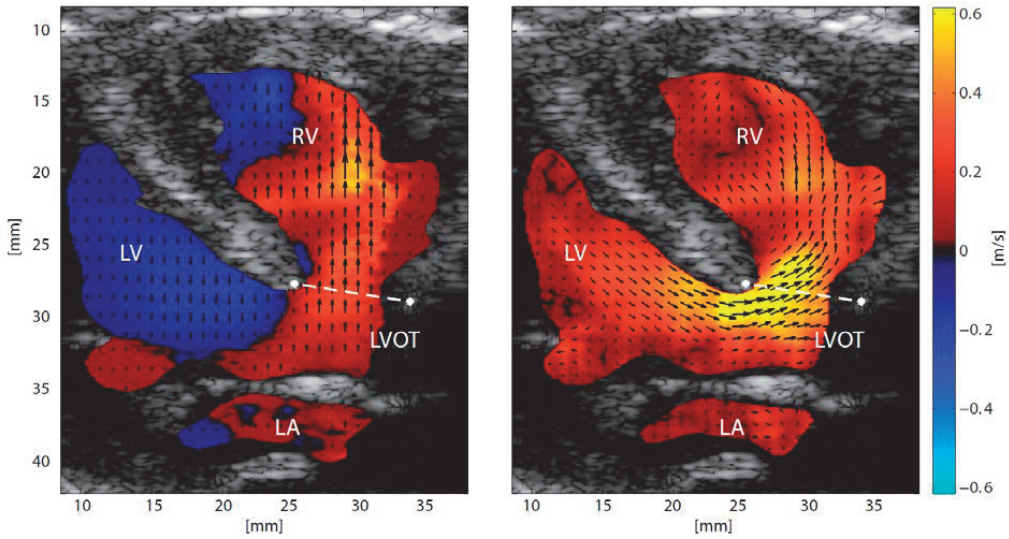

Figure 20: Reproduced from paper 4 with permission from Elsevier. The superimposed arrows in the color flow image to the left underline the one-dimensional velocity information acquired from the autocorrelation estimates. The colors in the image to the right represent the absolute velocity found from speckle tracking. The arrows represent the direction and magnitude of the speckle tracking estimates.

A vortex formation in the right ventricle due to the VSD shunt flow was visible with the 2-D velocity vector maps, but not in the color Doppler images.

Figure 21: Color Doppler and flow speckle tracking in an ASD

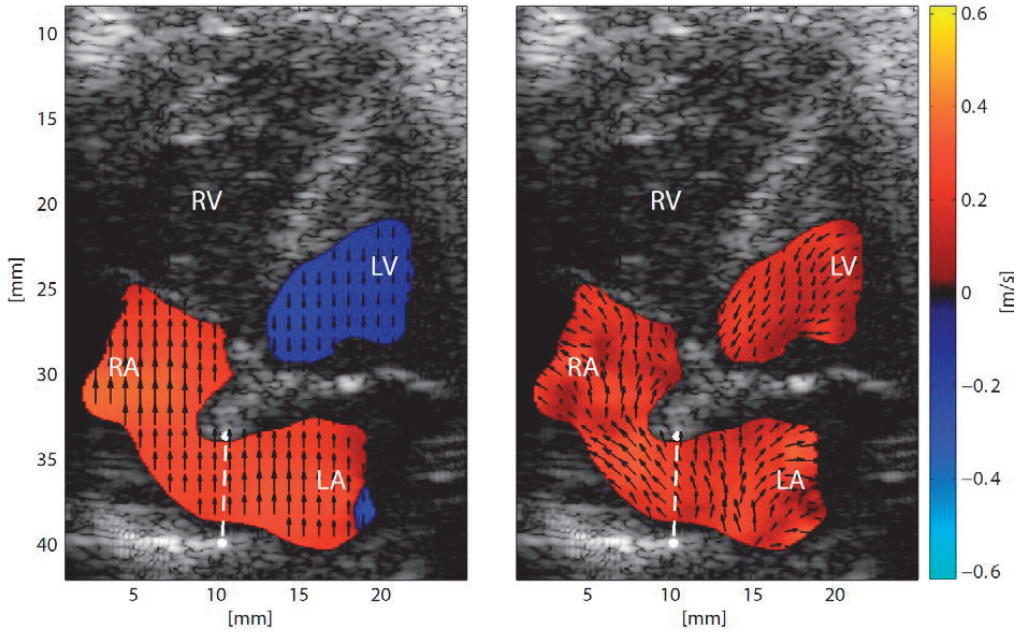

Figure 21: Reproduced from paper 4 with permission from Elsevier. The superimposed arrows in the color flow image to the left underline the one-dimensional velocity information acquired from the autocorrelation estimates. The colors in the image to the right represent the absolute velocity found from speckle tracking. The arrows represent the direction and magnitude of the speckle tracking estimates.

Both speckle tracking and color Doppler (autocorrelation velocity estimates) were validated with retrospective PW Doppler. The axial velocity estimates from speckle tracking agreed well with the PW spectrum and color Doppler estimates. The absolute velocity profiles for the speckle tracking and angle corrected autocorrelation estimates were reasonable and indicate that tracking works both in the axial and lateral direction. Please see the technical paper (paper 4) for further details.

6.5 Supporting online information

As the flow modalities are best appreciated by watching movie clips, such movie clips are available on the published articles journals webpages.

Study 2: http://onlinelibrary.wiley.com/doi/10.1111/j.1540-8175.2010.01206.x/suppinfo

Study 3: http://onlinelibrary.wiley.com/doi/10.1111/echo.12610/suppinfo

Study 4: http://www.sciencedirect.com/science/article/pii/S0301562914002154

7 DISCUSSION

With the aim of improving blood flow visualization in pediatric cardiology, we studied the novel flow imaging techniques of blood flow imaging and flow speckle tracking in this work. We performed three studies with blood flow imaging and one technical study with flow speckle tracing with focus on imaging of septal defects and pulmonary veins. A varied assortment of probes was tested: Phased array probes (7S, 4S), transesopageal probes (9T and 6T) and also a linear probe (4.9MHz). In addition we investigated a wide range of patient sizes, including premature and term neonates (study 2 and 4), children (study 1 and 3) and adult sized patients (study 3).

We found that BFI may improve the visualization of interatrial blood flow in children and the pulmonary veins in neonates (62, 63). We also compared transesophageal BFI to the established references or "gold standards" for ASD-sizing and pulmonary vein imaging (69). We found that transesophageal echocardiography with Blood Flow Imaging of the pulmonary veins agreed well with pulmonary angiography. BFI had lower estimates for ASD-size than BSD as expected, but with acceptable 95% limits of agreement. The repeatability of the BFI-measurements was close to the inherent measurement error of the ultrasound measurement itself. Study 3 represented the final step in the evaluation of BFI used in the imaging of atrial septal defects and pulmonary veins in children. If BFI is available on the scanner, the method may offer a complete assessment of ASD and has the potential to reduce radiation exposure time during ASD-closure.

During the project period, the engineers managed to take the blood flow imaging method one step further, and flow speckle tracking was introduced. Here the speckle pattern is not only detectable for our eyes as in BFI, but also for the computer. This allows velocities and flow direction to be measured. The technical article (study 4) demonstrates this technological development using a research ultrasound scanner. We found that flow speckle tracking may provide flow velocity estimates in a VSD and an ASD in two neonates. A vortex formation in the right ventricle due to the VSD shunt flow was visible with flow speckle tracking, but not in the color Doppler images.

7.1 Comparison between BFI and other modalities

7.1.1 ASD visualisation and sizing

Currently, echocardiography is the first line imaging modality for the diagnosis and follow up of

pediatric patients with ASDs. A detailed anatomical study is necessary to determine the defect size, morphology, the relationship with the surrounding structures and the hemodynamic consequences. The examination of blood flow direction through the ASD is also of high interest: Firstly to detect reversed shunting in pulmonary hypertension, and secondly to be watchful for other causes of reversed shunting in ASD, for instance pulmonary stenosis, tricuspid valve disease or the superior or inferior vena cava entering the left atrium.

Doppler-based modalities such as CDI are only able to measure the axial direction of flow, i.e. flow towards or away from the transducer surface. The BFI modality adds the speckle movement of blood to the Doppler information available with CDI, and is thereby able to visualize flow in any direction of the image plane. Thus, a more detailed and intuitive display of the flow conditions requiring less interpretation than CDI images may be provided. For example, interatrial flow is not only axial, and BFI may therefore provide more detailed information of interatrial blood flow than CDI. In one patient in study 1, BFI imaging revealed two ASDs, and not one defect as first suspected in a prior CDI examination. This is important information when planning catheter based device closure.

When presented with suboptimal color images (i.e. when color blooming artifacts were created), the rating differences between BFI and CDI were enlarged in favor of BFI for three of four observers in study 1. This finding indicates that BFI may be particularly useful when color image artefacts are present, or when too much color gain has been applied as can sometimes be an issue in a busy clinical practice. However, in pulmonary vein imaging in study 2, we found no difference between the optimal and suboptimal gain setting when comparing CDI and BFI.

The inclusion criteria for study 1 was ASD`s already visualized with CDI, and therefore angle was not an important factor in terms of ASD-detection. But angle may be a problem, especially in other views than the subcostal. The main reason that BFI may be advantageous over CDI in low pressure ASD-flow visualization is that interatrial blood flow may be shown in spite of non-axial flow and color blooming artifacts.

Since ASD flow may occur only during a limited portion of the cardiac cycle, CDI may not be able to visualize shunt flow because the frame rate is too low. Further, due to the low frame rate, the right-to-left component of the atrial shunt is usually not detectable with CDI (70). As BFI provides an increased frame rate of flow information, it may reduce this problem. Substantially higher frame rates than the BFI tested in study 1-3 are achieved with the plane wave flow speckle tracking technique

described in study 4. This increased amount of flow information is especially important in the imaging of neonates due to their high heart rates.

TEE is superior to TTE in detecting secundum ASD, sinus venosus defects and associated anomalous pulmonary venous return in adults (43). In children, routine transthoracic studies are generally adequate for ASD diagnosis, but TEE may be used in patients with poor image quality. TEE is the preferred imaging modality during guidance of catheter-based treatments of atrial septal defects in children (50).

High-quality imaging of atrial septal defect (ASD) size and morphology before transcatheter closure is essential for a successful outcome, and there has recently been much interest in advances in technology in order to improve visualization of the complex septal anatomy (71-76).
There has been less focus on further improving the flow visualization, even though this is important in identifying the number and size of ASDs, the direction of blood flow through the defects, and to differentiate dropouts in the region of the fossa ovalis from an ASD. Finally, since partial anomalous pulmonary venous connection is associated with ASD (77), thorough flow mapping of the pulmonary veins is essential (78).

Traditionally, transcatheter ASD-closure has included balloon sizing, fluoroscopy and pulmonary angiography. The radiation exposure from cardiac catheterization is of concern both to patients and operators (79), and should be limited to lowest possible values. Furthermore contrast agents may have side effects (80), and should be restricted whenever possible. The balloon sizing procedure has potential risks (81), and transcatheter closure of atrial septal defects following less invasive sizing techniques has been advocated (82-84).

ASD-measurements by Color Doppler Imaging (CDI) correlate with the balloon stretch diameter (54), and transcatheter ASD closure guided by the maximal color flow diameter has recently been shown to be feasible and safe (82). However, CDI has limitations that include angle dependence, aliasing and a frame rate which is considerably less than that of gray scale imaging (11). The reliability of color flow in predicting size is also limited by variability in gain settings. The additional speckle pattern in BFI has the potential to improve the ASD edge detection. This may diminish the sources of error in determining ASD size. Even though study 3 demonstrated quite equal overall results in CDI and BFI-measurements, the CDI measurements had two outliers with fairly large discrepancy compared to the BFI and BSD measurements. This would have been clinically significant

if the amplatzer device was chosen based on this measurement and no additional BSD-measurement was performed.

In study 3, BFI had lower estimates for ASD-size than BSD as expected, but with acceptable 95% limits of agreement. The mean maximum diameter measured by BFI was 3.8 mm less than the mean of BSD measurements. The paired CDI-measurement was 0.3 mm less than the BFI-measurement. Tzifa et al demonstrated similar results. They found that the mean maximal diameter measured with CDI was 4.6 mm and 3.3 mm less than the BSD-measurements in the prospective and retrospective groups respectively (82). The difference between the BFI and BSD measurements can be explained by the fact that BSD also provides information of physical stretch that cannot be predicted by echocardiography. The relationship between the maximal BFI-diameter measured in 2D echo and BSD is also influenced by the shape of the ASD (85).

The true ASD size was unknown in study 3, but we chose to compare the BFI measurements with the BSD, since this method still is regarded as the reference for measuring ASD maximal diameter to select the appropriate size of the device before closure. However, balloon sizing is not considered necessary by some authors (82-84), and BSD is consequently no longer performed in many centers that use Amplatzer devices to close ASDs. Balloon sizing may oversize an ASD (83), which may increase the risk of erosion. The stop flow technique was proposed to diminish this problem (86). Other potential disadvantages of balloon sizing are bradycardia, hypotension and enlargement of the defect. If there are multiple defects and a floppy septum, echocardiography may be better than BSD in the estimation of size (46).

The repeatability of the BFI-measurements in study 3 was consistent both between the observers and within each observer. Other studies measuring ASD-diameter with color flow diameter did not investigate the repeatability of the CDI- measurements (53, 82). It is important to be aware that some of the variability between measurements in different studies using two-dimensional imaging may be due to differences attained by different observers (87).

Improved echocardiographic imaging before and during transcatheter ASD-closure may reduce radiation exposure and possibly also the need for balloon sizing. We believe that BFI may be a suitable supplement to CDI in the complete echocardiographic ASD evaluation.

The new real time three-dimensional transesophageal echocardiography for guidance of percutaneous atrial septal defect closure seems promising, but there is still limited experience in

patients < 60 kg (71). To define the plane with the maximum ASD diameter may be easier using 3D TEE than 2D TEE (85). Even though 3D may be best for visualization of anatomy, this is not the case for flow, due to low frame rate and resolution. Another limitation of the current 3D TEE systems is dropout in the fossa ovale region (72). This dropout may be minimized by combining with 2D flow techniques. The best method for selecting an optimal device size may be to consider different measurements with different methods (85).

Echocardiography is usually sufficient in the diagnosis of a secundum ASD in children. However, if there is doubt regarding the anatomy, as discordance between the ASD size and the magnitude of the right ventricular enlargement, this should raise suspicion of an additional source of shunt, such as a sinus venosus defect or an anomalous pulmonary vein. Cardiovascular magnetic resonance (CMR) may then be a valuable supplement in the ASD evaluation (88). CMR may also identify an ASD or partial anomalous pulmonary venous connections in adults with right sided enlargement (89). In addition, quantification of shunt s with CMR is favorable compared to other imaging techniques, and should be considered in selected patients.(89)

7.1.2 Pulmonary vein imaging

Echocardiography is the most important imaging modality for visualizing the pulmonary veins (55, 56, 77, 90), but this is still a challenging area in the assessment of suspected congenital heart disease in the neonate. The pulmonary veins are among the top anatomic segments involved in diagnostic errors in pediatric echocardiography (7), and difficulties in the visualization of anomalous pulmonary return (57, 91, 92), pulmonary vein stenosis and also normally connecting pulmonary veins has been reported (59, 93, 94). We chose to look at neonates especially in study 2, since diagnostic errors in pediatric echocardiography occur more frequently in this low weight group (7, 9).

Cardiac catheterization with angiography, magnetic resonance angiography and computed tomography angiography are alternative diagnostic modalities in the evaluation of anomalies in the pulmonary veins (56). Seale at al looked at diagnostic imaging for total anomalous pulmonary venous connections in United Kingdom, Ireland and Sweden. They found that only 30% needed no further imaging after echocardiography (95). The same group found that 26% of the pulmonary vein stenoses in their population was not demonstrated by echocardiography and was subsequently diagnosed either on angiography or surgery (96). Because of the challenges in echo imaging of pulmonary vein anomalies, both cardiac magnetic resonance and computed tomography are increasingly being used

in the diagnosis and follow up of neonates and children (97). If the pulmonary veins are incompletely assessed with echocardiography, CMR is the first choice investigation if not obstructed total anomalous pulmonary veins are suspected. In this case an urgent definition of the pulmonary veins is needed and a short duration CT without sedation is preferred (97). However, CMR requires sedation in some age groups and is a resource demanding technique. CMR is therefore first of all is justified in the pediatric patients in whom clinical or echocardiographic data is insufficient for decision making (98). Then it supplements echocardiography and provides a non-invasive alternative to x-ray angiography and also avoids the ionizing radiation exposure from computed tomography (99). A cardiac CT leads to a radiation exposure of 1-2 milliSievert (equivalent to 100 chest x-rays), which limit the value in pediatric cardiology. Further improvement of the portable, safe, non-invasive and less resource demanding ultrasound technique is therefore still essential. However, the assessment of congenital heart disease must sometimes involve a variety of modalities used in a complementary fashion to ensure complete visualization of the cardiac anomalies, whilst minimizing harm (98).

The low velocities in the pulmonary veins are best recorded when the flow is near parallel to the sound beam. However, in the suprasternal short axis view where all the pulmonary veins may be visualized, the ultrasound beam is not parallel to the pulmonary blood flow, and the flow may be difficult to visualize and interpret using CDI. Study 2 confirms that BFI is beneficial in this setting.

To confirm normal pulmonary connections may be challenging in the critically ill neonate with pulmonary hypertension and constriction of the pulmonary veins (94). In study 2, four patients were critically ill on inclusion. Improved diagnostic imaging in these patients is valuable, because pulmonary vein anomalies may clinically mimic persistent pulmonary hypertension of the newborn.

Power Doppler Imaging has been shown to be superior to Color Doppler Imaging in the visualization of fetal pulmonary veins (100). Like BFI, Power Doppler Imaging is angle independent and without velocity aliasing. However, Power Doppler Imaging gives no information on the direction of flow, which is a disadvantage compared to BFI.

In study 3, we also compared visualization of the pulmonary veins using BFI with the traditional reference method, pulmonary angiography. Pulmonary angiography corresponded with the BFI visualization of the pulmonary veins in all patients except one patient. In that patient the left lower pulmonary vein was difficult to visualize using TEE with BFI. However, this pulmonary vein had been previously visualized using transthoracic echocardiography with BFI the day before the procedure.

Even though TEE images are usually of better quality than TTE images, the limited imaging windows and planes in TEE do restrict both imaging and alignment for Doppler velocity recording. Furthermore, the pulmonary veins may be too close to the TEE probe for proper imaging or flow evaluation (101). TTE and TEE together will usually be sufficient to map the pulmonary veins, and routine pulmonary angiography during ASD-closure has now been abandoned in the Department of Pediatric Medicine, Section for Pediatric Cardiology, Oslo University Hospital, Rikshospitalet, Norway.

7.2 Research methodology considerations

BFI is a qualitative, visual technology and this implies methodological challenges. To be able to compare BFI with standard CDI, we asked the observers to rate the methods on a visual analogue scale in study 1 and study 2. The observers had no access to the patient data and the cineloops were not labeled. However, it was still not possible to blind the observers with regard to which method was displayed, because there is an obvious visual difference between CDI and BFI. The variance of assessment differed among the observers. In study 2, they all consistently ranked BFI as better than CDI.

In study 3, we applied another design in order to test the method more quantitatively. Here we compared ASD-BFI measurements with the gold standard BSD and pulmonary vein angiography with the gold standard pulmonary vein angiography. In this way, testing was probably less biased. However, the multidirectional information provided by BFI was not assessed. Even though the angle independent technique BFI has theoretical advantages, this was not clearly demonstrated in the transesohageal study. This was probably due to a combination of the study design and the fact that in the assessment of ASD's by TEE, there is usually a reasonably parallel angle of Doppler interrogation. The same applies to pulmonary vein assessment by color Doppler when utilizing TEE.

By visualizing the pulmonary veins with BFI and CDI and later comparing with the reference method angiography, we planned to calculate both the sensitivity and specificity for the new method BFI and the conventional method CDI. However, no patients with pulmonary vein anomalies were found during the patient inclusion period at Rikshospitalet. Ideally we should have kept on including patents until we had a few patients with pulmonary vein anomalies.

7.3 Flow speckle tracking

There is a growing interest in understanding flow behavior inside the cardiac chambers. This is now possible thanks to new technology which can visualize and analyze complex flow patterns.(64, 102)

The pattern of blood flow in the developing heart has been proposed to play a significant role in cardiac morphogenesis (103-105), and intracardiac hemodynamics has been pointed out as a key epigenetic factor in embryonic cardiogenesis (106). A vortex flow is a circular or elliptical rotating mass of fluid spinning around. It is assumed that vortices play an important role in cardiac function (107, 108).

In study 4, vortex formations in the right ventricle due to the VSD shunt flow was visualized by flow speckle tracking, but not with color Doppler imaging, where only the axial velocity component is displayed. The shunt position tracking made it possible to generate spatial velocity profiles from the shunt throughout the cardiac cycle and to automatically find the peak velocity in the shunt for all frames. The speckle tracking estimates were validated towards PW Doppler and autocorrelation estimates in this work. The comparison was only performed as an initial validation of the axial speckle tracking. A general comparison of the accuracy needs a separate study.

Complex flow patterns such as left ventricular vortex flow have also been studied previously using MR phase contrast and contrast enhanced ultrasound (109, 110). Neither of these approaches is well suited in some age groups in pediatric cardiology. On the other hand, CMR has recently been applied using the “feed and sleep – technique” in term and preterm neonates. In this way the CMR can be performed without sedation or anesthesia in the first weeks of life (111, 112). However, the high heart rates in neonates and respiratory-motion artifacts because of the lack of breath-holding, may deteriorate the image quality. In addition, the scan time is usually longer than for echocardiography and the data is not displayed real-time (113). Ultrasound particle image velocimetry (echo-PIV) is able to map blood flow directions, streamlines and vortex flow (113), but used contrast agents not approved for the use in children in Norway.

8 LIMITATIONS

8.1 Materials

The number of study subjects in all sub-studies was relatively small. Consequently further studies are required to determine the clinical applicability of our findings. Ideally, patients should have been randomized to either CDI or BFI in the studies. However, such study design requires numerous patients and extensive inclusion time, which was not possible in this feasibility study. It would also be interesting to see if clinical endpoints improve in parallel with the introduction of new technology, but this also requires a high number of patients.

BFI is promising in the visualization of known ASDs, but the applicability of BFI during routine screening echocardiography remains to be evaluated. A limitation of study 1 was that the images that were presented to the observers did not include a control group without ASD. We do not therefore know if false positive findings may occur when using BFI. However, previous studies with CDI have not indicated problems with false positive flow images (114). On the contrary, false negative results in the detection of ASD have been reported (42, 43), and BFI may reduce the number of false negative findings. No patients in study 1 had sinus venosus defects or coronary sinus defects. It remains to be shown whether BFI simplifies the diagnosis of these defects, which may be missed with TTE.

In spite of recent advances in technology, we still lack a true gold standard for the measurement of ASD size and shape, and this is a limitation of the measurement comparison in study 3. CDI measurements of ASD have sources of error in determining the size of the jet, including CDI gain, examination depth and transducer frequency. CDI may also underestimate an irregular defect, because the 2 D ultrasound beam may not cut the defect in its maximal diameter. The same sources of error must be taken in account for BFI. However, a pilot study indicates that BFI is less dependent on gain setting (62).

Study 2 and 3 did not contain patients with pulmonary vein anomalies, and this is a limitation of the studies. Consequently, usefulness of BFI in detecting anomalous pulmonary veins was not tested in this thesis. However, an important aim was also to be able to demonstrate improved visualization of normally connecting veins.

8.2 Methods - Blood Flow Imaging

In its current implementation, the method Blood Flow Imaging is limited to imaging at shallow depths (< 10 cm), and is therefore suitable for vascular imaging and imaging in pediatric cardiology (61-63). In the neonate, the depths are shallow and the speckle pattern movement in BFI is clear. With increased imaging depths in adults, the speckle visualization may degrade, and blood flow direction become more challenging to perceive. Even though we did demonstrate acceptable speckle image quality in children up to 9 years (62), this is a weakness of the method in its current implementation. However, getting closer to the heart through the esophagus implies that the method should also have potential for cardiac imaging in adults using TEE. Study 3 had a variation in patient size from 6.2 to 67.5 kg which demonstrates this potential. With further utilization of parallel receive beam forming techniques as used in real-time 3D cardiac imaging systems (115), 2D BFI can be applicable for use at larger depths in the future.

The basic data acquisition scheme used in BFI and CDI is identical. However, there are some differences in the choice of ultrasound imaging parameters used. In BFI, a lower pulse repetition frequency (PRF) and higher spatial resolution may be preferred to improve the speckle visualization. This may in general come at the expense of a lowered image penetration, increased velocity aliasing artifacts in the underlying color images, and lowered overall color image frame rate.

In its current form BFI is best suitable to visualize low velocity flow. However, with further development of BFI using in plane wave imaging, the method will be more suitable for visualization of higher velocities. To switch between BFI and CDI is done quickly and easily, and we believe that alternating between the methods depending on the depth and case, would improve the ultrasound flow imaging.

8.3 Methods – Flow speckle tracking

Imaging with this technique is currently limited to linear array transducers. These transducers have a quite wide aperture, which may be a challenge in the imaging of the heart in the neonate. In addition the linear transducers have limited penetration when compared to passed-array transducers designed particular for cardiac imaging. Nevertheless, in the clinical project which study 4 was a part of, a sufficient penetration was achieved for CDI in all cases. We have subsequently examined 35 neonates

with this technique so far. In spite of a wider footprint of the linear probe, it was possible to obtain images from all standard views. However, the suprasternal view has been rather challenging.

Clutter filtering is necessary to suppress the strong tissue echo prior to the blood velocity estimation. However, clutter filtering is a remaining major challenge for large beam-to-flow angles, leading to signal drop-outs and corrupted velocity estimates. The signal drop-outs may influence the interpretation of the flow images.

The speckle pattern may decorrelate rapidly due to spatial and temporal velocity gradients, non-laminar flow and out-of- plane movement. With ultrahigh frame rates, the speckle decorrelation from frame to frame is reduced compared to conventional imaging.

Compared to focused imaging, the acquisition time for each frame is lowered significantly. Due to diffraction effects, the plane waves will naturally converge to a natural focus. For cardiac imaging transducers this limit occurs at about 15 cm, and for plane wave imaging the limit occurs at approximately 10 cm.

In plane wave imaging, the image contrast and the lateral resolution is compromised. This is particularly visible in B-mode imaging where a high dynamic range is shown, but less important in CDI where the dynamic range and signal-to-noise is substantially lower.

9 FUTURE PERSPECTIVES

Equipment malfunction, inherent limitations of echocardiography or imaging artefacts are significant contributors to diagnostic errors in pediatric echocardiography (7). Further work may uncover whether the angle-independent information provided by BFI may help reduce these errors. Technically, the BFI technique is continuously being improved in terms of increased imaging depths and speckle movement visualization. Further, by utilizing computer tracking algorithms, we have recently been able to quantify the 2-D blood velocity and direction (64), also demonstrated in a research scanner in study 4. This flow speckle tracking technique has the potential to demonstrate complex flow patterns in heart defects and to quantify shunt flow.

The focus in further work will first off all be additional investigation of this flow speckle tracking technique, including improved methods for visualization, for example with vector plot, streamlines or particle trace as demonstrated in figure 22.

Figure 22 – Blood Flow visualization

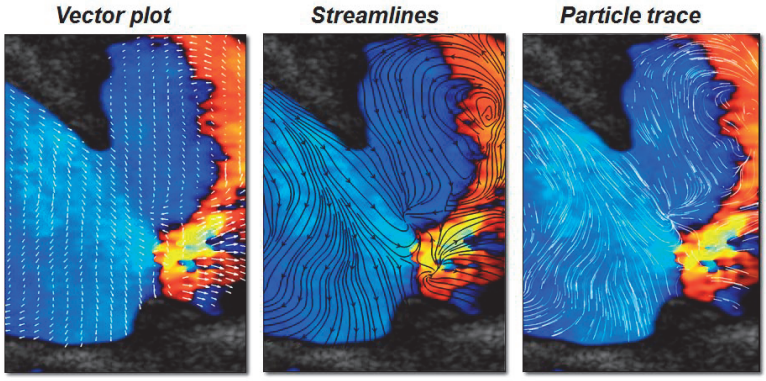

Further work will include an evaluation of high frame rate speckle tracking using phased array probes which are conventionally used in pediatric imaging. In this way, we have a smaller footprint and the penetration will improve. An imaging scheme where diverging (defocused) transmit beams are utilized together with parallel receive beam forming must then be implemented to achieve similar high frame rate flow images. In addition, methods for volume flow measurements to estimate shunt size and to quantitate valvular leakage will be investigated. In addition, potential solutions for the clutter filter issue and implementation of real time speckle tracking and visualization will be investigated.

We hope that improved flow imaging and visualization of the intracardiac flow pattern can improve the understanding of both physiological and pathological situations in congenital heart disease. Further studies will also explore if the method can improve the diagnostics of congenital heart disease and contribute to a more optimal treatment.

10 CONCLUSIONS

In the present work, we have demonstrated that:

- Using BFI to visualize ASD and pulmonary vein flow in children can be done as part of an ordinary 2D-TTE examination or TEE examination. The images can be obtained quickly with no need for offline post processing.

- BFI gives a better visualization of blood flow through the atrial septum than the traditional CDI method.

- BFI has lower estimates for ASD-size than BSD, but with acceptable 95% limits of agreement. The repeatability of the BFI-measurements was close to the inherent measurement error of the ultrasound measurement itself.

- Blood Flow Imaging may improve the visualization of the pulmonary veins in neonates.

- Transesophageal echocardiography with Blood Flow Imaging of the pulmonary veins agreed well with pulmonary angiography.

- By utilizing computer tracking algorithms, we have recently been able to quantify the 2-D blood velocity and direction.

- Flow speckle tracking technique has the potential to demonstrate complex flow patterns such as vortex flow, which is not visualized with today's Doppler techniques.

11 COPYRIGHT

12 REFERENCES

1. Dolk H, Loane M, Garne E. Congenital heart defects in Europe: prevalence and perinatal mortality, 2000 to 2005. Circulation. 2011;123(8):841-9.
2. O'Leary JM, Siddiqi OK, de Ferranti S, Landzberg MJ, Opotowsky AR. The Changing Demographics of Congenital Heart Disease Hospitalizations in the United States, 1998 Through 2010. JAMA. 2013;309(10):984-6.
3. Tworetzky W, McElhinney DB, Brook MM, Reddy VM, Hanley FL, Silverman NH. Echocardiographic diagnosis alone for the complete repair of major congenital heart defects. J Am Coll Cardiol. 1999;33(1):228-33.
4. Mertens L, Miller O, Fox K, Simpson J. Certification in echocardiography of congenital heart disease: experience of the first 6 years of a European process. European heart journal cardiovascular Imaging. 2013;14(2):142-8.
5. Stanger P, Silverman NH, Foster E. Diagnostic accuracy of pediatric echocardiograms performed in adult laboratories. Am J Cardiol. 1999;83(6):908-14.
6. Sharma S, Anand R, Kanter KR, Williams WH, Dooley KJ, Jones DW, et al. The usefulness of echocardiography in the surgical management of infants with congenital heart disease. Clin Cardiol. 1992;15(12):891-7.
7. Benavidez OJ, Gauvreau K, Jenkins KJ, Geva T. Diagnostic errors in pediatric echocardiography: development of taxonomy and identification of risk factors. Circulation. 2008;117(23):2995-3001.
8. Benavidez OJ, Gauvreau K, Geva T. Diagnostic errors in congenital echocardiography: importance of study conditions. J Am Soc Echocardiogr. 2014;27(6):616-23.
9. Dorfman AL, Levine JC, Colan SD, Geva T. Accuracy of echocardiography in low birth weight infants with congenital heart disease. Pediatrics. 2005;115(1):102-7.
10. Mitchell DG. Color Doppler imaging: principles, limitations, and artifacts. Radiology. 1990;177(1):1-10.
11. Ferrara K, DeAngelis G. Color flow mapping. Ultrasound Med Biol. 1997;23(3):321-45.
12. Bjaerum S, Martens D, Kristoffersen K, Torp H. Blood Motion Imaging - A new technique to visualize 2D blood flow. Proceedings of the IEEE Ultrasonics Symposium. 2002:1507-10.
13. Lovstakken L, Bjaerum S, Martens D, Torp H. Blood flow imaging--A new real-time, 2-D flow imaging technique. IEEE Trans Ultrason Ferroelectr Freq Control. 2006;53(2):289-99.
14. Edler I, Hertz CH. The use of ultrasonic reflectoscope for the continuous recording of the movements of heart walls. 1954. Clinical physiology and functional imaging. 2004;24(3):118-36.
15. Popp RL, Wolfe SB, Hirata T, Feigenbaum H. Estimation of right and left ventricular size by ultrasound. A study of the echoes from the interventricular septum. Am J Cardiol. 1969;24(4):523-30.
16. Skjærpe T, Hatle L. Ultralyd i Hjartediagnostikken: ein medisinsk og teknologisk triumf. In: Forfang K, Rasmussen K, editors. Det norske hjerte, Norsk kardiologis historie 2007. p. 91-102.
17. Holen J, Aaslid R, Landmark K, Simonsen S. Determination of pressure gradient in mitral stenosis with a non-invasive ultrasound Doppler technique. Acta Med Scand. 1976;199(6):455-60.
18. Edvardsen T, Urheim S, Skulstad H, Steine K, Ihlen H, Smiseth OA. Quantification of left ventricular systolic function by tissue Doppler echocardiography: added value of measuring pre- and postejection velocities in ischemic myocardium. Circulation. 2002;105(17):2071-7.
19. Edvardsen T, Gerber BL, Garot J, Bluemke DA, Lima JA, Smiseth OA. Quantitative assessment of intrinsic regional myocardial deformation by Doppler strain rate echocardiography in humans: validation against three-dimensional tagged magnetic resonance imaging. Circulation. 2002;106(1):50-6.
20. Skulstad H, Urheim S, Edvardsen T, Andersen K, Lyseggen E, Vartdal T, et al. Grading of myocardial dysfunction by tissue Doppler echocardiography: a comparison between velocity, displacement, and strain imaging in acute ischemia. J Am Coll Cardiol. 2006;47(8):1672-82.
21. Hatle L, Angelsen BAJ, editors. Doppler ultrasound in cardiology: Physical principles and clinical applications.: Philadelphia, Lea & Febiger.; 1985.
22. Hatle L, Angelsen BA, Tromsdal A. Non-invasive assessment of aortic stenosis by Doppler ultrasound. Br Heart J. 1980;43(3):284-92.
23. Hegrenaes L, Hatle L. Aortic stenosis in adults. Non-invasive estimation of pressure differences by continuous wave Doppler echocardiography. Br Heart J. 1985;54(4):396-404.
24. Skjaerpe T, Hatle L. Noninvasive estimation of systolic pressure in the right ventricle in patients with tricuspid regurgitation. Eur Heart J. 1986;7(8):704-10.

25. Rossvoll O, Hatle LK. Pulmonary venous flow velocities recorded by transthoracic Doppler ultrasound: relation to left ventricular diastolic pressures. J Am Coll Cardiol. 1993;21(7):1687-96.
26. Heimdal A, Stoylen A, Torp H, Skjaerpe T. Real-time strain rate imaging of the left ventricle by ultrasound. J Am Soc Echocardiogr. 1998;11(11):1013-9.
27. Blaas HG, Eik-Nes SH, Berg S, Torp H. In-vivo three-dimensional ultrasound reconstructions of embryos and early fetuses. Lancet. 1998;352(9135):1182-6.
28. Mahle WT, John JB, Silverman NH. The history of the development of paediatric echocardiography. Cardiol Young. 2009;19 Suppl 2:26-34.
29. Lundstrom NR, Edler I. Ultrasoundcardiography in infants and children. Acta Paediatr Scand. 1971;60(2):117-28.
30. Vermilion RP. Basic Physical Principles In: Snider AR, Serwer GA, Ritter S, editors. Echocardiography in Pediatric Heart Disease. Second ed. USA: Mosby; 1997. p. 1-10.
31. Claus P, D'Hooge J. Ultrasound Physics. In: Lai WW, Mertens L, Cohen MS, Geva T, editors. Echocardiography in pediatric and Congenital Heart Disease. Boston, USA: Wiley-Blackwell; 2009. p. 3-14.
32. Duck FA. The propagation of ultrasound through tissue. In: Haar Gt, editor. The Safe Use of Ultrasound in Medical Diagnosis. 3rd ed. London,UK: The British Institute of Radiology; 2012. p. 4-17.
33. Haar Gt. Guidelines and recommendations for the safe use of diagnostic ultrasound: the user's responsibilities. In: Haar Gt, editor. The Safe use of Ultrasound in Medical Diagnosis. 3rd ed. London, UK: The British Institute of Radiology; 2012. p. 142-57.
34. Shaw A, Martin K. The acoustic output of diagnostic ultrasound scanners. In: Haar Gt, editor. The Safe Use of Ultrasound in Medical Diagnosis. 3rd ed. London, UK: The British Institute of Radiology; 2012. p. 18-45.
35. Liu S, Joseph KS, Lisonkova S, Rouleau J, Van den Hof M, Sauve R, et al. Association between maternal chronic conditions and congenital heart defects: a population-based cohort study. Circulation. 2013;128(6):583-9.
36. Beerman LB, Zuberbuhler JR, editors. Atrial septal defect. 2nd Edition ed. London: Churchill Livingstone; 2002.
37. Stephensen SS, Sigfusson G, Eiriksson H, Sverrisson JT, Torfason B, Haraldsson A, et al. Congenital cardiac malformations in Iceland from 1990 through 1999. Cardiol Young. 2004;14(4):396-401.
38. Helgason H, Jonsdottir G. Spontaneous closure of atrial septal defects. Pediatr Cardiol. 1999;20(3):195-9.
39. McMahon CJ, Feltes TF, Fraley JK, Bricker JT, Grifka RG, Tortoriello TA, et al. Natural history of growth of secundum atrial septal defects and implications for transcatheter closure. Heart. 2002;87(3):256-9.
40. Hanslik A, Pospisil U, Salzer-Muhar U, Greber-Platzer S, Male C. Predictors of spontaneous closure of isolated secundum atrial septal defect in children: a longitudinal study. Pediatrics. 2006;118(4):1560-5.
41. Snider AR, Serwer GA, Ritter SB. Echocardiography in pediatric heart disease. 2nd ed. London: Mosby; 1997. X, 596 s. p.
42. Shub C, Dimopoulos IN, Seward JB, Callahan JA, Tancredi RG, Schattenberg TT, et al. Sensitivity of two-dimensional echocardiography in the direct visualization of atrial septal defect utilizing the subcostal approach: experience with 154 patients. J Am Coll Cardiol. 1983;2(1):127-35.
43. Hausmann D, Daniel WG, Mugge A, Ziemer G, Pearlman AS. Value of transesophageal color Doppler echocardiography for detection of different types of atrial septal defect in adults. J Am Soc Echocardiogr. 1992;5(5):481-8.
44. Morimoto K, Matsuzaki M, Tohma Y, Ono S, Tanaka N, Michishige H, et al. Diagnosis and quantitative evaluation of secundum-type atrial septal defect by transesophageal Doppler echocardiography. Am J Cardiol. 1990;66(1):85-91.
45. van den Bosch AE, Ten Harkel DJ, McGhie JS, Roos-Hesselink JW, Simoons ML, Bogers AJ, et al. Characterization of atrial septal defect assessed by real-time 3-dimensional echocardiography. J Am Soc Echocardiogr. 2006;19(6):815-21.
46. Abdel-Massih T, Dulac Y, Taktak A, Aggoun Y, Massabuau P, Elbaz M, et al. Assessment of atrial septal defect size with 3D-transesophageal echocardiography: comparison with balloon method. Echocardiography. 2005;22(2):121-7.
47. Wang ZJ, Reddy GP, Gotway MB, Yeh BM, Higgins CB. Cardiovascular shunts: MR imaging evaluation. Radiographics. 2003;23 Spec No:S181-94.

48. Piaw CS, Kiam OT, Rapaee A, Khoon LC, Bang LH, Ling CW, et al. Use of non-invasive phase contrast magnetic resonance imaging for estimation of atrial septal defect size and morphology: a comparison with transesophageal echo. Cardiovasc Intervent Radiol. 2006;29(2):230-4.
49. Bjornstad PG, Smevik B, Holmstrom H, Thaulow E, Hagemo PS, Ihlen H, et al. [Transcatheter closure of atrial septal defects in the oval fossa]. Tidsskr Nor Laegeforen. 2003;123(15):2052-4.
50. Kleinman CS. Echocardiographic guidance of catheter-based treatments of atrial septal defect: transesophageal echocardiography remains the gold standard. Pediatr Cardiol. 2005;26(2):128-34.
51. Chan KC, Godman MJ, Walsh K, Wilson N, Redington A, Gibbs JL. Transcatheter closure of atrial septal defect and interatrial communications with a new self expanding nitinol double disc device (Amplatzer septal occluder): multicentre UK experience. Heart. 1999;82(3):300-6.
52. Zhu W, Cao QL, Rhodes J, Hijazi ZM. Measurement of atrial septal defect size: a comparative study between three-dimensional transesophageal echocardiography and the standard balloon sizing methods. Pediatr Cardiol. 2000;21(5):465-9.
53. Faletra F, Scarpini S, Moreo A, Ciliberto GR, Austoni P, Donatelli F, et al. Color Doppler echocardiographic assessment of atrial septal defect size: correlation with surgical measurements. J Am Soc Echocardiogr. 1991;4(5):429-34.
54. Godart F, Rey C, Francart C, Jarrar M, Vaksmann G. Two-dimensional echocardiographic and color Doppler measurements of atrial septal defect, and comparison with the balloon-stretched diameter. Am J Cardiol. 1993;72(14):1095-7.
55. Seliem MA. Echocardiographic and color flow Doppler assessment of systemic and pulmonary venous connection and drainage in the neonate with congenital heart disease. Echocardiography. 1991;8(4):477-85.
56. Ucar T, Fitoz S, Tutar E, Atalay S, Uysalel A. Diagnostic tools in the preoperative evaluation of children with anomalous pulmonary venous connections. Int J Cardiovasc Imaging. 2008;24(2):229-35.
57. Wong ML, McCrindle BW, Mota C, Smallhorn JF. Echocardiographic evaluation of partial anomalous pulmonary venous drainage. J Am Coll Cardiol. 1995;26(2):503-7.
58. Anderson RH, Baker EJ, Macartney FJ, editors. Paediatric Cardiology. 2nd Ed ed. London: Churchill Livingstone; 2002.
59. Minich LL, Tani LY, Breinholt JP, Tuohy AM, Shaddy RE. Complete follow-up echocardiograms are needed to detect stenosis of normally connecting pulmonary veins. Echocardiography. 2001;18(7):589-92.
60. Chesarek RH, inventor; Quantum Medical Systems, Inc., assignee. Ultrasound imaging system for relatively low-velocity blood flow at relatively high framerates. United States of America patent 4888694. 1989 Dec 19.
61. Lovstakken L, Ibrahim KS, Vitale N, Henriksen ST, Kirkeby-Garstad I, Torp H, et al. Blood flow imaging: a new two-dimensional ultrasound modality for enhanced intraoperative visualization of blood flow patterns in coronary anastomoses. J Am Soc Echocardiogr. 2008;21(8):969-75.
62. Nyrnes SA, Lovstakken L, Torp H, Haugen BO. Blood flow imaging-a new angle-independent ultrasound modality for the visualization of flow in atrial septal defects in children. Echocardiography. 2007;24(9):975-81.
63. Nyrnes SA, Lovstakken L, Skogvoll E, Torp H, Haugen BO. Does a new ultrasound flow modality improve visualization of neonatal pulmonary veins? Echocardiography. 2010;27(9):1113-9.
64. Nyrnes SA, Lovstakken L, Torp H, Haugen BO. Flow speckle tracking for detailed visualization of flow patterns in neonates with congenital heart defects. Eur J Echocardiogr. 2011;12(Suppl 2):ii127.
65. Rosner B, editor. Fundamentals of Biostatistics. Sixth ed. United States of America: Thomson Brooks/Cole; 2006.
66. Altman DG, editor. Practical statistics for medical research. 1 st Ed ed. London: Chapmmann & Hall/CRC; 1991.
67. Team RDC. R: A language and environment for statistical computing. R Foundation for Statistical Computing, Vienna, Austria. 2012.
68. Bland JM, Altman DG. Statistical methods for assessing agreement between two methods of clinical measurement. Lancet. 1986;1(8476):307-10.
69. Nyrnes SA, Lovstakken L, Dohlen G, Skogvoll E, Torp H, Skjaerpe T, et al. Blood Flow Imaging in Transesophageal Echocardiography during Atrial Septal Defect Closure: A Comparison with the Current References. Echocardiography. 2014.
70. Lin FC, Fu M, Yeh SJ, Wu D. Doppler atrial shunt flow patterns in patients with secundum atrial septal defect: determinants, limitations, and pitfalls. J Am Soc Echocardiogr. 1988;1(2):141-9.

71. Lodato JA, Cao QL, Weinert L, Sugeng L, Lopez J, Lang RM, et al. Feasibility of real-time three-dimensional transoesophageal echocardiography for guidance of percutaneous atrial septal defect closure. European journal of echocardiography : the journal of the Working Group on Echocardiography of the European Society of Cardiology. 2009;10(4):543-8.
72. Saric M, Perk G, Purgess JR, Kronzon I. Imaging atrial septal defects by real-time three-dimensional transesophageal echocardiography: step-by-step approach. Journal of the American Society of Echocardiography : official publication of the American Society of Echocardiography. 2010;23(11):1128-35.
73. Johri AM, Witzke C, Solis J, Palacios IF, Inglessis I, Picard MH, et al. Real-time three-dimensional transesophageal echocardiography in patients with secundum atrial septal defects: outcomes following transcatheter closure. Journal of the American Society of Echocardiography : official publication of the American Society of Echocardiography. 2011;24(4):431-7.
74. Faletra FF, Nucifora G, Ho SY. Imaging the atrial septum using real-time three-dimensional transesophageal echocardiography: technical tips, normal anatomy, and its role in transseptal puncture. Journal of the American Society of Echocardiography : official publication of the American Society of Echocardiography. 2011;24(6):593-9.
75. Bhaya M, Mutluer FO, Mahan E, Mahan L, Hsiung MC, Yin WH, et al. Live/Real time three-dimensional transesophageal echocardiography in percutaneous closure of atrial septal defects. Echocardiography. 2013;30(3):345-53.
76. Garcia-Fuertes D, Mesa-Rubio D, Ruiz-Ortiz M, Delgado-Ortega M, Tejero-Mateo I, Pan-Alvarez-Ossorio M, et al. Monitoring complex secundum atrial septal defects percutaneous closure with real time three-dimensional echocardiography. Echocardiography. 2012;29(6):729-34.
77. Brown DW. Pulmonary Venous Anomalies. In: Lai WW, Mertens LL, Cohen MS, Geva T, editors. Echocardiography in pediatric and congenital heart disease : from fetus to adult. Chichester: Wiley-Blackwell; 2009. p. 119-42.
78. Amirghofran AA, Karimi A, Ajami GH, Rasekhi A. The importance of localizing pulmonary veins in atrial septal defect closure! J Cardiothorac Surg. 2011;6:41.
79. Picano E, Vano E, Rehani MM, Cuocolo A, Mont L, Bodi V, et al. The appropriate and justified use of medical radiation in cardiovascular imaging: a position document of the ESC Associations of Cardiovascular Imaging, Percutaneous Cardiovascular Interventions and Electrophysiology. Eur Heart J. 2014.
80. Brasch RC. Contrast media toxicity in children. Pediatr Radiol. 2008;38 Suppl 2:S281-4.
81. Amin Z. Transcatheter closure of secundum atrial septal defects. Catheterization and cardiovascular interventions : official journal of the Society for Cardiac Angiography & Interventions. 2006;68(5):778-87.
82. Tzifa A, Gordon J, Tibby SM, Rosenthal E, Qureshi SA. Transcatheter atrial septal defect closure guided by colour flow Doppler. Int J Cardiol. 2011;149(3):299-303.
83. Quek SC, Wu WX, Chan KY, Ho TF, Yip WC. Transcatheter closure of atrial septal defects--is balloon sizing still necessary? Ann Acad Med Singapore. 2010;39(5):390-3.
84. Wang JK, Tsai SK, Lin SM, Chiu SN, Lin MT, Wu MH. Transcatheter closure of atrial septal defect without balloon sizing. Catheterization and cardiovascular interventions : official journal of the Society for Cardiac Angiography & Interventions. 2008;71(2):214-21.
85. Seo JS, Song JM, Kim YH, Park DW, Lee SW, Kim WJ, et al. Effect of Atrial Septal Defect Shape Evaluated Using Three-Dimensional Transesophageal Echocardiography on Size Measurements for Percutaneous Closure. J Am Soc Echocardiogr. 2012;25(10):1031-40.
86. Carlson KM, Justino H, O'Brien RE, Dimas VV, Leonard GT, Jr., Pignatelli RH, et al. Transcatheter atrial septal defect closure: modified balloon sizing technique to avoid overstretching the defect and oversizing the Amplatzer septal occluder. Catheter Cardiovasc Interv. 2005;66(3):390-6.
87. Smallhorn JF, Khoo NS. Quantitative echocardiography in pediatrics--are we there yet? J Am Soc Echocardiogr. 2012;25(8):855-8.
88. Kutty S, Delaney JW, Latson LA, Danford DA. Can we talk? Reflections on effective communication between imager and interventionalist in congenital heart disease. J Am Soc Echocardiogr. 2013;26(8):813-27.
89. Pennell DJ, Sechtem UP, Higgins CB, Manning WJ, Pohost GM, Rademakers FE, et al. Clinical indications for cardiovascular magnetic resonance (CMR): Consensus Panel report. Eur Heart J. 2004;25(21):1940-65.
90. Huang X, Huang Y, Huang T, Huang W, Huang Z. Individual pulmonary vein imaging by transthoracic echocardiography: an inadequate traditional interpretation. Eur J Echocardiogr. 2008;9(5):655-60.

91. Stumper O, Vargas-Barron J, Rijlaarsdam M, Romero A, Roelandt JR, Hess J, et al. Assessment of anomalous systemic and pulmonary venous connections by transoesophageal echocardiography in infants and children. Br Heart J. 1991;66(6):411-8.
92. Hlavacek AM, Shirali GS, Anderson RH. Pulmonary venous abnormalities. In: Anderson RH, editor. Paediatric cardiology. 3rd ed. Philadelphia, Pa.: Churchill Livingstone/Elsevier; 2010. p. 497-522.
93. Latson LA, Prieto LR. Congenital and acquired pulmonary vein stenosis. Circulation. 2007;115(1):103-8.
94. Kimball TR, Weiss RG, Meyer RA, Daniels SR, Ryckman FC, Schwartz DC. Color flow mapping to document normal pulmonary venous return in neonates with persistent pulmonary hypertension being considered for extracorporeal membrane oxygenation. J Pediatr. 1989;114(3):433-7.
95. Seale AN, Uemura H, Webber SA, Partridge J, Roughton M, Ho SY, et al. Total anomalous pulmonary venous connection: outcome of postoperative pulmonary venous obstruction. J Thorac Cardiovasc Surg. 2013;145(5):1255-62.
96. Seale AN, Webber SA, Uemura H, Partridge J, Roughton M, Ho SY, et al. Pulmonary vein stenosis: the UK, Ireland and Sweden collaborative study. Heart. 2009;95(23):1944-9.
97. Vyas HV, Greenberg SB, Krishnamurthy R. MR imaging and CT evaluation of congenital pulmonary vein abnormalities in neonates and infants. Radiographics. 2012;32(1):87-98.
98. Ntsinjana HN, Hughes ML, Taylor AM. The role of cardiovascular magnetic resonance in pediatric congenital heart disease. Journal of cardiovascular magnetic resonance : official journal of the Society for Cardiovascular Magnetic Resonance. 2011;13:51.
99. Fratz S, Chung T, Greil GF, Samyn MM, Taylor AM, Valsangiacomo Buechel ER, et al. Guidelines and protocols for cardiovascular magnetic resonance in children and adults with congenital heart disease: SCMR expert consensus group on congenital heart disease. Journal of cardiovascular magnetic resonance : official journal of the Society for Cardiovascular Magnetic Resonance. 2013;15:51.
100. Chua LK, Twining P. A comparison of power colour flow with frequency based colour flow Doppler in fetal echocardiography. Clin Radiol. 1997;52(9):712-4.
101. Stevenson JG. Transesophageal Echocardiography. In: Lai WW, Mertens LL, Cohen MS, Geva T, editors. Echocardiography in Pediatric and Congenital Heart Disease. Chichester: Wiley-Blackwell; 2009. p. 671-86.
102. Udesen J, Gran F, Hansen KL, Jensen JA, Thomsen C, Nielsen MB. High frame-rate blood vector velocity imaging using plane waves: simulations and preliminary experiments. IEEE Trans Ultrason Ferroelectr Freq Control. 2008;55(8):1729-43.
103. Topper JN, Gimbrone MA, Jr. Blood flow and vascular gene expression: fluid shear stress as a modulator of endothelial phenotype. Mol Med Today. 1999;5(1):40-6.
104. Davies PF. Flow-mediated endothelial mechanotransduction. Physiol Rev. 1995;75(3):519-60.
105. Davies PF. Hemodynamic shear stress and the endothelium in cardiovascular pathophysiology. Nature clinical practice Cardiovascular medicine. 2009;6(1):16-26.
106. Hove JR, Koster RW, Forouhar AS, Acevedo-Bolton G, Fraser SE, Gharib M. Intracardiac fluid forces are an essential epigenetic factor for embryonic cardiogenesis. Nature. 2003;421(6919):172-7.
107. Kilner PJ, Yang GZ, Wilkes AJ, Mohiaddin RH, Firmin DN, Yacoub MH. Asymmetric redirection of flow through the heart. Nature. 2000;404(6779):759-61.
108. Rodriguez Munoz D, Markl M, Moya Mur JL, Barker A, Fernandez-Golfin C, Lancellotti P, et al. Intracardiac flow visualization: current status and future directions. European heart journal cardiovascular Imaging. 2013;14(11):1029-38.
109. Hong GR, Pedrizzetti G, Tonti G, Li P, Wei Z, Kim JK, et al. Characterization and quantification of vortex flow in the human left ventricle by contrast echocardiography using vector particle image velocimetry. JACC Cardiovascular imaging. 2008;1(6):705-17.
110. Chai P, Mohiaddin R. How we perform cardiovascular magnetic resonance flow assessment using phase-contrast velocity mapping. Journal of cardiovascular magnetic resonance : official journal of the Society for Cardiovascular Magnetic Resonance. 2005;7(4):705-16.
111. Groves AM, Chiesa G, Durighel G, Goldring ST, Fitzpatrick JA, Uribe S, et al. Functional cardiac MRI in preterm and term newborns. Arch Dis Child Fetal Neonatal Ed. 2011;96(2):F86-91.
112. Groves AM, Durighel G, Finnemore A, Tusor N, Merchant N, Razavi R, et al. Disruption of intracardiac flow patterns in the newborn infant. Pediatr Res. 2012;71(4 Pt 1):380-5.
113. Sengupta PP, Pedrizzetti G, Kilner PJ, Kheradvar A, Ebbers T, Tonti G, et al. Emerging trends in CV flow visualization. JACC Cardiovascular imaging. 2012;5(3):305-16.

114. Khandheria BK, Shub C, Tajik AJ, Taylor CL, Hagler DJ, Seward JB. Utility of color flow imaging for visualizing shunt flow in atrial septal defect. Int J Cardiol. 1989;23(1):91-8.
115. Hergum T, Bjastad T, Kristoffersen K, Torp H. Parallel beamforming using synthetic transmit beams. IEEE Trans Ultrason Ferroelectr Freq Control. 2007;54(2):271-80.

13 PAPERS

Paper 1

Nyrnes SA, Løvstakken L, Torp H, Haugen BO. Blood Flow Imaging - A new angle-independent ultrasound modality for the visualization of flow in atrial septal defects in children. Echocardiography. 2007;24(9):975-981.

DOI: 10.1111/j.1540-8175.2007.00508.x

Blood Flow Imaging—A New Angle-Independent Ultrasound Modality for the Visualization of Flow in Atrial Septal Defects in Children

Siri Ann Nyrnes, M.D.,* Lasse Løvstakken, M.Sc., Ph.D.,† Hans Torp, M.Sc., Ph.D.,† and Bjørn Olav Haugen, M.D., Ph.D.†

*Department of Pediatrics, University Hospital of Trondheim, Norway, †Department of Circulation and Medical Imaging, Norwegian University of Science and Technology, Trondheim, Norway

Background: Color Doppler imaging (CDI) is the most applied method for evaluation of flow in atrial septal defects (ASD). A new real time ultrasound flow imaging modality called blood flow imaging (BFI) is able to visualize the blood flow in any direction of the image and is not limited by velocity aliasing. The method thereby overcomes the two limitations most often encountered in CDI. In this study we compared BFI with CDI for the visualization of interatrial blood flow in children. Methods: We studied ASD flow in 13 children using both CDI and BFI in the same examination. CDI and BFI cineloops were prepared off-line and both optimal and suboptimal (increased color artifacts) images were presented in random order to four observers. They were asked to range from 0–100 on a visual analogue scale how certain they were of interatrial blood flow. The CDI and BFI ratings were compared using the exact Wilcoxon signed rank test for paired samples. Results: All ASDs visualized with CDI were confirmed using BFI. Two of the observers ranked BFI as being significantly better than CDI when the images were optimized. When the images were suboptimal three of the observers rated BFI as being significantly better. Conclusions: This pilot study indicates that BFI improves the visualization of interatrial blood flow in children. To include BFI in the ordinary echocardiography examination is easy and not time consuming. The method may prove to be a useful supplement to CDI in ASD imaging. (ECHOCARDIOGRAPHY, Volume 24, October 2007)

atrial septal defect (ASD), *angle-independent flow visualization*, *blood flow imaging (BFI)*, *echocardiography*, *color Doppler imaging (CDI)*

Defects of the atrial septum may be visualized using 2D transthoracic echocardiography (TTE), which may also demonstrate the functional consequences with enlargement of the right atrium and right ventricle. Additional pulsed Doppler studies and pulmonary venous flow pattern studies can further help evaluate the atrial septal defect (ASD) hemodynamics.[1,2] In the apical four-chamber view the parallel angle of the echo beam and the thinness of the fossa ovalis can cause artifactual echo dropouts of the septum and thereby lead to an inaccurate diagnosis.[3] Subcostal imaging minimize the dropouts of the atrial septal echoes, but some defects may be missed. The subcostal image view may further be suboptimal for obese patients.[4]

Transesophageal echocardiography (TEE) provides improved images of the interatrial septum.[5,6] But TEE applicability is limited by the need for general anesthesia in children, and is mostly used to guide catheter closure. Both TTE and TEE may be combined with microbubble contrast imaging to increase the sensitivity for the detection of interatrial shunts.[4]

Recent studies have presented real time 3D echocardiography[7,8] and magnetic resonance imaging[9,10] as useful imaging modalities. But the need for sedation in small children, and the fact that these modalities are time consuming limits the use of these methods in daily clinical practice.

In spite of all new modalities for ASD-visualization, 2D-TTE with color Doppler imaging (CDI) still is the most commonly used technique for ASD visualization. The addition

Address for correspondence and reprints request: Siri Ann Nyrnes, M.D., Department of Pediatrics, St. Olavs Hospital, 7006 Trondheim, Norway. Fax: +47 72574708; E-mail: siranyr@online.no

of color flow imaging increase the diagnostic sensitivity for ASD-detection and nearly eliminate false positive diagnoses.[11] CDI is useful both to confirm the presence of an ASD in patients where direct imaging of the atrial septum is inadequate, and also for distinguishing a true ASD from a echocardiographic dropout. CDI also show the direction of flow and may be used to estimate the size of the defect.[12]

However, CDI has some limitations that may lessen its diagnostic value, and down to 64% overall ASD detection rates has been reported.[5] Due to a false coloring of the interatrial septum from overlapping color and B-mode images (i.e., color blooming artifacts) the flow through ASDs are not always easy to detect, especially when 2D images are suboptimal and when defects are small. Also, Doppler-based imaging techniques are only able to measure velocities along the ultrasound beam. They are thus angle dependent, and require knowledge of the relative angle between the ultrasound beam and direction of flow. Further, when the Nyquist limit for blood velocity is reached, aliasing artifacts will occur, obscuring the true velocity and the direction of flow.[13]

A new real time 2D flow imaging modality called blood flow imaging (BFI) has been described.[14] This modality extends CDI with information of flow direction that is not dependent on the relative angle of the ultrasound beam, and which is not limited by velocity aliasing. The method thereby overcomes the two limitations most often encountered in CDI, and may provide a more detailed image of the blood flow.

The BFI modality is commercially available for vascular imaging, and has previously successfully been applied in visualization of flow in the carotid arteries.[15] Our aim was to examine the potential benefits of using BFI in cardiac imaging. To the authors knowledge this has not previously been investigated. The movement of blood in BFI may be seen in spite of nonaxial flow and color blooming artifacts. In addition, BFI is improved in shallow depths and in the visualization of low velocity flow. In the light of this, we chose to study flow in ASD, which is one of the most common congenital heart disorders.[16,17] The aim of this pilot study was to explore whether the addition of BFI to ordinary CDI in 2D-TTE improves the visualization of ASD flow in children.

Materials and Methods

Patients

This pilot study was performed at the Pediatric Department, University Hospital of Trondheim, Norway. A total of 13 children with a diagnosis of ASD were evaluated between March and August 2006. The age ranged from newborns to 9 years, with a median age of 12 months. The inclusion criterion was ASD sized 4 mm or more at the time of diagnosis. Patients were recruited in the outpatient clinic and from the hospital ward, and both newly diagnosed and previously diagnosed patients were included. The reason for referral to a pediatric cardiologist in most of the patients was the presence of a heart murmur. In one patient, hemiparesis and cerebral infarction led to further investigation with echocardiography. One patient with previously diagnosed ASD was excluded due to closure of the defect discovered at the time of study inclusion.

An ethical committee approval was obtained, and the parents of all study subjects provided written informed consent for participation in the study.

Equipment

All the TTEs were performed using a GE Vingmed Vivid 7 (GE Vingmed, Horten, Norway) with a GE M4S cardiac probe (GE Healthcare, Princeton, NJ, USA). Although offline analysis is not required in daily practice, CDI and BFI images were analyzed in MATLAB (The MathWorks, Inc.) in this study for comparison by the independent observers.

Aspects of BFI

BFI extends CDI with qualitative information of flow. This is achieved through the preservation and visualization of the speckle pattern originating from the blood signal echoes. The speckle pattern is present inside the vessel lumens and heart ventricles, but is normally not visible in the B-mode image due the weak strength of the echoes from blood compared with the surrounding tissue structures. The movement of this speckle pattern between image acquisitions correlates to the actual blood cell movement, and can be captured by acquiring images with a high frame rate. By using a slow motion display of these images, the

movement of the speckle pattern can be tracked by the human eye.

Data Acquisition and Processing

The blood flow through the ASDs was first studied in a conventional TTE examination using CDI. BFI was supplemented as a part of the same examination. BFI data acquisition is identical to that of CDI. The BFI application was optimized by altering an existing CDI application. The image quality (spatial resolution) was increased on the expense of frame rate to ensure a proper visualization of the speckle movement of blood.

A pediatric cardiologist and an accompanying ultrasound technician performed the scans. Subcostal views were used to compare the methods, because this imaging plane has been shown to be most sensitive.[4] The application of BFI has the same limitations by acoustic windows as CDI. When all patient data had been collected, CDI and BFI cineloops for each patient were prepared offline. The color image information presented was identical in both modalities, i.e., in the BFI cineloops speckle movement images were added to the ordinary color images. Two different cineloops were prepared for each modality. In one cineloop, the color images were optimized for best possible visualization of the flow through the ASD. In a second cineloop, the amount of color-gain was increased to simulate the color blooming artifact which may arise in CDI. This was introduced in order to evaluate the potential of BFI when CDI images are suboptimal.

The echocardiograms were independently reviewed by two pediatric cardiologists, one adult cardiologist, and one physician with ultrasound experience from research. All the observers were otherwise uninvolved in the study. The two pediatric cardiologists had no previous experience with BFI, but were introduced to the concept prior to the evaluation. The other observers were familiar with the technique from vascular applications. The images from the two modalities were presented to the observers in random order. The observers were then asked to range from 0 to 100 on a visual analogue scale (VAS) how certain they were that there was blood flow across the atrial septum.

The observers were also asked to rank the general quality of the images on a VAS from 0 to 100, where 100 was the best possible image quality. They were asked to rank the general ultrasound quality for each clip, and the presentation of the anatomy.

Statistical Methods

The null hypothesis was that there is no difference between BFI and CDI in the visualization of interatrial blood flow, versus the alternative hypothesis that BFI improves the ASD visualization.

The degree of certainty (VAS scale 0–100) was compared within each observer using the exact 2-tailed Wilcoxon signed-rank test for paired samples.[18] Ratings of the optimal and suboptimal cineloops were analyzed separately. The difference between CDI and BFI ratings were considered significant when the P-value were less than 0.05. The statistical analysis and plotting was done in the numerical MATLAB software with the statistics toolbox (The MathWorks Inc., Natick, MA, USA).

Results

Patient Characteristics

The patient material is described in Table I. One patient had a primum ASD and the others had secundum defects. The ASD size ranged from 2 to 9 mm. All defects were 4 mm or larger at time of diagnosis. Because of the natural history of secundum ASDs,[19] some of the defects were smaller at the study investigation. Two of the patients had two defects. One patient had bidirectional shunt; a newborn who still had raised vascular pulmonary resistance. The others had left to right shunting across the ASD. Both patients with pulmonary stenosis had small shunts and mild stenosis. The patient with mild pulmonary hypertension had broncopulmonary dysplasia, and the ASD shunting was small.

In one patient, the recordings with BFI revealed two ASDs and not one as first suspected in the prior CDI recording. Eight of the patients were girls. Seven patients had additional cardiac anomalies. One of the patients had total atriovetricular (AV) block, while the others had sinus rhythm. Three patients had significant right ventricular volume overload. The Qp/Qs value in the patient with a 7-mm ASD and a small patent ductus arteriosus was 1.8. This patient has been accepted for device closure. The patient with a 9-mm ASD has now had device closure. The 12-month-old girl who presented with a stroke had a 5 mm secundum ASD.

TABLE I

Patient Characteristics

Age	Diagnosis	ASD Size (mm)	Other Cardiac Anomalies
9 years	Secundum	7	Small patent ductus arteriosus
12 months	Secundum	5	
22 months	Secundum	4 and 2	Mild pulmonary hypertension
4 months	Primum	6	Atrioventricular septal defect
1 month	Secundum	4	Muscular ventricular septum defect (VSD)
13 months	Secundum	3	Pulmonary valve stenosis
19 months	Secundum	4	Pulmonary valve stenosis
2 weeks	Secundum	4	Perimembranous VSD
2 months	Secundum	3	
3 years	Secundum	9	
21 months	Secundum	6 and 3	
5 days	Secundum	4	Grade III atrioventricular (AV)-block
6 weeks	Secundum	4	

2D Echocardiography

All ASDs visualized using CDI in the examinations were confirmed using BFI.

BFI imaging prolonged the echocardiographic examination with no more than five minutes. No children needed sedation during the ultrasound examination.

Examples of ASD flow visualization with BFI is shown in Figures 1 and 2. In Figure 1, color blooming artifacts can be observed, and the example demonstrates that the speckle pattern visualization can provide additional directional information which may be helpful to distinguish ASD flow from normal flow and color artifacts. In Figure 2, BFI imaging revealed two ASDs, and not one defect as first suspected in a prior CDI examination. Knowing there were two defects, we did additional CDI in the same patient and could then visualize both defects. As the

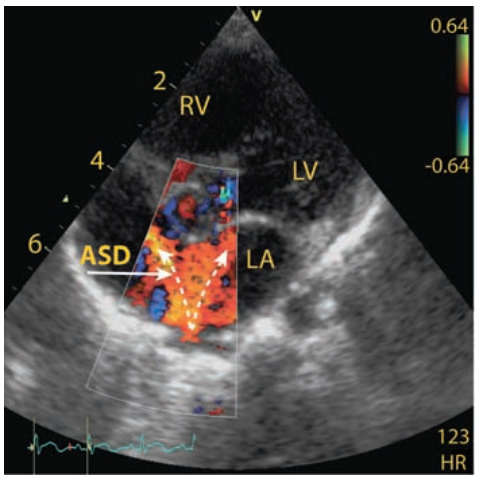

Figure 1. *BFI image of a small secundum ASD. The arrows indicate direction of flow as visualized by the speckle pattern movement. Machine settings; frequency 2.5 MHz, pulse repetition frequency 4 kHz. ASD = atrial septal defect; BFI = blood flow imaging; LA = left atrium; LV = left ventricle; RV = right ventricle.*

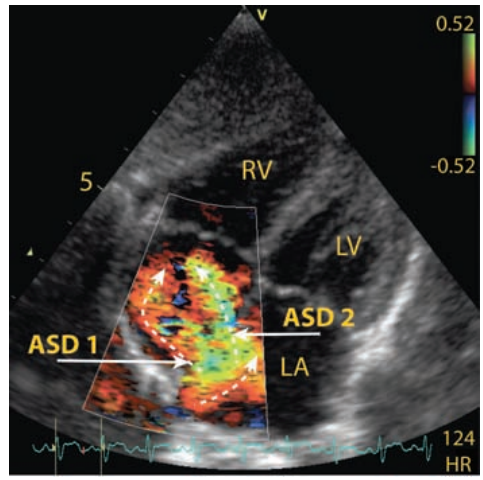

Figure 2. *BFI image of a double ASD, 6 and 3 mm. The arrows indicate the direction and flow as visualized by the speckle pattern movement. Machine settings; frequency 2.7 MHz, pulse repetition frequency 3.5 kHz. ASD = atrial septal defect; BFI = blood flow imaging; LA = left atrium; LV = left ventricle; RV = right ventricle.*

BFI modality can only really be appreciated by watching cineloops, we encourage the reader to download the generated MPEG video clips from the journal WebPages (http://www.blackwell-synergy.com/loi/echo), in which BFI and CDI are presented side by side.

The four observers reviewed the images from the 13 patients. All four observers ranked the BFI very high. When the presented color images were optimal, two observers ranked BFI as significantly better than CDI in the visualization of interatrial blood flow (Fig. 3). The two other observers also ranked CDI very high (near 100%), and no significant difference could be measured. When the color images were suboptimal (i.e., color blooming artifacts were created), the BFI was ranked significantly higher than CDI in three of the observers (Fig. 4). The physician with ultrasound experience from research (observer number 4) regarded the two methods as equal in both scenarios. The mean value in the ranking of the general quality of the image was 52 (2 SD ± 23) for both of the questions.

Discussion

This pilot study implies that BFI, a new angle independent ultrasound modality, may improve the visualization of blood flow through the atrial septum in children compared to the CDI method. To include BFI in the TTE examination is easy and not time consuming.

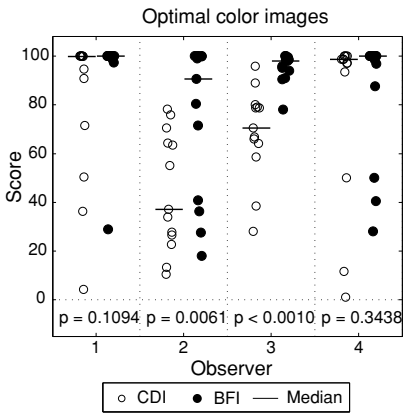

Figure 3. *Dot plot showing the observers assessments of CDI versus BFI when the color images were optimal. The observers were asked to range from 0 to 100 on a VAS how certain they were that there was blood flow across the atrial septum. Random noise is added to enhance visual quality. BFI = blood flow imaging; CDI = color Doppler imaging; VAS = visual analogue scale.*

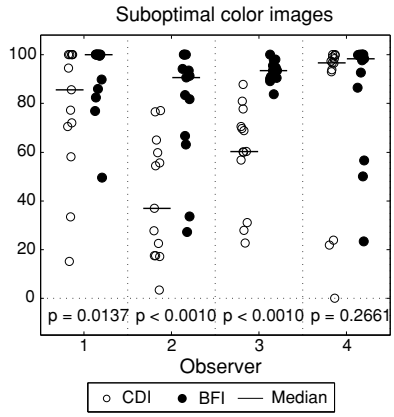

Figure 4. *Dot plot showing the observers assessments of CDI versus BFI when the color images were suboptimal. The observers were asked to range from 0 to 100 on a VAS how certain they were that there was blood flow across the atrial septum. Random noise is added to enhance visual quality. BFI = blood flow imaging; CDI = color Doppler imaging; VAS = visual analogue scale.*

Current Doppler-based modalities such as CDI are only able to measure the axial direction of flow, i.e., flow towards or away from the transducer surface. The BFI modality adds the speckle movement of blood to the Doppler information available with CDI, and is thereby able to visualize flow in any direction of the image plane. Thus, a more detailed and intuitive display of the flow conditions requiring less interpretation than CDI images may be provided. Since several speckle images are generated for each CDI image (4 additional images in our application), the frame rate of the speckle visualization in BFI is increased compared to CDI.

As interatrial flow is not only axial, BFI may provide more detailed information of interatrial blood flow than CDI. In one patient in this study, BFI imaging revealed two ASDs, and not one defect as first suspected in a prior CDI examination. This is important information when planning catheter based device closure.

When presented with suboptimal color images (i.e., when color blooming artifacts were created), the rating differences between BFI and CDI were enlarged in favor of BFI for three of four observers. This finding indicates that BFI may be especially useful when color image artifacts are present or when too much color

gain has been applied, which may be a problem in daily clinical practice. This is illustrated in Figure 1.

In our pilot study, we could not determine whether ASD size or patient age had any bearing on ASD detection. Reasonably good visualization of the atrial septum was possible in all the study patents. One of the general considerations of BFI is that the method is not limited by velocity aliasing. However, we did not experience significant aliasing in our study on interatrial flow.

The inclusion criteria for the study was ASDs already visualized with CDI, and therefore angle was not an important factor in terms of ASD-detection. But angle may be a problem, especially in other views than the subcostal. The main reason that BFI may be advantageous over CDI in low pressure ASD-flow visualization is that interatrial blood flow may be shown in spite of nonaxial flow and color blooming artifacts.

Several investigators have used CDI to estimate the size of the ASD,[12,20] but even if the CDI-jet width give an indication of ASD size, reliability of color flow in predicting size is limited by variability in gain settings and alignment of the scanning plane relative to the shunt.[16] In addition, estimation of jet-width size does not take into account shunt flow due to associated anomalous pulmonary connections. We do not know if the use of BFI may improve the sizing of ASDs, but this study indicates that a better visualization of blood flow is obtained.

Since ASD flow may occur only during a limited portion of the cardiac cycle, CDI may not be able to visualize shunt flow because the frame rate is too low. Further, due to the low frame rate, the right-to-left component of the atrial shunt is usually not detectable with CDI.[21] As BFI provides an increased framerate of flow information, it may reduce this problem. This increased amount of flow information is especially important in the imaging of children due to their high heart rates.

The BFI modality has previously been studied in vascular imaging.[15] More detailed flow patterns in the areas of stenosis and branching of the carotid artery were observed.[15] This is the first study that evaluate BFI in cardiac imaging. The increased imaging depths and more complex flow patterns in cardiac imaging degrade the speckle visualization of BFI.[14] Speckle directions in adult TTE can therefore be challenging to perceive. When imaging children, the probe may be placed closer to the heart and a better visualization can be obtained.

TEE is superior to TTE in detecting secundum ASD, sinus venosus defects and associated anomalous pulmonary venous return in adults.[5] In children, routine transthoracic studies are generally adequate of ASD diagnosis, but TEE may be used in patients with poor image quality. TEE is the preferred imaging modality during guidance of catheter-based treatments of ASDs in children.[22] BFI can easily be added during a TEE investigation, and as the probe is placed close to the heart in TEE, a detailed speckle pattern may be visualized. But to establish this, further studies are necessary.

A limitation of the study was that the images that were presented to the observers did not include a control group without ASD. We therefore do not know if false positive findings may occur when using BFI. However, previous studies with CDI have not indicated problems with false-positive flow images.[11] On the contrary, false-negative results in the detection of ASD have been reported,[4,5] and BFI may reduce the amount of false-negative findings. No patients in our study had sinus venosus defects or coronary sinus defects. It remains to be shown whether BFI simplify the diagnosis of these defects, which may be missed with TTE.

BFI is promising in the visualization of known ASD, but the applicability of BFI during routine screening echocardiography remains to be evaluated. Further investigations are necessary to study the sensitivity and specificity of the method. To accomplish this, BFI should be compared to the gold standard of ASD visualization, which at present is balloon sizing during catheterization.

Conclusion

Using BFI to visualize ASD flow in children can be done as part of an ordinary 2D-TTE examination. The images can be obtained quickly with no need for off-line postprocessing and without sedation. This pilot study indicates that BFI gives a better visualization of blood flow trough the atrial septum than the traditional CDI method, and we believe the method could be a useful supplement to CDI in the diagnosis and follow up of children with ASD.

Acknowledgment: We thank the observers. We also thank Eirik Skogvoll for advise on the statistics.

References

1. Dittmann H, Jacsch R, Voelker W, et al: Accuracy of Doppler echocardiography in quantification of left to right shunts in adult patients with atrial septal defect. *J Am Coll Cardiol* 1988;11:338–342.
2. Chockalingam A, Dass SH, Alagesan R, et al: Role of transthoracic Doppler pulmonary venous flow pattern in large atrial septal defects. *Echocardiography* 2005;22:9–13
3. Snider AR, Serwer GA, Ritter SB: *Echocardiography in Pediatric Heart Disease*, *2nd Ed*. Mosby, United States of America, 1997, pp. 235–296.
4. Shub C, Dimopoulos IN, Seward JB et al: Sensitivity of two-dimensional echocardiography in the direct visualization of atrial septal defect utilizing subcostal approach: Experience with 154 patients. *J Am Coll Cardiol* 1983;2:127–135.
5. Hausmann D, Daniel WG, Mugge A, et al: Value of transesophageal color Doppler echocardiography for detection of different types of atrial septal defect in adults. *J Am Soc Echocardiogr* 1992;5:481–488.
6. Morimoto K, Matsuzaki M, Tohma Y, et al: Diagnosis and quantitative evaluation of secundum-type atrial septal defect by transesophageal Doppler echocardiography. *Am J Cardiol* 1990;66:85–91.
7. Van Den Bosch AE, Ten Harkel DJ, McGhie JS, et al: Characterization of atria septal defect assessed by real time 3-dimensional echocardiography. *J Am Soc Echocardiogr* 2006;19:815–821.
8. Abdel-Massih T, Dulac Y, Taktak A, et al: Assessment of atrial septal defect size with 3D-transesophageal echocardiography: Comparison with balloon method. *Echocardiography* 2005;22:121–127.
9. Wang ZJ, Reddy GP, Gotway MB, et al: Cardiovascular shunts: MR-imaging evaluation. *Radiographics* 2003;23:81–94.
10. Piaw CS, Kiam OT, Rapaee A, et al: Use of noninvasive phase contrast magnetic resonance imaging for estimation of atrial septal defect size and morphology: A comparison with transesophageal echo. *Cardiovasc Intervent Radiol* 2006;29:230–234.
11. Khanderia BK, Shub C, Tajik AJ, et al: Utility of color flow imaging for visualization shunt flow in atrial septal defects. *Int J Cardiol* 1989;23:91–98.
12. Faletra F, Scarpini S, Moreo A, et al: Color Doppler echocardiographic assessment of atrial septal defect size: Correlation with surgical measurements. *J Am Soc Echocardiogr* 1991;4:429–434.
13. Ferrara K, DeAngelis G: Color flow mapping. *Ultrasound Med Biol* 1997;23:321–345.
14. Løvstakken L, Bjærum S, Martens D, et al: Blood flow imaging—A new real time, 2D flow imaging technique. *IEEE Trans Ultrason, Ferroelec, Freq Contr* 2006;53:289–299.
15. Amundsen BH, Løvstakken L, Samstad SO, et al: Ultrasound blood flow imaging—A new method for improved visualization of flow direction in carotid stenosis. *Eur Heart J* 2005;26(Abstract Supplement): 698.
16. Beerman LB, Zuberbuhler JR: Atrial septal defect. In Anderson RH, Baker EJ, Macartney FJ, et al. (eds): *Paediatric Cardiology, 2nd Ed*. London, Churchill Livingstone; 2002, pp. 901–930.
17. Stephensen SS, Sigfusson G, Eiriksson H, et al: Congenital cardiac malformations in Iceland from 1990 through 1999. *Cardiol Young* 2004;14:396–401.
18. Rosner B: Nonparametric methods. *Fundamentals of Biostatistics*, *5th Ed*. Duxbury, Brooks/Cole, Pacific Grove, USA, 2000, pp. 331–353.
19. McMahon CJ, Feltes TF, Fraley JK, et al: Natural history of growth of secundum atrial septal defects and implications for transcatheter closure. *Heart* 2002;87:256–259.
20. Pollick C, Sullivan H, Cujec et al: Doppler color-flow imaging assessment of shunt size in atrial septal defect. *Circulation* 1988;78:522–528.
21. Lin F-C, Fu M, Yeh S-J, et al: Doppler atrial shunt flow patterns in patients with secundum atrial septal defect: determinants, limitations and pitfalls. *J Am Soc Echocardiogr* 1988;1:141–149.
22. Kleinman CS: Echocardiographic guidance of catheter-based treatments of atrial septal defect: Transesophageal echocardiography remains the gold standard. *Pediatr Cardiol* 2005;26:128–134.

Supplementary Material

The following supplementary material is available online—Video clips:
Figure 1–2.

Paper 2

Nyrnes SA, Løvstakken L, Skogvoll E, Torp H, Haugen BO. Does a new ultrasound flow modality improve visualization of neonatal pulmonary veins? Echocardiography. 2010;27(9):1113-1119.

DOI: 10.1111/j.1540-8175.2010.01206.x

Echocardiography

Does a New Ultrasound Flow Modality Improve Visualization of Neonatal Pulmonary Veins?

Siri Ann Nyrnes, M.D.,*† Lasse Lovstakken, M.Sc., Ph.D.,*‡ Eirik Skogvoll, M.D., Ph.D.,*§ Hans Torp, M.Sc., Dr.Tech.,* and Bjørn Olav Haugen, M.D., Ph.D.*¶

*Department of Circulation and Medical Imaging, Norwegian University of Science and Technology (NTNU), Trondheim, Norway; †Department of Pediatrics, St. Olav's University Hospital, Trondheim, Norway; ‡St. Olav's University Hospital, Trondheim, Norway; §Department of Anesthesiology and Emergency Medicine, St. Olav's University Hospital, Trondheim, Norway; and ¶Department of Cardiology, St. Olav's University Hospital, Trondheim, Norway

Background: Blood flow imaging is a new ultrasound modality that supplements color Doppler imaging with angle-independent information of flow direction that is not influenced by velocity aliasing. This is done by visualizing the blood speckle movement superimposed on the color Doppler images. This study aimed to investigate whether this method improves the visualization of the pulmonary veins in neonates. Methods: Twenty-six neonates with suspected congenital heart disease were prospectively examined with echocardiography and blood flow imaging of the pulmonary veins after parental consent. For each patient, blood flow imaging and color Doppler imaging cine loops were presented to four observers (pediatric cardiologist/cardiologists) in a random order. Questions regarding the pulmonary venous connections and the overall quality of the pulmonary vein imaging were evaluated on a visual analogue scale from 0 (worst) to 100 (best). The methods were compared within each observer using the Wilcoxon's exact signed-rank test. Results: Blood flow imaging (color Doppler imaging combined with the blood speckle movement) was consistently ranked as better than conventional color Doppler imaging for visualization of the pulmonary veins for all observers (all P-values < 0.002). Conclusion: Blood flow imaging may improve the visualization of the pulmonary veins in neonates. (Echocardiography 2010;27:1113-1119)

Key words: echocardiography, heart defects, congenital, pulmonary veins, flow visualization, blood flow imaging

Echocardiography is the most important imaging modality for visualizing the pulmonary veins,[1–4] but still this is a challenging area in the assessment of suspected congenital heart disease in the neonate. The pulmonary veins are among the top anatomic segments involved in diagnostic errors in pediatric echocardiography,[5] and difficulties in the visualization of anomalous pulmonary return,[6–8] pulmonary vein stenosis, and also normally connecting pulmonary veins have been reported.[9–11] Further, in views where the pulmonary blood flow is not parallel to the ultrasound beam, the flow direction may be difficult to visualize using color Doppler imaging (CDI). We chose to look into neonates especially, since diagnostic errors in pediatric echocardiography occur more frequently in this low-weight group.[5,12]

A new real time ultrasound flow modality called blood flow imaging (BFI) supplements CDI with additional angle-independent information of flow direction. This is done by visualizing the blood speckle movement superimposed on the color Doppler images. BFI has been shown to improve the visualization of interatrial blood flow in children[13] and coronary flow imaging during coronary bypass surgery in an experimental porcine model.[14]

This prospective study aimed to investigate whether BFI improves visualization of the pulmonary veins in neonates.

Funding: From 01.10.07 to 28.02.09 the first author had a half-time position as assistant professor in Norwegian University of Science and Technology (NTNU), Institute for Circulation and medical imaging. This position was financed from the Medical Imaging Laboratory for Innovative Future Healthcare. From 01.03.09 until the present the first author had a half-time position as PhD candidate in the Liaison Committee between the Central Norway Regional Health Authority (RHA) and the Norwegian University of Science and Technology (NTNU).

Address for correspondence and reprint requests: Siri Ann Nyrnes, M.D., Department of Circulation and Medical, Imaging, Norwegian University of Science and Technology, Olav Kyrresgt. 9, 7489 Trondheim, Norway. Fax: +47 73598613; E-mail: siri.a.nyrnes@ntnu.no

Methods:

Patients:

The study was performed at the Department of Pediatrics, St. Olav's University Hospital in Trondheim, Norway. A total of 26 newborn children referred to a pediatric cardiologist because of suspected congenital heart disease were included prospectively from February to April 2008.

Patients were recruited from the hospital ward. The reasons for referral to a pediatric cardiologist were either the presence of a heart murmur, other congenital defects, asphyxia or arrhythmias.

Informed consent was obtained from the parents. The study was approved by The Regional Committee for Medical and Health Research Ethics (REK) and the Norwegian Social Science Data Services (NSD).

Equipment:

All transthoracic echocardiography examinations (TTE) were performed using a GE Vingmed Vivid 7 (GE Vingmed, Horten, Norway) with a GE 7S cardiac probe (GE Healthcare, Milwaukee, WI, USA).

Blood Flow Imaging:

The ultrasound research environment in Trondheim has developed a new real time ultrasound flow modality called BFI,[15,16] which is a visual method aimed to image the blood flow in more detail than today's Doppler techniques. BFI is patented and currently commercially available for vascular imaging.[17] In this work, the ultrasound scanner settings were modified to adapt this method to cardiac imaging in neonates.

In all ultrasound imaging, there is a so-called speckle pattern that is recognized as an irregular pattern where homogenous tissue is expected. The ultrasound speckle pattern from blood is present inside the vessel lumens and heart ventricles, but is normally not visible in the B-mode (B = brightness) image due to the weak strength of the echoes from blood compared to the surrounding tissue structures. However, this blood speckle pattern can be visualized by first filtering out the stronger tissue echoes (wall filtering). The movement of the blood speckle pattern between image acquisitions corresponds to the actual blood cell movement, but can only be captured by acquiring images with a frame rate in the kilohertz range. In an image-acquisition scheme termed beam interleaved acquisition,[18] such high frame rates can be achieved for separately acquired subregions of the total image sector. On display, speckle images acquired for different subregions are shown at a rate equal to the total image sector frame rate, leading to a slow motion display of the speckle movement, which can be tracked by the human eye. In BFI, this speckle pattern technique is combined with regular CDI. The speckle pattern in BFI is angle independent and has no upper velocity scale limitation.

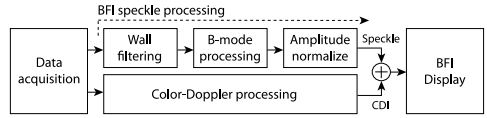

Figure 1. A block diagram illustrating the data acquisition and processing scheme utilized in BFI. The general data acquisition is identical for CDI and BFI. In parallel to conventional CDI processing, speckle images from blood are produced by wall filtering and conventional B-mode processing. A normalization procedure is applied to avoid flashing artifacts in the speckle images due to discontinuities in signal power. In the end, the speckle image variation is added to the Doppler power estimates in CDI and displayed using a two-dimensional color map including both Doppler power and mean frequency. BFI = blood flow imaging; B-mode = brightness mode; CDI = color Doppler imaging.

The data acquisition and data processing scheme used in BFI is schematically shown in Figure 1. As illustrated, both color Doppler and speckle images are produced from the same data recording. In parallel to conventional color Doppler processing, speckle images from blood are produced by wall filtering followed by conventional B-mode processing. Further, an amplitude-normalization procedure is applied to avoid flashing artifacts due to discontinuities in the blood signal power. Finally CDI and speckle images are combined by adding the speckle variation to the Doppler power estimates. On display, a two-dimensional (2D) color scale is used where both the mean Doppler frequency and power is included. Based on the 8–12 temporal image samples typically acquired in CDI, one color image and 4–8 speckle images can be produced. For more details on the implementation of BFI, we refer to information in a technical paper.[16]

Data Acquisition and Processing:

A full standard echocardiography examination was done in all the patients, and BFI scanning of the pulmonary veins by a pediatric cardiologist was supplemented as a part of the same examination. Flow in the pulmonary veins was examined from the suprasternal short-axis view, the apical, subcostal, and long-axis view.

When all patient data had been collected, CDI and BFI cine loops were prepared offline from the same data recordings, that is, the only difference between the two was the additional speckle visualization in BFI. The adjustments of the color information presented were identical in CDI and

BFI. The same cineloops were also presented with increased color gain (color blooming artifacts) in both modalities.

For each patient, images of the pulmonary veins from the suprasternal short-axis view and one additional view were selected and presented in a random order to four independent observers (pediatric cardiologist/cardiologists) for evaluation. The observers were not otherwise involved in the study or had information about the patients. All observers were experienced echocardiographers without previous experience with BFI. They were introduced to the method through a short presentation prior to the evaluation. The presented CDI and BFI images were not labeled in any way. However, since there is a visible difference between the methods, the observers were able to recognize the flow method presented. The observers evaluated the quality of the diagnostic imaging using a visual analogue scale (VAS), score 0% (worst) to 100% (best):

1. Clinical question: On a scale from 0% to 100%, how certain are you that there are normal pulmonary venous connections? (90% certainty means 10% chance of anomalous venous connections.)
2. General question: Please rank the general quality of the ultrasound images for the assessment of pulmonary veins (Complete evaluation including image view, image quality, color blooming, flow direction). A 100% score on the VAS scale corresponds to best possible image quality ("good"), 50% corresponds to satisfactory image quality ("fair"), and 0% corresponds to "poor" image quality.

Statistical Methods:

The null hypothesis corresponds to no difference between BFI and CDI in the visualization of flow in the pulmonary veins, and the alternative hypothesis that BFI improves the visualization.

In a prior feasibility study,[13] an absolute difference between the methods of 19% on the VAS scale was observed, a difference considered to be of clinical interest. With an observed standard deviation of 31% (absolute), a two-sided paired-samples *t*-test requires 24 observations to have a power of 80% at the 5% significance level.[19] This number was rounded upwards to accommodate deviations from normality and the use of a nonparametric test.

The methods (BFI vs. CDI) were compared within each observer using Wilcoxon's exact signed-rank test for paired samples.[20] The variability of this evaluation of quality between observers and methods was investigated using Bartlett's test of homogeneity of variance.[21] Ratings of the optimal cine loops and the cine loops with too much color gain were analyzed separately. P-values less than 0.05 were considered to be statistically significant. The statistical analysis and plotting was done in the numerical MATLAB software with the statistics toolbox (The MathWorks Inc., Natick, MA, USA), and the statistical software R.[22]

Results:

Patient Characteristics:

The age of the patients ranged from a few hours to 33 days (median age of 5.9 days). There were 17 boys and 9 girls. The patients' conditions varied from critically ill to healthy. Five patients received ventilation support during echocardiography; two patients with conventional mechanical ventilation, two patients with high-frequency ventilation and one patient with continuous positive airway pressure (CPAP). Two patients had pulmonary hypertension and 18 patients had shunts at inclusion. All patients had normal venous connections. For further patient characteristics, see Table I.

Echocardiography:

BFI was consistently ranked as better than CDI in the visualization of the pulmonary veins (Figs. 2 and 3). Median differences on the VAS scale in favor of BFI among the observers regarding pulmonary venous connections and overall pulmonary vein imaging quality ranged from 0–8% and 4–34%, respectively (all P-values $<$ 0.002). Moreover, the variance of assessment differed significantly among the observers and methods ($P < 0.001$). The difference between the methods was not altered when the color gain was increased (i.e., color blooming artifacts created).

The mean pulse repetition frequency (PRF) used during the imaging of the pulmonary veins images in this study was 3120 Hz. The mean overall color Doppler image frame rate was 23 Hz (default CDI frame rate 65 Hz) and the mean BFI frame rate was 92 Hz (The speckle images were acquired at a rate in the kilohertz range given by the PRF, and played back to the user in real time at a rate given by the total acquisition time of the whole frame of color flow data. As four speckle images were generated per color image in our data set, the frame rate of BFI is given as four times the color frame rate.) Additional BFI of the pulmonary veins prolonged the echocardiography examination with approximately 5 minutes.

Examples of BFI visualization in suprasternal short-axis view and subcostal view are shown in Figures 4 and 5 (movie clips 1 and 2).

TABLE I

Patient Characteristics

Patient	Age/days	Echocardiography Findings	Supplementary Information
1	4	Normal	Intrauterine supraventricular tachycardia
2	10	Tetralogy of Fallot	Di George syndrome, inguinal hernia, supraventricular tacycardia
3	0	Pulmonary hypertension, PDA	Duodenal atresia, infantile myofibromatosis
4	0	Muscular VSD, PDA	
5	5	Pericardial effusion, pulmonary hypertension, PDA	Diaphragmatic hernia, primary intestinal lyphangiactasia
6	21	Peripheral pulmonary stenosis	Prematurity (31weeks + 2 days)
7	2	Muscular VSD, reduced left ventricular contractility	Prematity (34 weeks), asphyxia, RDS
8	6	Secundum ASD, peripheral pulmonary stenosis	
9	0	Atrial septal aneurysm	
10	2	Muscular VSD, secundum ASD	
11	6	Normal	Prader Willi syndrome, hip dysplasia
12	2	PDA, frequent supraventricular extrasystoles	
13	1	PDA	Esophageal atresia
14	3	Normal	Hypospadia
15	0	Secundum ASD, PDA	Asphyxia
16	4	PDA	Prematurity (28 weeks + 5 days)
17	33	Peripheral pulmonary stenosis	
18	1	PDA	
19	0	Transposition of the great arteries, PDA	
20	13	Two muscular VSDs, secundum ASD	
21	3	Secundum ASD	Bilateral radial aplasia
22	0	PDA	Did not pass pulse oximetry screening (saturation 94%)
23	0	PDA, atrial septal aneurysm	Oesophageal atresia
24	20	Normal	Tacypnoea
25	5	Muscular VSD, secundum ASD	
26	12	AVSD	Down's syndrome NEC in newborn period, colonic strictures

VSD = ventricular septal defect; PDA = patent ductus arteriosus; RDS = respiratory distress syndrome; ASD = atrial septal defect; NEC = necrotizing enterocolitis; AVSD = atrioventricular septal defect.

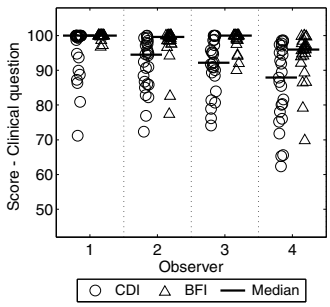

Figure 2. The clinical question to the observers: On a scale from 0% to 100% how certain are you that there are normal pulmonary venous connections? The observers' rating of CDI versus BFI is presented in this dot plot, all P-values < 0.002. Random noise is added to enhance visualization. BFI = blood flow imaging; CDI = color Doppler imaging; VAS = visual analogue scale.

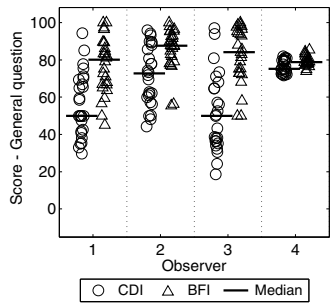

Figure 3. The general question to the observers: On a scale from 0% to 100%, please rank the general quality of the ultrasound images for the assessment of pulmonary veins (image view, image quality, color blooming, flow direction). The observers' rating of CDI versus BFI is presented in this dot plot, all P-values < 0.001. Random noise is added to enhance visualization. BFI = blood flow imaging; CDI = color Doppler imaging; VAS = visual analogue scale.

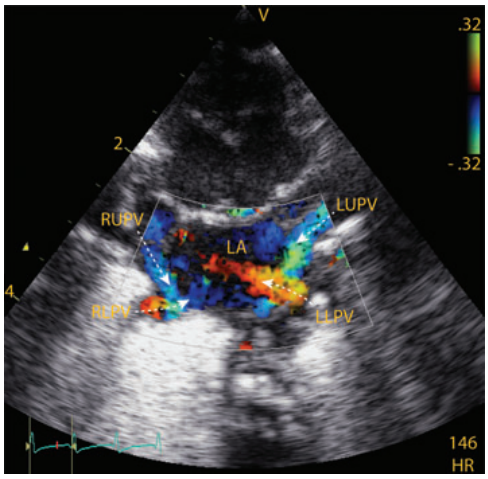

Figure 4. The pulmonary veins visualized by blood flow imaging in suprasternal short-axis view. LA = left atrium; LLPV = left lower pulmonary vein; LUPV = left upper pulmonary vein; RLPV = right lower pulmonary vein; RUPV = right upper pulmonary vein.

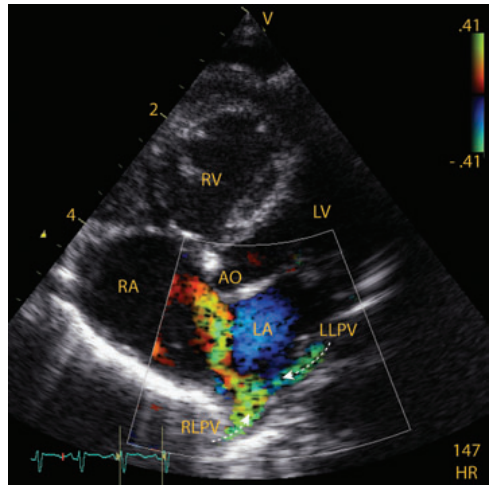

Figure 5. The pulmonary veins visualized by blood flow imaging in the subcostal view. This neonate had a small secundum atrial septal defect. Ao = aorta; LA = left atrium, LLPV = left lower pulmonary vein; RA = right atrium; RLPV = right lower pulmonary vein; RV = right ventricle.

Discussion:

We found that the new method BFI (CDI combined with the blood speckle movement) improves the imaging of the pulmonary veins in neonates compared to conventional CDI. The low velocities in the pulmonary veins are best recorded when the flow is near parallel to the sound beam. However, in the suprasternal short-axis view where all the pulmonary veins may be visualized, the ultrasound beam is not parallel to the pulmonary blood flow, and the flow may be difficult to visualize and interpret using CDI. Our study confirms that BFI is beneficial in this setting.

The speckle pattern in BFI is angle independent and thereby overcomes the main limitation of CDI. The semiquantitative color information in CDI is also available in BFI, and regions with disturbed flow are discovered in the same way as with CDI. In case of aliasing in the color, as in pulmonary vein stenosis, the speckle pattern is not influenced by this and displays the true direction of flow.

Power Doppler imaging has been shown to be superior to CDI in the visualization of fetal pulmonary veins.[23] Like BFI, Power Doppler imaging is angle independent and without velocity aliasing. However, Power Doppler imaging gives no information on the direction of flow, which is a disadvantage compared to BFI.

Cardiac catheterization with angiography, magnetic resonance angiography, and computed tomography angiography are alternative diagnostic modalities in the evaluation of anomalies in the pulmonary veins.[3] However, the need for sedation, the invasive nature, and the radiation exposure limit the value of these modalities. Further improvement of the noninvasive and less-demanding ultrasound technique is therefore still essential.

To confirm normal pulmonary connections may be challenging in the critically ill neonate with pulmonary hypertension and constriction of the pulmonary veins.[11] In our study, four patients were critically ill on inclusion. Improved diagnostic imaging in these patients is valuable, because pulmonary vein anomalies may clinically mimic persistent pulmonary hypertension.

Our prospective study did not contain neonates with pulmonary vein anomalies, and this is a limitation of the study. However, the main purpose of this first study was to demonstrate improved visualization of normally connecting veins.

BFI is a qualitative, visual technology and this implies methodological challenges. To be able to compare BFI with standard CDI, we asked the observers to rate the methods on a VAS. The observers had no access to the patient data and the cineloops were not labeled, still it was not

possible to blind the observers with regard to which method displayed, because there is a visual difference between CDI and BFI. The variance of assessment differed among the observers. Apparently, observer 2 and 4 ranked BFI and CDI in question 2 unlike observer 1 and 3. However, they all consistently ranked BFI as better than CDI.

The basic data-acquisition scheme used in BFI and CDI is identical. However, there are some differences in the choice of ultrasound imaging parameters used. In BFI, a lower PRF and higher spatial resolution may be preferred to improve the speckle visualization. This may in general come at the expense of a lowered image penetration, increased velocity aliasing artifacts in the underlying color images, and lowered overall color image frame rate. However, in the case of pulmonary vein imaging in neonates, we did not experience difficulties due to these trade-offs in the imaging setup.

In the neonate, the depths are shallow and the speckle pattern movement in BFI is clear. With increased imaging depths, as in adults, the speckle visualization may degrade, and blood flow direction becomes more challenging to perceive. Even though we did demonstrate acceptable speckle image quality in children up to 9 years,[13] this is a weakness of the method in its current implementation. However, with further utilization of parallel receive beam-forming techniques as used in real time three-dimensional cardiac imaging systems,[24] 2D BFI can be applicable for use at larger depths in the future.

Conclusion:

BFI may improve the visualization of the pulmonary veins in neonates. Switching between BFI and CDI is done quickly and easily, and we believe that alternating between the methods depending on the depth and case, would improve the ultrasound imaging.

Acknowledgments: The authors thank the observers: Anders Thorstensen, Thomas Renhult Skaug, Finn Høivik, and Terje Skjærpe for their contributions to this study.

References

1. Brown DW: Pulmonary venous anomalies. In Lai WW, Mertens LL, Cohen MS, et al. (eds): Echocardiography in Pediatric and Congenital Heart Disease: From Fetus to Adult. Chichester: Wiley-Blackwell; 2009. pp. 119–142.
2. Seliem MA: Echocardiographic and color flow Doppler assessment of systemic and pulmonary venous connection and drainage in the neonate with congenital heart disease. *Echocardiography* 1991;8:477–485.
3. Ucar T, Fitoz S, Tutar E, et al: Diagnostic tools in the preoperative evaluation of children with anomalous pulmonary venous connections. *Int J Cardiovasc Imaging* 2008;24:229–235.
4. Huang X, Huang Y, Huang T, et al: Individual pulmonary vein imaging by transthoracic echocardiography: An inadequate traditional interpretation. *Eur J Echocardiogr* 2008;9:655–660.
5. Benavidez OJ, Gauvreau K, Jenkins KJ, et al: Diagnostic errors in pediatric echocardiography: Development of taxonomy and identification of risk factors. *Circulation* 2008;117:2995–3001.
6. Stumper O, Vargas-Barron J, Rijlaarsdam M, et al: Assessment of anomalous systemic and pulmonary venous connections by transoesophageal echocardiography in infants and children. *Br Heart J* 1991;66:411–418.
7. Wong ML, McCrindle BW, Mota C, et al: Echocardiographic evaluation of partial anomalous pulmonary venous drainage. *J Am Coll Cardiol* 1995;26:503–507.
8. Hlavacek AM, Shirali GS, Anderson RH: Pulmonary venous abnormalities. In Anderson RH (ed): Paediatric Cardiology. Philadelphia, PA., Churchill Livingstone/Elsevier, 2010. pp. 497–522.
9. Minich LL, Tani LY, Breinholt JP, et al: Complete follow-up echocardiograms are needed to detect stenosis of normally connecting pulmonary veins. *Echocardiography* 2001;18:589–592.
10. Latson LA, Prieto LR: Congenital and acquired pulmonary vein stenosis. *Circulation* 2007;115:103–108.
11. Kimball TR, Weiss RG, Meyer RA, et al: Color flow mapping to document normal pulmonary venous return in neonates with persistent pulmonary hypertension being considered for extracorporeal membrane oxygenation. *J Pediatr* 1989;114:433–437.
12. Dorfman AL, Levine JC, Colan SD, et al: Accuracy of echocardiography in low birth weight infants with congenital heart disease. *Pediatrics* 2005;115:102–107.
13. Nyrnes SA, Lovstakken L, Torp H, et al: Blood flow imaging-a new angle-independent ultrasound modality for the visualization of flow in atrial septal defects in children. *Echocardiography* 2007;24:975–981.
14. Lovstakken L, Ibrahim KS, Vitale N, et al: Blood flow imaging: A new two-dimensional ultrasound modality for enhanced intraoperative visualization of blood flow patterns in coronary anastomoses. *J Am Soc Echocardiogr* 2008;21:969–975.
15. Bjaerum S, Martens D, Kristoffersen K, et al: Blood motion imaging—a new technique to visualize 2D blood flow. *Proceedings of the IEEE Ultrasonics Symposium* 2002;1507–1510.
16. Lovstakken L, Bjaerum S, Martens D, et al: Blood flow imaging—a new real-time, 2-D flow imaging technique. *IEEE Trans Ultrason Ferroelectr Freq Control* 2006;53:289–299.
17. Torp HG, Bjaerum S: Method and apparatus for visualization of motion in ultrasound flow imaging using packet data acquisition. GE Medical Systems Global Technology Company, LLC; 2003.
18. Chesarek RH: Ultrasound imaging system for relatively low-velocity blood flow at relatively high framerates. United States of America: Quantum Medical Systems, Inc.; 1989. US Patents.
19. Machin D: Sample size tables for clinical studies. Oxford, Blackwell Science; 1997, pp. 65.
20. Rosner B, ed. Fundamentals of Biostatistics. 6th ed. Pacific Grove, CA: Thomson Brooks/Cole, 2006. pp. 366–372.
21. Altman DG, ed: Practical statistics for medical research. 1st ed. London, Chapman & Hall/CRC, 1991. pp. 206–209.
22. Team RDC: R: A language and environment for statistical computing. Vienna, Austria, R Foundation for Statistical Computing, 2008.
23. Chua LK, Twining P: A comparison of power colour flow with frequency based colour flow Doppler in fetal echocardiography. *Clin Radiol* 1997;52:712–714.

24. Hergum T, Bjastad T, Kristoffersen K, et al: Parallel beamforming using synthetic transmit beams. *IEEE Trans Ultrason Ferroelectr Freq Control* 2007;54:271–280.

Supporting Information

Additional Supporting Information may be found in the online version of this article:

Movie clip 1: The pulmonary veins visualized in suprasternal short-axis view: color Doppler imaging to the left and blood flow imaging to the right.

Movie clip 2: The two lower pulmonary veins visualized from the subcostal view: color Doppler imaging to the left and blood flow imaging to the right.

Please note: Wiley-Blackwell are not responsible for the content or functionality of any supporting materials supplied by the authors. Any queries (other than missing material) should be directed to the corresponding author for the article.

Paper 3

Nyrnes SA, Løvstakken, Døhlen G, Skogvoll E, Torp H, Skjærpe T, Norgård G, Samstad S, Graven T, Haugen BO. Transesophageal echocardiography with Blood Flow Imaging during atrial septal defect closure: A comparison with the current references. Echocardiography. 2014; Apr 5. Epub ahead of print.

DOI: 10.1111/echo.12610
Echocardiography

ORIGINAL INVESTIGATION

Blood Flow Imaging in Transesophageal Echocardiography during Atrial Septal Defect Closure: A Comparison with the Current References

Siri Ann Nyrnes, M.D.,*,† Lasse Løvstakken, M.Sc., Ph.D.,* Gaute Døhlen, M.D., Ph.D.,‡ Eirik Skogvoll, M.D., Ph.D.,*,§ Hans Torp, M.Sc., Dr.Tech.,* Terje Skjærpe, M.D., Ph.D.,¶ Gunnar Norgård, M.D., Ph.D.,‡ Stein Samstad, M.D., Ph.D.,*,¶ Torbjørn Graven, M.D.,** and Bjørn Olav Haugen, M.D., Ph.D.¶,††

*Department of Circulation and Medical Imaging, Norwegian University of Science and Technology (NTNU), Trondheim, Norway; †Department of Pediatrics, St. Olav's University Hospital, Trondheim, Norway; ‡Department of Pediatric Medicine, Section for Pediatric Cardiology, Oslo University Hospital, Oslo, Norway; §Department of Anesthesiology and Emergency Medicine, St. Olav's University Hospital, Trondheim, Norway; ¶Department of Cardiology, St. Olav's University Hospital, Trondheim, Norway; **Levanger Hospital, Nord-Trøndelag Health Trust, Levanger, Norway; and ††MI-Laboratory, Department of Circulation and Medical Imaging, NTNU, Trondheim, Norway

Background: Flow visualization before transcatheter atrial septal defect (ASD) closure is essential to identify the number and size of ASDs and to map the pulmonary veins (PV). Previous reports have shown improved visualization of ASD and PV using blood flow imaging (BFI), which supplements color Doppler imaging (CDI) with angle-independent information of flow direction. In this study, we compared transesophageal BFI with the current references in ASD sizing (balloon stretched diameter, BSD) and PV imaging (pulmonary angiography). Methods: In this prospective study, 28 children were examined with transesophageal echocardiography (TEE) including BFI of the secundum ASD and the PV before interventional ASD closure. The maximum ASD diameter measured with BFI by 4 observers was compared to the corresponding BSD and CDI measurements. The repeatability of the BFI measurements was calculated as the residual standard deviation. BFI of the PV was compared to PV angiography. Results: The mean maximum diameter measured by BFI was 12.1 mm (±SD 2.4 mm). The corresponding BSD and CDI measurements were 15.9 mm (±SD 3.0 mm) and 11.8 mm (±SD 2.5 mm), respectively. The residual standard deviation was 1.2 mm. Compared to PV angiography, the sensitivity of BFI in detecting the correct entry of the PV was 0.96 (95% CI: 0.82–1.0). Conclusion: Transesohageal echocardiography with BFI of the PV agreed well with pulmonary angiography. BFI had lower estimates for ASD size than BSD, but with acceptable 95% limits of agreement. The repeatability of the BFI measurements was close to the inherent ultrasound measurement error. (Echocardiography 2014;00:1–8)

Key words: atrial septal defect, pulmonary veins, flow visualization, blood flow imaging, transesophageal echocardiography

High-quality imaging of atrial septal defect (ASD) size and morphology before transcatheter closure is essential for a successful outcome, and there has recently been much interest in advances in technology to improve visualization of the complex septal anatomy.[1–6]

Less interest has been set on further improvements of flow visualization, which is important to identify the number and size of ASDs, the direction of blood flow through the defects, and to differentiate dropouts in the region of the fossa ovalis from an ASD. Finally, as partial anomalous pulmonary venous connection is associated with ASD,[7] thorough flow-mapping of the pulmonary veins (PV) is essential.[8]

Traditionally, transcatheter ASD closure has included balloon sizing, fluoroscopy, and pulmonary angiography. The radiation exposure from

Funding Sources: The work was financially supported by a grant from Liaison Committee between the Central Norway Regional Health Authority (RHA) and the Norwegian University of Science and Technology (NTNU) and the MI-laboratory, Department of Circulation and Medical Imaging, NTNU, Trondheim.
Address for correspondence and reprint requests: Siri Ann Nyrnes, M.D., Department of Circulation and Medical Imaging, Norwegian University of Science and Technology, Olav Kyrresgt. 9, 7489 Trondheim, Norway. Fax: +47 73598613; E-mail: siri.a.nyrnes@ntnu.no

cardiac catheterization is of concern both to patients and operators,[9] and should be limited to lowest possible values. Furthermore, contrast agents may have side effects,[10] and should be restricted whenever possible. The balloon sizing procedure has potential risks,[11] and transcatheter closure of ASDs following less invasive sizing techniques has been advocated.[12–14]

Atrial septal defect measurements by color Doppler imaging (CDI) correlate with the balloon stretch diameter,[15] and transcatheter ASD closure guided by the maximal color flow diameter has recently been shown to be feasible and safe.[12] However, CDI has limitations that include angle dependence, aliasing, and a frame rate which is considerably less than that of grayscale imaging.[16]

Blood flow imaging (BFI) is a new ultrasound modality which supplements CDI with angle-independent information of flow direction that is not influenced by velocity aliasing.[17] This is done by visualizing the blood speckle movement superimposed on the color Doppler images. Previous reports using BFI in comparison with CDI in transthoracic echocardiography (TTE) (GE Vingmed Vivid 7, GE Vingmed, Horten, Norway) with GE M4S and GE 7S cardiac probes (GE Healthcare, Milwaukee, WI, USA) has shown better visualization of flow both through the ASD and in the mapping of PV.[18,19] The aim of this study was to compare the new method BFI with current references in ASD sizing (balloon stretched diameter [BSD]) and PV imaging (pulmonary angiography) for a complete assessment of ASD, and for the first time transesophageally.

Methods:

Patients:

This prospective study was a collaboration project between the Department of Pediatric Medicine, Section for Pediatric Cardiology, Oslo University Hospital, Rikshospitalet, Norway and the Norwegian University of Science and Technology (NTNU)/St. Olav's University Hospital, Trondheim, Norway. Patient inclusion took place in Rikshospitalet, were all interventional pediatric ASD closures in Norway are centralized. NTNU/St Olav's University Hospital contributed with the new technology BFI and echocardiography.

The inclusion criteria in the study were children aged 0–16 years with isolated secundum ASD accepted for interventional ASD closure. To be accepted for interventional closure, the secundum ASD had to be hemodynamic significant, that is, there was signs of pulmonary hyperflow with qualitative evidence of right ventricular and/or right atrial dilatation on echocardiography. A total of 28 children scheduled to interventional ASD closure were included prospectively from February 2008 to February 2009. The patients were recruited from hospitals all over Norway. The ratio of pulmonary to systemic blood flow (Qp/Qs) was calculated from saturations obtained from superior and inferior vena cava, PV and artery and systemic saturation. ASD closure device was chosen based on balloon sizing using the stop flow technique.[11]

Informed consent was obtained from all the parents and also from children above 12 years of age. The study was approved by The Regional Committee for Medical and Health Research Ethics (REK) and the Norwegian Social Science Data Services (NSD).

Equipment:

The transesophageal echocardiography (TEE) examinations were performed using a GE Vingmed Vivid 7 with a 9T or 6T probe. (GE Healthcare, Milwaukee, WI, USA). Image analysis was done in a custom software package (GcMat, GE Vingmed), while statistical analysis was done using IBM (Armonk, NY, USA) SPSS version 19 and package lme4 of the software R version 2.15.[20]

Imaging by using BFI has the same restrictions regarding patient security as conventional CDI, and satisfy the requirements from the American Food and Drug Administration.

BFI in Transesophageal Echocardiography:

The BFI technique is commercially available for vascular imaging on GE systems, but was not initially available for use with TEE probes. For this project development, efforts were made to make the BFI technique available for TEE probes, and to make suitable applications for BFI in TEE during ASD closure.

In CDI, the velocity component transversal to the ultrasound beam cannot be estimated from the received Doppler signal. The BFI technique supplements CDI with an angle- and aliasing-independent visualization of blood speckle movement.[17] By displaying this additional speckle pattern, acquired with a high frame rate in slow motion, the human eye can detect blood flow in any direction of the ultrasound image. The BFI technique is based on the same data acquisition scheme as CDI, but some trade-offs regarding optimal CDI setup is often needed to ensure suitable blood speckle visualization. The pulse repetition frequency (PRF) often needs to be reduced which may increase aliasing artifacts in CDI. Further, the image resolution and line density needs to be increased to ensure sufficient quality of speckle images, something which may lead to a

reduced penetration and color Doppler frame rate. However, in BFI 4–8 speckle images are produced for each color Doppler image, and the imaging frame rate of the speckle information is higher than the Doppler information in CDI.

The lateral image resolution in this setup was approximately 1.0–1.3 mm for the 6T probe and 1.0–1.4 mm for the 9T probe. The axial image resolution was approximately 0.4–0.5 mm for both probes.

Data Acquisition and Processing:
A full-standard TEE examination was done in all the patients before the transcatheter closing procedure, and BFI scanning of the ASD and the PV was supplemented as a part of the same examination.

ASD Sizing: When all patient data had been collected, BFI and CDI movie clips were prepared off line from the data recordings. The only difference between the 2 was the additional speckle visualization in BFI. The technical adjustments of the color information presented were identical in CDI and BFI.

The movie clips were presented to 4 observers who were blinded to the patient data. The observers were experienced echocardiographers (consultant cardiologists) without previous experience with BFI. They were given a short introduction to the BFI method prior to the evaluation. The presented CDI and BFI images were not labeled in any way, neither with respect to patient number. However, as there is an obvious visible difference between the methods, the observers were able to recognize the flow method presented. The observers were asked to measure the ASD size in the presented BFI and CDI images. If there were more than 1 ASD present in 1 movie clip, they were asked to measure the largest defect.

The process of measurements of the BFI and CDI movie clips is described in Figure 1. In each patient, a screen with 2 movie clips showing the ASD in the 2 widest planes (movie clips 1 and 2) were presented with BFI. The same BFI screen was repeated once during the measurement process. Identical screens showing the ASD visualized with CDI from the same patient were presented in the same manner. This means that the process described in Figure 1 was performed once for each method (BFI and CDI). Thus, every observer made 8 ASD measurements in each patient (4 measurements with BFI and 4 measurements with CDI). The BFI and CDI screens and replications were presented to the observers in a random order.

To reflect the clinical reality, we chose the maximum ASD diameter measured with BFI (BFI-max, later referred to as "BFI" only) in each observer for comparison with BSD and CDI measurements.

Pulmonary Veins: The PV were evaluated during the examination by an echo technician in cooperation with a pediatric cardiologist using BFI. The results were recorded as one of the following: Normal PV, 1 anomalous PV, 2 anomalous PV, or PV stenosis. The BFI investigations were finished and documented before the PV eventually were examined by routine angiography by the interventionist.

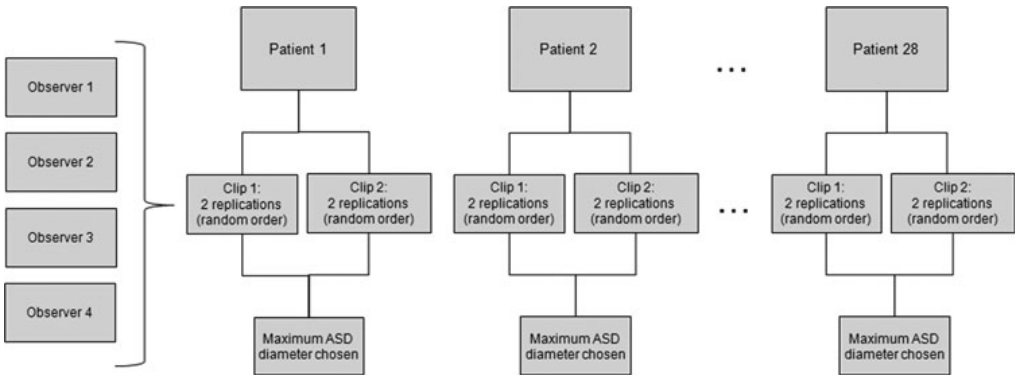

Figure 1. Description of method for atrial septal defect (ASD) measurements with blood flow imaging (BFI) and color Doppler imaging (CDI) in 4 observers: In each patient, 2 identical screens (2 replications) with movie clips displaying the ASD in the 2 widest planes (movie clips 1 and 2) were presented with BFI and CDI. The observers thus measured the ASD in 2 planes twice with both methods (4 BFI measurements and the corresponding 4 CDI measurements). For each patient, the maximum ASD diameter was chosen for further analysis. This figure also illustrates the linear mixed-effects model which was used to assess repeatability.

Statistical Methods:
ASD Sizing: The mean difference between the BFI and BSD measurements and the BFI and CDI measurements were analyzed using a paired samples *t*-test. Furthermore, the BFI and BSD measurements and the BFI and CDI measurements were plotted against the other. Finally, agreement between the BFI and BSD measurements and the BFI and CDI measurement were evaluated using Bland–Altman plots, in which the difference between BSD and BFI measurements and BFI and CDI measurement were plotted against their respective means.[21]

To assess repeatability, a linear mixed-effects model with BFI as the outcome variable was employed in a variance components model. We treated observers and patients as crossed random factors (Fig. 1), whose net effects are assumed to be zero. The residual error of this model yields a measure of repeatability, that is, the remaining variation when different observers do measure identical movie clips in the same patient. Estimation was done with restricted maximum likelihood using the *lmer* command of R version 2.15.[20]

Pulmonary Veins: By visualizing the PV with BFI and compared with the reference method angiography, one can calculate sensitivity and specificity for the new method. Point estimates with exact 95% confidence intervals (CI) were calculated based on the binomial distribution.

Results:
Patient Characteristics:
The age of the patients ranged from 8.5 months to 16 years. There were 19 girls and 9 boys, and 9 patients had more than 1 ASD. The BSD ranged from 9.5 to 20.5 mm and the ratio of pulmonic (Qp) to systemic (Qs) blood flow ranged from 1.2 to 4. Four patients had Qp/Qs < 1.5. However, closure was considered reasonable because these patients had echocardiographic evidence of right atrium and right ventricular dilatation. Furthermore, they had a rather large ASD and/or more than one defect. None of the patients had pulmonary hypertension, 19 patients had a systolic murmur, and 18 patients had a split second sound.

A total of 27 patients underwent successful ASD Amplatzer closure; 2 of these patients required 2 devices. In 1 patient, closure attempt was unsuccessful because of insufficient attachment of the Amplatzer device to the atrial septal rims.

By June 2012 (3–4 years after closure), there were no registered complications among the patients. In 2 patients the Amplatzer device was touching the mitral valve, but there were no mitral obstruction or insufficiency. One patient had a large device related to septal size. In this patient, there were temporary increased flow velocities in the upper left PV. But from 1 year after closure, there were no signs of obstruction of this PV.

Echocardiography Probes:
The transesophageal examination was done using the 6T probe in 4 patients and the 9T probe in 24 patients.

ASD Sizing:
The mean maximum diameter measured by BSD was 15.9 mm (±SD 3.0 mm), and the mean maximum diameter measured by BFI was 12.1 mm (±SD 2.4 mm); yielding a mean difference between the measurements of 3.8 mm (±SD 2.2 mm), with a 95% confidence interval (CI) from 3.4 to 4.2 mm. The 95% limits of agreement extended from −0.7 to 8.3 mm with no obvious trend in the data.

Figure 2 shows the scatter plot of the BSD measurements versus the BFI ASD diameter measurements and Figure 3 shows the Bland–Altman plot with 95% limits of agreement for the difference between the BSD and BFI measurements.

The corresponding ASD diameter measured by CDI was 11.8 mm (±SD 2.5 mm); yielding a mean difference between the CDI and BFI measurements of −0.3 mm (±SD 1.3 mm) with a 95% CI from −0.6 to −0.1 mm. The 95% limits of agreement extended from −3.0 to 2.3 with no obvious trend in the data.

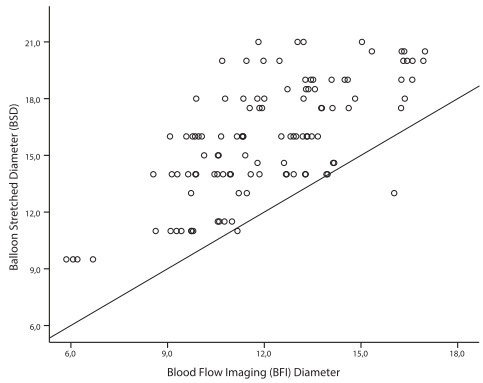

Figure 2. Two methods of measuring atrial septal defect (ASD) size, in mm: The maximum ASD diameter measured by blood flow imaging (BFI) and balloon stretched diameter (BSD) in 28 patients measured by 4 observers. In the scatter plot, the 2 methods of measurements (BSD and BFI) are plotted against each other. The figure demonstrates that almost all BSD measurements were larger than BFI measurements.

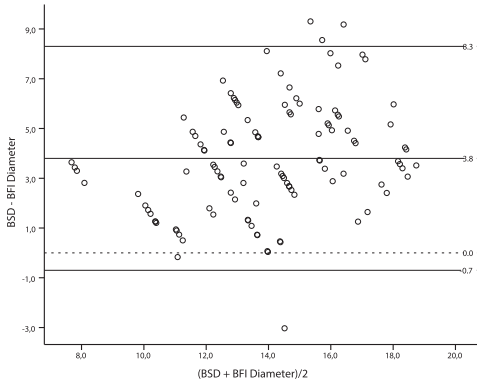

Figure 3. Two methods of measuring atrial septal defect (ASD) size, in mm: The maximum ASD diameter measured by blood flow imaging (BFI) and balloon stretched diameter (BSD) in 28 patients measured by 4 observers. The Bland–Altman plot shows differences against the mean and 95% limits of agreement.

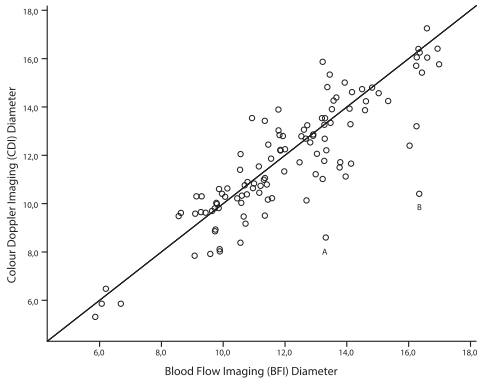

Figure 4. Two methods of measuring atrial septal defect (ASD) size, in mm: The maximum ASD diameter measured by blood flow imaging (BFI) and the paired color Doppler imaging (CDI) measurements in 28 patients measured by 4 observers. In the scatter plot, the 2 methods of measurements (CDI and BFI) are plotted against each other. There were 2 outliers labeled A and B. The corresponding balloon stretched diameter (BSD) measurements for A and B were 16 mm and 20.5 mm, respectively.

Figure 4 shows the scatter plot of the CDI measurements versus the corresponding BFI measurements and Figure 5 shows the Bland–Altman plot with 95% limits of agreement for the difference between the BFI and CDI measurements. There were 2 outliers labeled A and B in Figures 4 and 5. The outlier A measurements were CDI 8.6 mm, BFI 13.3 mm, and corresponding BSD 16 mm. The outlier B measurements were

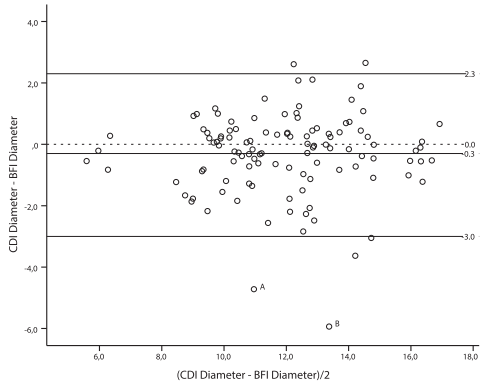

Figure 5. Two methods of measuring atrial septal defect (ASD) size, in mm: The maximum ASD diameter measured by blood flow imaging (BFI) and the paired color Doppler imaging (CDI) measurements in 28 patients measured by 4 observers. The Bland–Altman plot shows differences against the mean with 95% limits of agreement. There were 2 outliers labeled A and B. The corresponding balloon stretched diameter (BSD) measurements for A and B were 16 mm and 20.5 mm, respectively.

CDI 10.4 mm, BFI 16.3, and corresponding BSD 20.5 mm. As we could not identify obvious errors regarding these outliers, we kept them in the material.

Figure 6 demonstrates the transesophageal examination (6T probe) from a patient who had 2 separate ASDs. This patient was 14 years old, 176 cm, and 61.8 kg. The BSD in the largest defect were 13 mm. A corresponding movie clip demonstrating ASD flow in the transesophageal examination from this patient (movie clip S1) can be downloaded from the additional supporting information in the online version of this article. BFI is best demonstrated through movie clips, and in movie clip S2 there is another example from a 16-year-old patient with 1 ASD (BSD 18 mm).

The Repeatability of the BFI Measurements:
The linear mixed-effects model (Fig. 1) yielded the following standard deviation estimates; patient 2.1 mm, observer 0.4 mm, and residual (i.e. the movie clips presented) 1.2 mm. Given a mean BFI value of 12.1 mm this corresponds to coefficients of variation (CV) of 18%, 4%, and 9.6%, respectively. The latter may be taken as a measure of repeatability, the remaining variation when different observers do measure identical movie clips in the same patient.

The Pulmonary Veins:
Pulmonary angiography demonstrated normal pulmonary connections for all PV branches in the

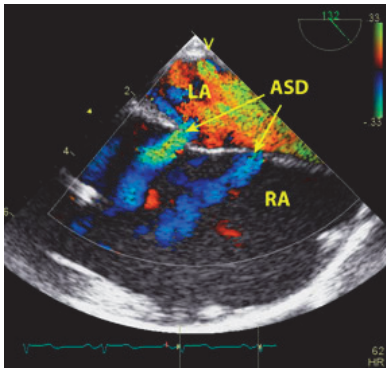

Figure 6. Transesophageal long-axis view of the atrial septum: Blood flow imaging in the visualization of 2 atrial septal defects (ASD), the left atrium (LA) and the right atrium (RA). A movie clip of this figure can be seen in the corresponding movie clip S1.

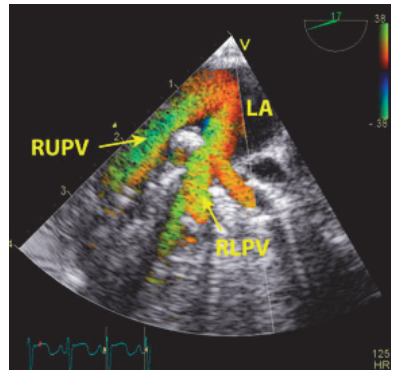

Figure 7. Transesophageal blood flow imaging in the visualization of the right upper (RUPV) and right lower pulmonary vein (RLPV) entering the left atrium (LA). A movie clip of this figure can be seen in the corresponding movie clip S3.

28 patients. Visualization of the upper left and the upper and lower right PV using transesophageal examination with BFI was successful in all patients. The site of drainage of the left lower PV was identified in 27 of the 28 patients studied. In 1 patient, the left lower PV was difficult to visualize using BFI (and CDI) in TEE. Pulmonary angiography visualized the lower left pulmonary artery in this patient, and the drainage was normal—as were the other PV in this patient. Pulmonary angiography corresponded with the BFI visualization of PV branches in all patients except in this case. This leads to a sensitivity of BFI in detecting the correct entry of the PV of 0.96 (95% CI: 0.82–1.0).

An example of transesophageal BFI visualization of the right-sided PV is shown in Figure 7. This image is from a patient who was 1 year and 3 months old, 81 cm, and 11.7 kg. We used the 9T probe in this examination. A corresponding movie clip (movie clip S3) can be downloaded from the additional supporting information in the online version of this article.

Discussion:

We have previously found that TTE with the new flow imaging technique BFI may improve the visualization of interatrial blood flow in children and the PV in neonates.[18,19] In this transesophageal echo study, we compared this technique with the current reference methods for ASD sizing BSD and PV imaging (pulmonary angiography). We have described and quantified the agreement between the corresponding BSD and BFI ASD measurements and assessed repeatability of BFI measurements. BFI had lower estimates for ASD size than BSD, but with acceptable 95% limits of agreement. The mean maximum diameter measured by BFI was 3.8 mm less than the mean of BSD measurements. The paired CDI measurement was 0.3 mm less than the BFI measurement. Tzifa et al.[12] demonstrated similar results; they found that the mean maximal diameter measured with CDI was 4.6 mm and 3.3 mm less than the BSD measurements in the prospective and retrospective groups, respectively. The difference between the BFI and BSD measurements can be explained by the fact that BSD also provides information of physical stretch that cannot be predicted by echocardiography. The relationship between the maximal BFI diameter measured in two-dimensional (2D) echo and BSD is also influenced by the shape of the ASD.[22]

The true ASD size was unknown in this study, but we chose to compare the BFI measurements with the BSD, as this method still is regarded as the reference for measuring ASD maximal diameter to select the appropriate size of the device before closure. However, balloon sizing is not considered necessary by some authors,[12–14] and BSD are consequently no longer performed in many centers that use Amplatzer devices to close ASDs. Balloon sizing may oversize an ASD,[13] which may increase the risk of erosion. The stop flow technique was proposed to diminish this problem.[23] Other potential disadvantages of balloon sizing are bradycardia, hypotension, and enlargement of the defect. If there are multiple defects and a floppy septum, echocardiography may be better than BSD in the estimation of size.[24]

The repeatability of the BFI measurements in this study was consistent both between the observers and within each observer. Other studies measuring ASD diameter with color flow

diameter did not investigate the repeatability of the CDI measurements.[12,25] It is important to be aware that some of the variability between measurements in different studies using 2D imaging may be due to differences attained by different observers.[26]

In the present study, we also compared visualization of the PV using BFI with the traditional reference method; pulmonary angiography. Pulmonary angiography corresponded with the BFI visualization of PV branches in all patients except in 1 patient; here, the left lower PV was difficult to visualize using TEE with BFI. However, this PV was visualized using TTE with BFI the day before the procedure. Even though TEE images are usually of better quality than TTE images, the limited imaging windows and planes in TEE do restrict both imaging and alignment for Doppler velocity recording. Furthermore, the PV may be too close to the TEE probe for proper imaging or flow evaluation.[27] TTE and TEE together will usually be sufficient to map the PV, and routine pulmonary angiography during ASD closure has now been abandoned in Department of Pediatric Medicine, Section for Pediatric Cardiology, Oslo University Hospital, Rikshospitalet, Norway.

The new real time 3DTEE for guidance of percutaneous ASD closure seems promising, but still there is limited experience in patients <60 kg.[1] To define the plane with the maximum ASD diameter may be more easy using 3DTEE than 2DTEE.[22] Even though 3D may be best for visualization of anatomy, this is not the case for flow, due to low frame rate and resolution. Another limitation of the current 3DTEE systems is dropouts in the fossa ovale region.[2] These dropouts may be minimized by combining with 2D flow techniques. The best method for selecting an optimal device size may be to consider different measurements with different methods.[22]

Color Doppler imaging measurements of ASD have sources of error in determining the size of the jet, including CDI gain, examination depth, and transducer frequency. CDI may also underestimate an irregular defect, because the 2D ultrasound beam may not cut the defect in its maximal diameter. The same sources of error must be taken in account using BFI. However, a pilot study indicates that BFI is less dependent on gain setting.[18] The additional speckle pattern in BFI has the potential to improve the ASD edge detection. This may diminish the sources of error in determining ASD size.

In spite of recent advances in technology, we still lack a true gold standard for the measurement of ASD size and shape, and this is a limitation of the measurement comparison in this study. An additional limitation of this study was that no patients had anomalous PV and therefore, usefulness of BFI in detecting anomalous PV was not tested.

In its current implementation, the method BFI is limited to imaging shallow depths (<10 cm), suitable for instance for vascular imaging and imaging in pediatric cardiology.[18,19,28] However, getting closer to the heart through the esophagus implies that the method should also have potential for cardiac imaging in adults using TEE. Our study had a variation in patient size from 6.2 to 67.5 kg which demonstrates this potential. Two of the movie clip examples are from patients with adult size (movie clips S1 and S2).

Improved echocardiographic imaging before and during transcatheter ASD closure may reduce radiation exposure and possible also the need for balloon sizing. We believe that BFI may be a suitable supplement in this complete echocardiographic ASD evaluation.

Equipment malfunction, inherent limitations of echocardiography, or imaging artifacts are significant contributors to diagnostic errors in pediatric echocardiography.[29] Further work may uncover whether the angle-independent information provided by BFI may help reduce these errors. Technically, the BFI technique is continuously being improved in terms of increased imaging depths and speckle movement visualization. Further, by utilizing computer tracking algorithms, we have recently been able to quantify the 2D blood velocity and direction.[30] This flow speckle tracking technique has the potential to demonstrate complex flow patterns in heart defects and to quantify shunt flow.

Conclusion:

Transesophageal echocardiography with BFI of the PV agreed well with pulmonary angiography. BFI has lower estimates for ASD size than BSD, but with acceptable 95% limits of agreement. The repeatability of the BFI measurements was close to the inherent measurement error of the ultrasound measurement itself. BFI may offer a complete assessment of ASD and has the potential to reduce radiation exposure time during ASD closure.

Acknowledgments: Thanks to echo technician Kjetil Lenes who at time of patient inclusion worked in Department of Pediatric Medicine, Section for Pediatric Cardiology, Oslo University Hospital, Rikshospitalet, Norway.

References

1. Lodato JA, Cao QL, Weinert L, et al: Feasibility of real-time three-dimensional transoesophageal echocardiography for guidance of percutaneous atrial septal defect closure. *Eur J Echocardiogr* 2009;10:543–548.
2. Saric M, Perk G, Purgess JR, et al: Imaging atrial septal defects by real-time three-dimensional transesophageal

echocardiography: Step-by-step approach. *J Am Soc Echocardiogr* 2010;23:1128–1135.
3. Johri AM, Witzke C, Solis J, et al: Real-time three-dimensional transesophageal echocardiography in patients with secundum atrial septal defects: Outcomes following transcatheter closure. *J Am Soc Echocardiogr* 2011;24:431–437.
4. Faletra FF, Nucifora G, Ho SY: Imaging the atrial septum using real-time three-dimensional transesophageal echocardiography: Technical tips, normal anatomy, and its role in transseptal puncture. *J Am Soc Echocardiogr* 2011;24:593–599.
5. Bhaya M, Mutluer FO, Mahan E, et al: Live/Real time three-dimensional transesophageal echocardiography in percutaneous closure of atrial septal defects. *Echocardiography* 2013;30:345–353.
6. Garcia-Fuertes D, Mesa-Rubio D, Ruiz-Ortiz M, et al: Monitoring complex secundum atrial septal defects percutaneous closure with real time three-dimensional echocardiography. *Echocardiography* 2012;29:729–734.
7. Brown DW: Pulmonary venous anomalies. In Lai WW, Mertens LL, Cohen MS, Geva T (eds): *Echocardiography in Pediatric and Congenital Heart Disease: From Fetus to Adult*. Chichester, UK: Wiley-Blackwell, 2009, pp. 119–142.
8. Amirghofran AA, Karimi A, Ajami GH, et al: The importance of localizing pulmonary veins in atrial septal defect closure!. *J Cardiothorac Surg* 2011;6:41.
9. Picano E, Vano E, Rehani MM, et al: The appropriate and justified use of medical radiation in cardiovascular imaging: A position document of the ESC Associations of cardiovascular imaging, percutaneous cardiovascular interventions and electrophysiology. *Eur Heart J*. 2014;35:665–672.
10. Brasch RC: Contrast media toxicity in children. *Pediatr Radiol* 2008;38(Suppl 2):S281–S284.
11. Amin Z: Transcatheter closure of secundum atrial septal defects. *Catheter Cardiovasc Interv* 2006;68:778–787.
12. Tzifa A, Gordon J, Tibby SM, et al: Transcatheter atrial septal defect closure guided by colour flow Doppler. *Int J Cardiol* 2011;149:299–303.
13. Quek SC, Wu WX, Chan KY, et al: Transcatheter closure of atrial septal defects–is balloon sizing still necessary? *Ann Acad Med Singapore* 2010;39:390–393.
14. Wang JK, Tsai SK, Lin SM, et al: Transcatheter closure of atrial septal defect without balloon sizing. *Catheter Cardiovasc Interv* 2008;71:214–221.
15. Godart F, Rey C, Francart C, et al: Two-dimensional echocardiographic and color Doppler measurements of atrial septal defect, and comparison with the balloon-stretched diameter. *Am J Cardiol* 1993;72:1095–1097.
16. Ferrara K, DeAngelis G: Color flow mapping. *Ultrasound Med Biol* 1997;23:321–345.
17. Lovstakken L, Bjaerum S, Martens D, et al: Blood flow imaging–A new real-time, 2D flow imaging technique. *IEEE Trans Ultrason Ferroelectr Freq Control* 2006;53:289–299.
18. Nyrnes SA, Lovstakken L, Torp H, et al: Blood flow imaging-a new angle-independent ultrasound modality for the visualization of flow in atrial septal defects in children. *Echocardiography* 2007;24:975–981.
19. Nyrnes SA, Lovstakken L, Skogvoll E, et al: Does a new ultrasound flow modality improve visualization of neonatal pulmonary veins? *Echocardiography* 2010;27:1113–1119.
20. Team RDC: *R: A Language and Environment for Statistical Computing*. Vienna, Austria: R Foundation for Statistical Computing, 2012.
21. Bland JM, Altman DG: Statistical methods for assessing agreement between two methods of clinical measurement. *Lancet* 1986;1:307–310.
22. Seo JS, Song JM, Kim YH, et al: Effect of atrial septal defect shape evaluated using three-dimensional transesophageal echocardiography on size measurements for percutaneous closure. *J Am Soc Echocardiogr* 2012;25:1031–1040.
23. Carlson KM, Justino H, O'Brien RE, et al: Transcatheter atrial septal defect closure: Modified balloon sizing technique to avoid overstretching the defect and oversizing the Amplatzer septal occluder. *Catheter Cardiovasc Interv* 2005;66:390–396.
24. Abdel-Massih T, Dulac Y, Taktak A, et al: Assessment of atrial septal defect size with 3D-transesophageal echocardiography: Comparison with balloon method. *Echocardiography* 2005;22:121–127.
25. Faletra F, Scarpini S, Moreo A, et al: Color Doppler echocardiographic assessment of atrial septal defect size: Correlation with surgical measurements. *J Am Soc Echocardiogr* 1991;4:429–434.
26. Smallhorn JF, Khoo NS: Quantitative echocardiography in pediatrics–are we there yet? *J Am Soc Echocardiogr* 2012;25:855–858.
27. Stevenson JG: Transesophageal Echocardiography. In Lai WW, Mertens LL, Cohen MS, et al, (eds): *Echocardiography in Pediatric and Congenital Heart Disease*. Chichester, UK: Wiley-Blackwell, 2009, pp. 671–686.
28. Lovstakken L, Ibrahim KS, Vitale N, et al: Blood flow imaging: A new two-dimensional ultrasound modality for enhanced intraoperative visualization of blood flow patterns in coronary anastomoses. *J Am Soc Echocardiogr* 2008;21:969–975.
29. Benavidez OJ, Gauvreau K, Jenkins KJ, et al: Diagnostic errors in pediatric echocardiography: Development of taxonomy and identification of risk factors. *Circulation* 2008;117:2995–3001.
30. Nyrnes SA, Lovstakken L, Torp H, et al: Flow speckle tracking for detailed visualization of flow patterns in neonates with congenital heart defects. *Eur J Echocardiogr* 2011:12:ii127.

Supporting Information

Additional Supporting Information may be found in the online version of this article:

Movie clip S1. Blood flow imaging in the visualization of 2 atrial septal defects (ASD), the left atrium (LA) and the right atrium (RA).

Movie clip S2. Blood flow imaging in the visualization of an atrial septal defect (ASD), the left atrium (LA), left ventricle (LV), right atrium (RA), and right ventricle (RV).

Movie clip S3. Blood flow imaging in the visualization of the right upper (RUPV) and right lower (RLPV) pulmonary vein entering the left atrium (LA).

Paper 4

Fadnes S, Nyrnes SA, Torp H, Løvstakken L. Shunt flow evaluation in congenital heart disease based on Two-Dimensional Speckle tracking. Ultrasound Med Biol;2014;40(10):2379-2391.

Ultrasound in Med. & Biol., Vol. 40, No. 10, pp. 2379–2391, 2014

0301-5629/$ - see front matter

http://dx.doi.org/10.1016/j.ultrasmedbio.2014.03.029

● *Original Contribution*

SHUNT FLOW EVALUATION IN CONGENITAL HEART DISEASE BASED ON TWO-DIMENSIONAL SPECKLE TRACKING

Solveig Fadnes,* Siri Ann Nyrnes,*† Hans Torp,* and Lasse Lovstakken*
*MI Lab and the Department of Circulation and Medical Imaging, Norwegian University of Science and Technology, Trondheim, Norway; and †Department of Pediatrics, St. Olav's University Hospital, Trondheim, Norway

(*Received* 12 *April* 2013; *revised* 25 *March* 2014; *in final form* 31 *March* 2014)

Abstract—High-frame-rate ultrasound speckle tracking was used for quantification of peak velocity in shunt flows resulting from septal defects in congenital heart disease. In a duplex acquisition scheme implemented on a research scanner, unfocused transmit beams and full parallel receive beamforming were used to achieve a frame rate of 107 frames/s for full field-of-view flow images with high accuracy, while also ensuring high-quality focused B-mode tissue imaging. The setup was evaluated *in vivo* for neonates with atrial and ventricular septal defects. The shunt position was automatically tracked in B-mode images and further used in blood speckle tracking to obtain calibrated shunt flow velocities throughout the cardiac cycle. Validation toward color flow imaging and pulsed wave Doppler with manual angle correction indicated that blood speckle tracking could provide accurate estimates of shunt flow velocities. The approach was less biased by clutter filtering compared with color flow imaging and was able to provide velocity estimates beyond the Nyquist range. Possible placements of sample volumes (and angle corrections) for conventional Doppler resulted in a peak shunt velocity variations of 0.49–0.56 m/s for the ventricular septal defect of patient 1 and 0.38–0.58 m/s for the atrial septal defect of patient 2. In comparison, the peak velocities found from speckle tracking were 0.77 and 0.33 m/s for patients 1 and 2, respectively. Results indicated that complex intraventricular flow velocity patterns could be quantified using high-frame-rate speckle tracking of both blood and tissue movement. This could potentially help increase diagnostic accuracy and decrease interobserver variability when measuring peak velocity in shunt flows. (E-mail: solveig.fadnes@ntnu.no) © **2014 World Federation for Ultrasound in Medicine & Biology.**

Key Words: **2-D blood flow imaging, Speckle tracking, *In vivo*, Atrial septal defect, Ventricular septal defect.**

INTRODUCTION

Atrial (ASDs) and ventricular (VSDs) septal defects are the two most common forms of congenital heart defects (van der Linde et al. 2011). The natural history of small septal defects may be regression or spontaneous closure (Hanslik et al. 2006; Penny and Vick 2011), whereas more severe defects must be repaired by catheter closure or corrective surgery. The management of an ASD or VSD depends on the location, size, hemodynamic consequences, associated defects and the symptomatology of the patient. Generally, the clinical approach is to repair an isolated ASD or VSD when there is a large left-to-right shunt (Driscoll et al. 1994). In pediatric cardiology today, 2-D echocardiography with color flow imaging (CFI) is used to detect and visualize septal defects. Continuous wave Doppler and pulsed wave (PW) Doppler are utilized to estimate the peak velocity and evaluate the shunt flow (Forbus and Shirali 2009).

Color flow imaging and continuous wave and pulsed wave Doppler have been extensively validated and are used in a wide range of clinical settings, but the methods have fundamental limitations. The frequency shifts between the transmitted and received ultrasound waves are used to estimate the blood velocity components along the ultrasound beam axis. The velocity estimates are thus limited to one component of the velocity vector and dependent on the angle between the ultrasound beam and the blood flow direction, and the resulting color flow images can be difficult to interpret. In addition, CFI and PW Doppler are based on pulsed transmission of ultrasound waves, and the pulse repetition frequency limits the highest measurable velocities according to the Nyquist sampling theorem. Velocities above the Nyquist limit are commonly encountered and will give aliasing

Address correspondence to: Solveig Fadnes, MI Lab and Department of Circulation and Medical Imaging, NTNU, Postboks 8905, 7491 Trondheim, Norway. E-mail: solveig.fadnes@ntnu.no

artifacts in the image where high velocities will not be displayed correctly. These fundamental limitations may lead to undetected defects and misdiagnosis (Benavidez et al. 2008).

To improve imaging and evaluation of shunt flows, other modalities have been suggested. Real-time 3-D echocardiography has yielded promising results in the visualization of septal defects (Acar et al. 2007; Cheng et al. 2004), but the blood flow estimation is still angle dependent. In transesophageal echocardiography, the probe is led down the patient's esophagus, and cardiac images of higher quality are achieved. Also, cardiac magnetic resonance imaging is a useful modality, not limited by the acoustic window, but the need for general anesthesia or sedation in these methods limits their use in pediatric cardiology (Oliver-Ruiz and Bret-Zurita 2007).

Several flow velocity estimators for estimating both the axial and lateral velocity components have been proposed. Speckle tracking (Bohs et al. 2000) and vector Doppler (Dunmire et al. 2000) are the two main research lines for 2-D flow estimation, but recently new techniques such as echo particle image velocimetry (PIV) (Poelma et al. 2009; Zheng et al. 2006) have been suggested. For the latter, the need for contrast agents makes it currently not suitable for pediatric imaging. The speckle tracking technique uses the speckle in the ultrasound image, which is a result of the constructive and destructive interference from the backscattered echoes, to estimate the velocity of the scatterers. The movement of the blood speckle is correlated with the movement of the blood, and the speckle can be tracked from frame to frame to obtain information on blood velocities. The vector Doppler technique combines the Doppler estimates from two transmit and/or receive angles to obtain angle-independent velocity measurements. Several studies have been performed to evaluate the speckle tracking and vector Doppler techniques for numerically simulated flow patterns, *in vitro* flow phantoms and *in vivo* in human vessels (Bohs and Gebhart 2001; Bohs et al. 1995; Pastorelli et al. 2008; Steel et al. 2004; Swillens et al. 2010; Tortoli et al. 2010). However, neither speckle tracking nor vector Doppler has yet been established for clinical use in blood flow estimation. This can, in our experience, be attributed to a lack of robustness and limitations related to data acquisition and processing capabilities for real-time imaging.

Recent developments in ultrasound imaging technology provide a substantially higher acquisition rate which offers new possibilities in 2-D flow estimation. By transmitting broad unfocused ultrasound pulses, parallel receive beamforming can be used to increase the acquisition rate, resulting in instantaneous full field-of-view images at high frame rates. The technique has been suggested for elastography (Tanter et al. 2002), compound Doppler imaging (Bercoff et al. 2011) and vector velocity imaging (Udesen et al. 2008). The high acquisition rate also makes it possible to have a higher ensemble size for improved clutter filtering possibilities and to achieve more robust velocity estimates without compromising a high frame rate, which is advantageous when imaging complex blood flow (Ekroll et al. 2013).

Quantitative vector velocity imaging has, to the authors' knowledge, not previously been evaluated for use in pediatric cardiology. However, a qualitative method based on the direct visualization of blood speckle has been suggested, and was shown to increase the certainty in ASD shunt flow evaluation (Lovstakken et al. 2006; Nyrnes et al. 2007). In this work, we investigate 2-D speckle tracking for quantitative blood flow velocity estimation in ASDs and VSDs in newborns. The overall objective was to achieve angle-independent peak shunt flow velocity estimates for better shunt evaluation. To find the true peak velocity throughout the cardiac cycle, we further propose the use of tissue speckle tracking to follow the shunt position in the 2-D image plane throughout the cardiac cycle.

METHODS

Two patients from the ongoing feasibility study are the subjects in this study. Patient 1, a boy, was 8 days old and 3340 g at the time of the ultrasound recordings. He had a perimembranous VSD, which was focused on in this study. He was also born with a secundum ASD, a pulmonary artery sling (the left pulmonary artery anomalously originating from the right pulmonary artery) and an anal atresia. Patient 2, a girl, was born prematurely at 31 + 4 weeks and diagnosed with a secundum ASD. She was 25 days old and 2165 g when included and had no additional congenital malformations. Written informed consent was obtained from the parents of the participants before the examination. The study was approved by the Norwegian Regional Committee for Medical and Health Research Ethics, and patient safety measurements were within the guidelines from the U.S. Food and Drug Administration.

In vivo *and* in vitro *setup*

We used a SonixMDP ultrasound scanner (Ultrasonix, Richmond, BC, Canada) with a 4- to 9-MHz linear transducer and a Sonix DAQ for channel data acquisition for *in vivo* and *in vitro* recordings. In the duplex acquisition scheme implemented, separate acquisition setups were used for B-mode and flow imaging to ensure sufficient image quality for both modalities. Figure 1 is a schematic of data acquisition and post-processing used in this

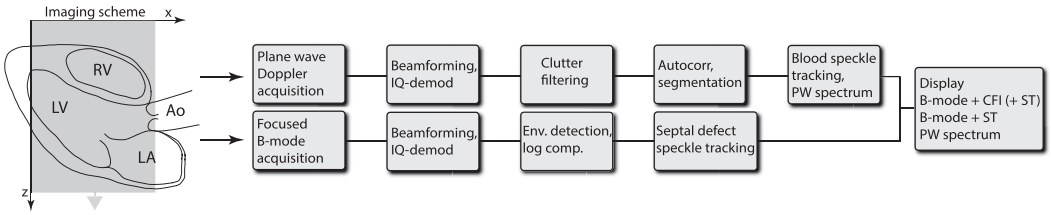

Fig. 1. Schematic overview of data acquisition and post-processing setup. The channel data are acquired, and beamforming is done off-line. The plane wave data are clutter filtered before blood velocity estimation is done using the autocorrelation approach and speckle tracking. The B-mode images are used for septal defect speckle tracking. On the left is a parasternal long-axis view of a heart where the left atrium (LA), left ventricle (LV), right ventricle (RV) and outflow tract to the aorta (Ao) are visible. One plane transmit beam is covering the region of interest. IQ-demod = In-phase and Quadrature demodulation, CFI = color flow imaging, ST = speckle tracking, PW = pulsed wave.

work, where the top and bottom line represent acquisition and processing of blood flow images and B-mode images, respectively.

Unfocused transmit beams transmitted at a pulse repetition frequency (PRF) of 8 kHz were used for the flow imaging with an ensemble size of 32. The transmit beams covered a region equal to the transducer width, and full parallel receive beamforming was used, achieving a frame rate of 107 frames/s (fps) when interleaved with the separate B-mode scan sequence. Channel radiofrequency (RF) data (128 channels) were stored for up to 2 s (limited by 16 GB of channel data memory), and beamforming and processing were done off-line. The data were beamformed using a hamming apodization window over the active receive aperture to reduce side lobes. A high-pass clutter filter was applied to separate the blood signal from the strong tissue signal, before blood velocity estimation. Conventional Doppler and 2-D speckle tracking estimation of the blood velocity were done after clutter filtering. The color flow power and velocity estimates and the intensity in the B-mode images were used for segmentation of areas containing blood. Threshold values were set empirically for the given data sets.

The B-mode scan sequence was interleaved with the flow acquisition, and two interleave groups of 64 focused pulses were used to cover the whole transducer width, resulting in a B-mode frame rate of 54 fps. A PRF of 12 kHz was used for the B-mode images. Additional imaging parameters for the duplex acquisition are given in Table 1.

An *in vitro* flow phantom was used to validate and investigate the accuracy of the speckle tracking blood flow estimation algorithm. The setup consisted of a pump (PhysioPulse 100 Flow System, Shelley Medical Imaging Technologies, London, ON, Canada) connected to a straight-tube flow phantom (ATS Laboratories, Bridgeport, CT, USA) with a blood-mimicking fluid (Ramnarine et al. 1998). The tube had a diameter of 6 mm, and a stationary flow scenario with a beam-to-flow angle of 60° and a maximum velocity of approximately 1 m/s was investigated. We used the same acquisition and processing setup used for the *in vivo* recordings. The reference velocities used for comparison were calculated under the assumption of a fully developed laminar flow and based on the tube diameter and the programmed volume flow rate.

Data acquisition

In conventional ultrasound imaging, the image is built line by line. One focused pulse is transmitted at the time, and the received echoes form one line in the image as illustrated to the left in Figure 2. Recent development in ultrasound technology allows for multiple image lines to be generated in parallel (Udesen et al. 2008). The approach may to some extent be used for focused transmit pulses, but to cover a wide imaging region, unfocused or diverging beams must be emitted.

Today's research scanners can store and process the RF data from all the channels in the transducer. When the channel data are available, any number of receive lines can be beamformed simultaneously in software, and a full image may result from the transmission of just one full field plane wave, as illustrated to the right in Figure 2. The ultrahigh acquisition rate obtained by plane wave imaging and parallel receive beamforming makes it

Table 1. Image acquisition parameters

Probe	UX L9-4/38	
	128 element linear array	
Probe type	Flow acquisition	B-Mode acquisition
Pulse center frequency (MHz)	5	6.67
Transmit aperture (cm)	3.89 (full aperture)	1.5
Transmit *F*-number	—	2
Receive *F*-number	1.1	1.1
Pulse repetition frequency (Hz)	8000	12,000
Ensemble size	32	—
Frame rate (Hz)	107	54

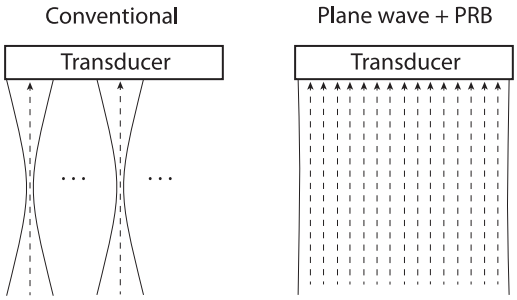

Fig. 2. Comparison of conventional ultrasound acquisition scheme with parallel receive beamforming (PRB). Left: In the conventional setup, one focused transmit line and one focused receive line are acquired at a time. Right: A broad unfocused wave is transmitted and multiple image lines are received simultaneously.

possible to have a wide region of interest, with dense lateral image sampling at high frame rates. The highly dynamic and complex blood flow in the heart makes high frame rates crucial and plane wave imaging favorable for blood flow imaging. There is, however, a loss in penetration with plane wave imaging, compared with focused imaging, and also a decrease in image contrast and lateral resolution. The latter is particularly visible in B-mode imaging, but is, in our experience, less deteriorating and often negligible for blood flow imaging, where the dynamic range is significantly lower; that is, the elevated side lobe level is often below the noise floor, and the parametric image display typically uses a low dynamic range.

Conventional color flow imaging and processing

In CFI, the estimated axial blood velocity is displayed as a 2-D color map, where the colors correspond to the blood velocity components along the beam axis. The image region is scanned line by line, where a series of ultrasound pulses are emitted in each beam direction at a given PRF. The movement of the blood scatterers indicates a shift in the received signal from pulse to pulse. The part of the received signal coming from the stationary tissue is called the clutter signal, whereas the signal originating from the moving blood scatterers is called the Doppler signal. The Doppler signal is separated from the clutter signal using a high-pass filter, for example, a polynomial regression, finite impulse response (FIR) or infinite impulse response (IIR) filter (Bjaerum et al. 2002). The number of emitted pulses in each beam direction used to generate one image line is referred to as the ensemble size. The blood velocity estimation is typically based on the autocorrelation method (ACM), where the mean velocity is estimated from the correlation of the Doppler signal from pulse to pulse (lag 1), $\widehat{R}(1)$ (Kasai et al. 1985),

$$\widehat{v}_{\text{axial}} = \frac{c \times \text{PRF}}{4\pi f_0} \angle \widehat{R}(1), \tag{1}$$

where c is the speed of sound, and f_0 is the center frequency of the transmitted pulse. The autocorrelation function is calculated as

$$\widehat{R}(1) = \frac{1}{N_p} \sum_{0}^{Np-1} x(k)^* x(k+1), \tag{2}$$

where $x(k)$ is a fixed spatial position, * denotes the complex conjugate and N_p is the ensemble size. The autocorrelation function is also spatially averaged to decrease estimator variance. In this work, a polynomial regression filter of order 2 was chosen as the clutter filter for the autocorrelation estimation, with a –3-dB cutoff at 0.05 m/s.

Blood flow estimation using speckle tracking

Speckle is an interference pattern in the backscattered signal from many subresolution scatterers, for example, the red blood cells. The movement of the speckle pattern is correlated with the movement of the scatterer ensemble, and the 2-D blood velocities can thus be estimated by tracking the movement of the blood speckle pattern from frame to frame using pattern matching techniques (Bohs et al. 2000). The speckle tracking principle is illustrated in Figure 3. A kernel region is defined in a first image acquisition, and the best pattern match of the kernel is searched for in a following image, determining the displacement of the kernel.

Different pattern matching algorithms can be used, for example, 2-D normalized cross-correlation, sum of absolute differences and sum of squared differences. When the most likely displacement is found, the velocity can be estimated given the time between the two acquisitions. After this process is repeated for the whole imaging area, a vector velocity map of the blood flow is obtained.

In this work, pattern matching was done using the sum of squared differences algorithm,

$$d(\alpha, \beta) = \sum_{x,y} (I(x+\alpha, y+\beta) - K(x,y))^2, \tag{3}$$

where I is the image displaced (α, β) from the original kernel position, and K is the original kernel. The minimum sum of squared differences coefficient, $d(\alpha_{\min}, \beta_{\min})$, reveals the most likely displacement of the kernel. The minimum measurable velocity is limited by the sampling resolution in the data, which can be quite crude. Linear interpolation of the IQ data and parabolic subsample interpolation of the estimated displacement were used to improve the velocity resolution. If $f_1 = d(\alpha_{\min}, \beta_{\min})$, and f_0 and f_2 are the two nearest neighbors, the subsample

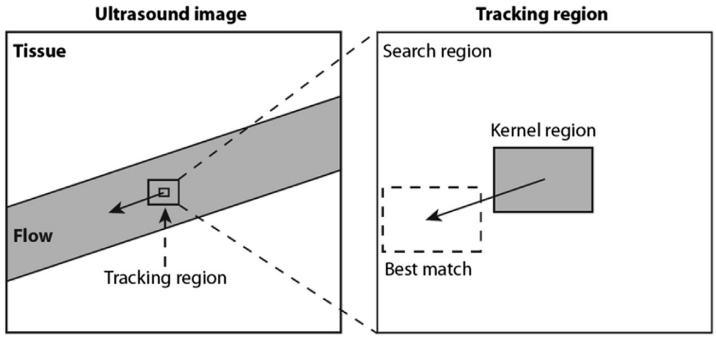

Fig. 3. Speckle tracking principle. A kernel is defined in the first acquisition, and the best match of this kernel is searched for in the next acquisition.

offset correction for the estimated displacement is given by (Cespedes et al. 1995)

$$\hat{\delta} = \frac{f_0 - f_2}{2(f_0 - 2f_1 + f_2)}. \quad (4)$$

The maximum measurable velocity is determined by the size of the search region. The velocity estimates were subjected to median averaging over the temporal ensemble of 32 to minimize the effect of spurious tracking errors. The acquisition rate of 8 kHz made averaging over a large packet of 32 pulses possible while still achieving a high flow frame rate. Additional temporal averaging over five flow frames was done in a non-causal way according to the weights [0.1 0.2 0.4 0.2 0.1] to smooth the flow patterns throughout the cardiac cycle. The velocity estimates were also spatially averaged in a region of 2 × 2 mm to reduce the variance of the estimates.

A time-invariant clutter filter is preferable for speckle tracking methods to ensure that every speckle image is filtered equally. This is important to maximize temporal and spatial correlation. In this work, a fourth-order FIR filter with a –3-dB cutoff at $0.33 \times V_{\text{Nyquist}} = 0.2$ m/s was used.

The accuracy of the speckle tracking velocity estimation was investigated for stationary flow in an *in vitro* flow phantom. After one recording of 130 flow frames, the velocity estimates were averaged as described above, where $N = 26$ independent realizations were used to estimate the expected value and standard deviation of the method *in vitro*.

To validate the velocity estimates in the *in vivo* cases, PW spectra were made retrospectively from the same recording used for speckle tracking and autocorrelation estimation. The Doppler ensemble lengths of 32 are sufficient to make a conventional PW spectrum for the intended use of validation in this work. A PW spectrum could thus be made from any given point in the image and was estimated using the discrete Fourier transform

$$\hat{P}(\omega) = \frac{1}{RB} \sum_{r=0}^{R-1} \sum_{b=0}^{B-1} \left| \sum_{n=0}^{N-1} w(n) x_{r,b}(n) e^{-i\omega n} \right|^2, \quad (5)$$

where $x_{r,b}(n)$ is the IQ signal from a range, beam position for a given ensemble sample n, $w(n)$ is a smooth window function, R is the number of range samples, B is the number of receive beams and N is the ensemble length. In this work, a Hamming window was used, and the averaging region was 1 mm in the axial direction and 0.5 mm in the lateral direction.

Semi-automatic tracking of septal defect using speckle tracking

The objective of this work was to estimate shunt flow velocities. During the contraction and relaxation of the myocardium, the shunt is shifted in the ultrasound image plane, and the shunt size may also vary. To keep track of the velocities in the shunt flow, it is therefore important to track the septal defect position during the cardiac cycle. The same speckle tracking algorithm was used for tissue tracking by using a larger kernel region and assuming a maximum tissue velocity of 5–10 cm/s. The kernel size was 1.1 mm in the lateral direction and 1.3 mm in the axial direction. An area of 45 overlapping kernel regions was defined around the start and end points of the septal defect in the image, as indicated by the two squares in Figure 4. The median of all the displacement vectors in each of the squares defined the start or end point of the defect in the next frame.

The septal defect position was manually marked in two different frames, corresponding to end-systole and end-diastole. These known positions were used as attractors to ensure robust tracking results throughout the cardiac cycle. The new position of the septal defect found

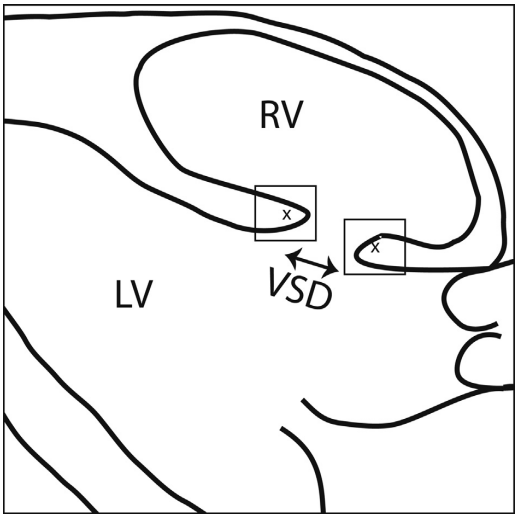

Fig. 4. Tissue speckle tracking of a ventricular septal defect (VSD) in the septum between the left (LV) and right (RV) ventricles. The defect is marked in the first acquisition. Many overlapping large kernels are defined around the marked beginning and end of the defect in the image (inside the *squares* indicated).

from speckle tracking was for each frame corrected using the predefined positions $(x,z)_{\text{systole}}$ and $(x,z)_{\text{diastole}}$ as

$$\Delta x_{\text{attractor}}(t) = (x(t)-x_{\text{s}})k_{\text{s}}(t)+(x(t)-x_{\text{d}})k_{\text{d}}(t) \quad (6)$$

$$x_{\text{corrected}}(t) = x(t)-\Delta x_{\text{attractor}}(t), \quad (7)$$

where $x(t)$ and $x_{\text{corrected}}(t)$ are the shunt positions before and after the correction. The attraction parameters $k_{\text{s}}(t)$ and $k_{\text{d}}(t)$ have values between 0 and 1, as illustrated in Figure 5, and describe the attraction strength as a function of time. At end-systole and end-diastole, k_{s} and k_{d} are equal to 1, respectively, and the shunt positions are thus equal to the predefined positions for these frames.

The shunt tissue tracking approach was validated by visual inspection of the example data used in this work. Based on the tissue tracking of the shunt position, it was possible to have a PW Doppler sample volume automatically moving with the maximum velocity in the shunt for all frames in the cardiac cycle. This differs from conventional PW Doppler, where a fixed sample volume is manually placed where the seemingly highest axial shunt velocities are present according to the color flow images.

RESULTS

Speckle tracking of blood flow

To the left in Figure 6 is a color flow image of stationary flow in an *in vitro* tube phantom, with the speckle tracking estimates overlaid as *arrows*. Speckle tracking and angle-corrected autocorrelation velocity estimates from the region marked by *dashed lines* at 25-mm depth were used to estimate velocity profiles and standard deviations for N = 26 independent realizations. To the right in Figure 6, the velocity profiles are compared with the expected parabolic profile for a fully developed laminar flow.

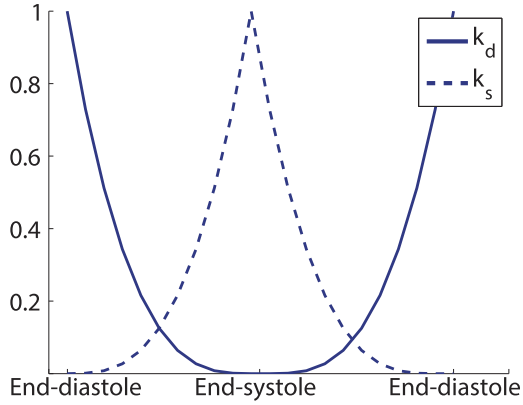

Fig. 5. Shunt tracking attractor parameters, k_{s} and k_{d}, as a function of time. The parameters define the attraction strength.

For a 1 × 1- mm area in the middle of the tube, the mean axial velocity was 0.50±0.02 m/s for the autocorrelation method and 0.51±0.01 m/s for speckle tracking. The mean lateral velocity was 0.88±0.03 m/s for speckle tracking. The resulting absolute velocity was 0.99±0.04 m/s for the angle-corrected ACM and 1.02±0.02 m/s for speckle tracking. The reference velocity in the same region was 0.98 m/s.

To the left in Figure 7 is a color flow image of blood flow in the heart of patient 1, a newborn with a VSD. The image was acquired from a parasternal long-axis view, in which the left atrium, the left ventricle and the right ventricle were visible. The septum between the ventricles is distinct, and shunt flow is clearly visible in the image (marked by the *white dashed line*). The color flow image contains only the 1-D velocity information along the beam direction, underlined here by the superimposed *arrows*. To the right in the figure is the same image frame, with the colors representing the absolute velocities found from speckle tracking instead of the autocorrelation estimates. The direction of the speckle tracking estimates is indicated by *arrows* (Supplementary Videos 1–4).

As can be observed, the shunt flow is differently highlighted in the image when the absolute velocities are displayed. The highest absolute velocities are found in the shunt region, but because of a large lateral component that is not measured with CFI, this is not directly seen in the color flow image. In addition, the direction of the flow is not easily interpreted from the color flow

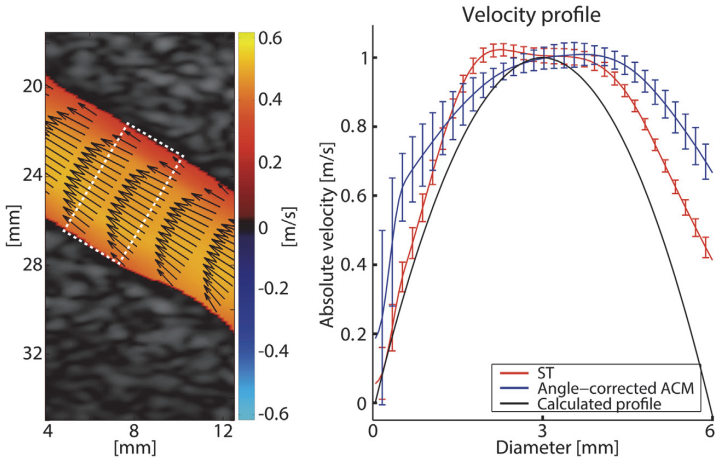

Fig. 6. Stationary flow in an *in vitro* straight-tube phantom with a beam-to-flow angle of 60°. Left: Color flow image with speckle tracking estimates overlaid as *arrows*. Right: Mean speckle tracking (ST) and angle-corrected autocorrelation method (ACM) velocity profiles with standard deviations from 26 measurements compared with the calculated reference velocity profile. The velocity profiles are estimated from the area indicated by the *dashed lines*.

image, which consequently makes it difficult to correctly angle-correct the autocorrelation estimates. The speckle tracking estimates directly give the information about directions and absolute velocities of the blood flow in the image plane. In addition, it was observed that the speckle tracking method tracked beyond the Nyquist limit in areas where aliasing artifacts were present in the color flow image (see Supplementary Video 1).

In Figure 8 are color flow and speckle tracking velocity images of patient 2 with an ASD. These images were acquired from a subcostal oblique long-axis view in which all four chambers were visible. The defect is in the septum between the atria in the lower part of the images. In the color flow image, uniform color distribution in the shunt area is seen. This could be mistaken for color blooming into the tissue for cases where the septal defect is not clearly visible in the B-mode image. The 2-D velocity information from speckle tracking to the right in this figure better indicates the flow from the left to the right atrium.

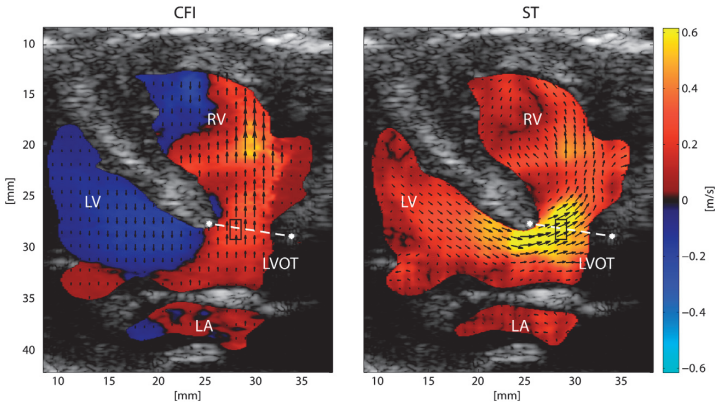

Fig. 7. Color flow and speckle tracking images of patient 1 (8 days, 3340 g) indicating a ventricular septal defect from a parasternal long-axis view. The septal defect is approximately 6 mm wide in this view, and the left-to-right shunt flow is marked with a *white dashed line*. The sample volume for the retrospective pulsed wave spectrum in Figure 10 is indicated in the shunt region. The superimposed *arrows* in the color flow image to the left underline the 1-D velocity information acquired from the autocorrelation estimates. The colors in the image to the right represent the absolute velocity found from speckle tracking. The *arrows* represent the direction and magnitude of the speckle tracking estimates. LV = left ventricle, RV = right ventricle, LA = left atrium, LVOT = left ventricular outflow tract.

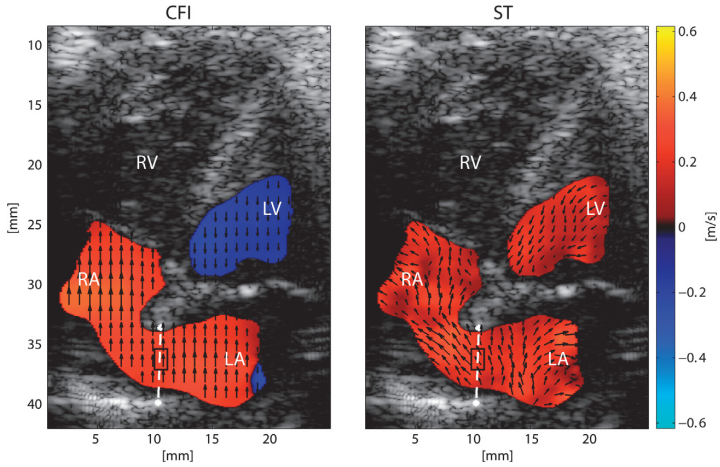

Fig. 8. Color flow and speckle tracking images of patient 2 (premature, 2165 g) indicating an atrial septal defect from a subcostal oblique long-axis view. The septal defect is approximately 5 mm wide in this view, and the left-to-right shunt flow is marked with a *white dashed line*. The sample volume for the retrospective pulsed wave spectrum in Figure 11 is indicated in the shunt region. The superimposed *arrows* in the color flow image to the left underline the 1-D velocity information acquired from the autocorrelation estimates. The colors in the image to the right represent the absolute velocities found from speckle tracking. The arrows represent the direction and magnitude of the speckle tracking estimates. LV = left ventricle, RV = right ventricle, LA = left atrium, RA = right atrium.

Speckle tracking of septal defect

Figure 9 provides examples of tissue tracking results of the VSD in patient 1 for three different frames corresponding to early diastole, late diastole and mid-systole. The frame times are 0.07, 0.18 and 0.31 s, where 0.39 s is a full cycle. The starting and ending positions of the septal defect in the images were found for all B-mode frames, and the maximum displacement in the image plane was 3–5 mm. The speckle tracking algorithm gave robust tracking results when the movement was in the image plane, and the end-systole and end-diastole attractors helped to ensure robust results even with out-of-plane-movement.

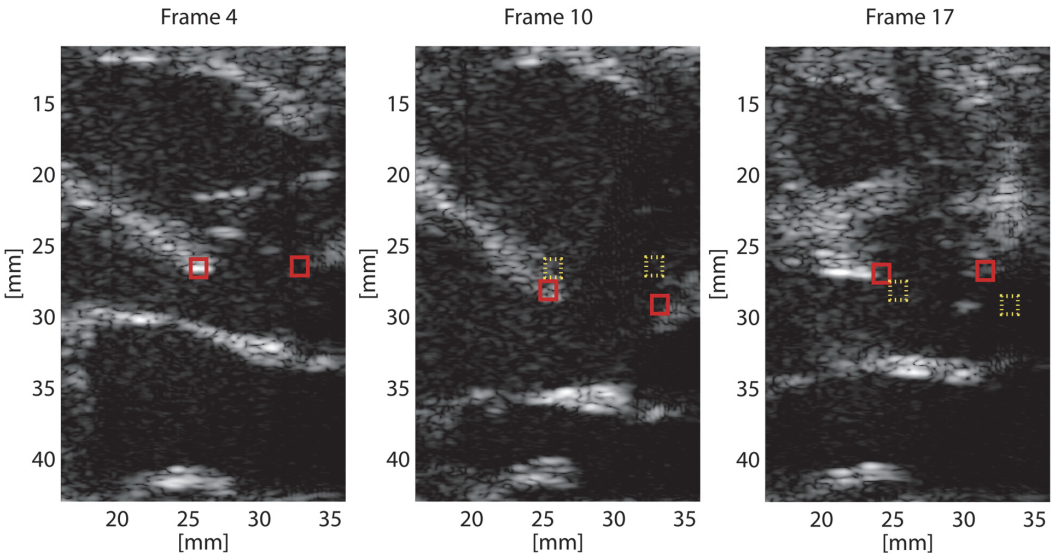

Fig. 9. Three different time frames showing tissue tracking results of the ventricular septal defect in patient 1. The *yellow dotted squares* represent the defect's position at the previous displayed frame. Dynamic range = 50 dB.

Shunt flow evaluation

Both speckle tracking and autocorrelation velocity estimates were validated with retrospective PW Doppler. The velocity estimates were compared with those of conventional PW Doppler and PW Doppler from a moving sample volume based on shunt tracking. For the conventional PW Doppler, a fixed sample volume was placed manually by a pediatric cardiologist. In Figure 10, the PW spectrum of the VSD is shown with and without a moving sample volume together with the velocity estimates from color flow and speckle tracking. When the sample volume is not moving with the septal defect in the image plane (right), potentially important shunt flow information is missed for parts of the cycle. In this example, the shunt is bidirectional, and the reversed flow from the right to the left ventricle is missed when the sample volume is fixed, as indicated by the *yellow circle* on the right in Figure 10. The axial velocity estimates from speckle tracking agreed well with the PW spectrum and autocorrelation estimates.

In Figure 11 is the PW spectrum of the ASD in patient 2 together with the speckle tracking and autocorrelation velocity estimates. The velocities in the ASD are lower than the velocities in the VSD and the beam-to-flow angle is high, resulting in axial velocities around the cutoff velocity of the FIR filter of 0.2 m/s. To the right in Figure 11 the FIR filter was used for the autocorrelation estimates as well to compare the filter effect on the two estimators. The autocorrelation method overestimates the velocities in the filter transition region. A much better result is therefore obtained with the polynomial regression filter with a 0.05 m/s cutoff, as seen to the left in Figure 11. With this filter, the autocorrelation and speckle tracking estimates correspond better.

To the left in Figure 12, the angle-corrected autocorrelation estimates from the moving sample volume in patient 1 are compared with the absolute velocities from speckle tracking for all frames. The angle correction factor was estimated for each frame based on the flow direction estimates from speckle tracking. The maximum left-to-right shunt velocity measured in this view was 0.77 m/s. The VSD was bidirectional, and the maximum right-to-left shunt velocity measured was approximately 0.3 m/s. The gray region indicates the variation in manually angle-corrected autocorrelation estimates from different fixed sample volume positions. The peak velocity found manually varied from 0.49 to 0.56 m/s, an underestimation compared with the peak velocity found from speckle tracking.

To the right in Figure 12 are the absolute velocities in the shunt for patient 2. The manually found absolute velocities from the autocorrelation method were in general higher than the absolute velocities found from speckle tracking. The peak velocity found manually varied from 0.38 to 0.58 m/s, compared with the speckle tracking peak velocity of 0.33 m/s.

The speckle tracking velocity profiles from the shunt region in the VSD and ASD are illustrated in Figure 13. The *red* profiles in the VSD are from frames where the flow has been reversed and is going from the right ventricle into the left ventricle. In the VSD, the flow profile develops from a relatively flat to a more complex profile, with skewed peak velocities as the velocity in the shunt increases. The velocity profiles are more plug-shaped throughout the cycle for the ASD, as seen to the right in Figure 13.

DISCUSSION

In this work, our aim was to investigate if 2-D speckle tracking of blood velocities could be used to provide angle-independent velocity measurements in the context of shunt flow evaluation in congenital heart disease. In current clinical routine, peak velocity is one of the important measures in shunt evaluation. However, when peak velocity is measured with PW Doppler, a manual angle correction is needed, leading to a potentially inaccurate measurement, especially for high

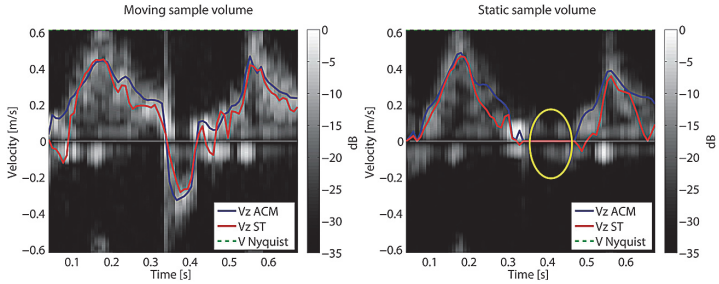

Fig. 10. Retrospective pulsed wave spectrum from the shunt region in patient 1. The spectrum is shown together with the speckle tracking (ST) and autocorrelation method (ACM) velocity estimates from the same sample volume. Left: The sample volume is automatically placed at the location of the highest velocity in the shunt for all frames. Right: A static sample volume is manually placed in the shunt region.

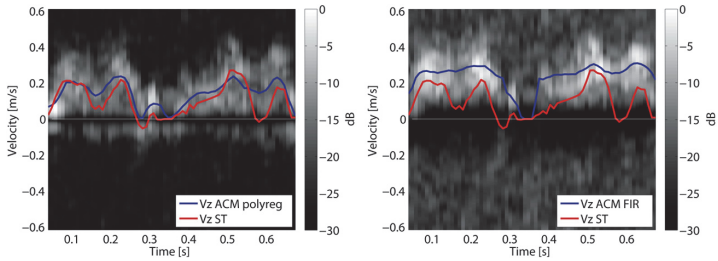

Fig. 11. Retrospective pulsed wave spectrum from the shunt region in patient 2. The spectrum is shown together with the speckle tracking (ST) and autocorrelation method (ACM) estimates. Right: The FIR filter is used for both autocorrelation and speckle tracking estimates. Left: The FIR filter is used for the speckle tracking estimates and the polynomial regression filter is used for the autocorrelation estimates.

beam-to-flow angles (Thrush 2010). Further, several measurements from different image views may be needed to ensure that the peak velocity is found. With our acquisition scheme, high-frame-rate flow images are acquired where color flow imaging, blood flow speckle tracking and PW Doppler estimation can be done from the same data set. In addition, tissue speckle tracking based on B-mode images was used to provide the shunt position throughout the cardiac cycle to ensure that the true peak velocity was found in the imaging plane.

An *in vitro* flow phantom was used to test the acquisition setup and speckle tracking algorithm. The speckle tracking velocity estimates for the N = 26 independent measurements had a low standard deviation (1–3 cm/s) and were in good agreement with the reference velocities as seen in Figure 6. The increased deviation at the edges of the tube can be attributed to the limited spatial resolution of the imaging system, as well as to the clutter filter for low velocities.

The *in vivo* results indicate that speckle tracking may indeed provide angle-independent flow velocity estimates in ASD and VSD shunts throughout the cardiac cycle. The manual angle correction in the Doppler-based methods may infer a variation in peak velocity estimate especially for large beam-to-flow angles, as seen for the ASD in Figure 12. For the VSD in Figure 12, the timing of the peak velocity estimate was also observed to differ, where the absolute peak velocity occurred later in the cycle than the manual angle-corrected peak axial velocity. For the speckle tracking estimates, no angle correction is needed, and improved measurements of peak velocities may therefore be acquired. The speckle tracking angle estimates can also be used to automatically angle-correct the PW Doppler estimates in more complex flow situations where the beam-to-flow angle is difficult to determine manually. Also, for cases where the beam-to-flow angle exceeds the recommended limit for angle correction (60° [Thrush 2010]), the angle-independent speckle tracking estimate still provides an estimate of the absolute velocity.

The 2-D velocity vector maps provide new information on the potentially complex flow patterns and dynamics that may occur in congenital heart disease. Vortex formation in the right ventricle caused by VSD shunt flow is, for example, visualized with the 2-D velocity vector maps. In color flow images, where only the axial velocity component is displayed, small defects can be missed, as the shunt flow could be mistaken as

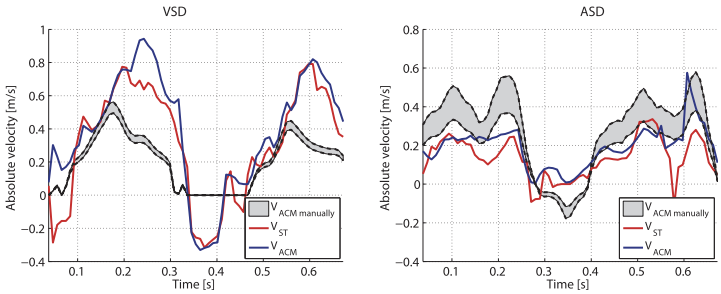

Fig. 12. Comparison of absolute velocities from speckle tracking (V_{ST}) with angle-corrected autocorrelation estimates (V_{ACM}) from the moving sample volume in the ventricular septal defect in patient 1 and the atrial septal defect in patient 2. The speckle tracking estimates were used to angle-correct the autocorrelation estimates. The variation in absolute velocity estimation using manual angle correction and a fixed sample volume is also indicated.

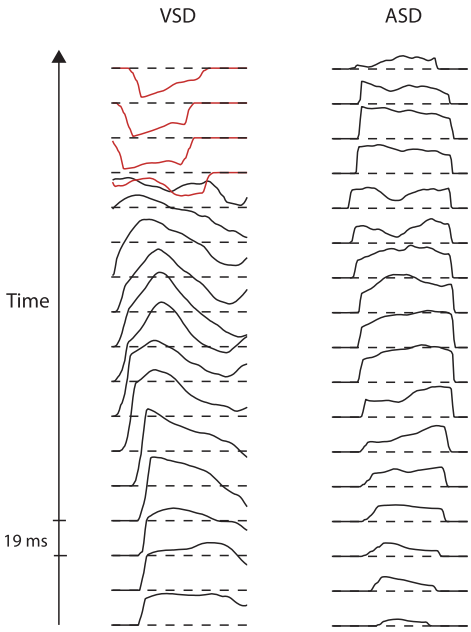

Fig. 13. Estimated velocity profiles over the shunt region indicated by the *white lines* in Figures 7 and 8 for one cardiac cycle. VSD = ventricular septal defect, ASD = atrial septal defect.

color blooming into the tissue (Benavidez et al. 2008). Further, the shunt position tracking made it possible to generate spatial velocity profiles from the shunt throughout the cardiac cycle and to automatically find the peak velocity in the shunt, for all frames. These flow profiles can provide new information on the shunt flow in general; for instance, it could be observed that the peak velocity was not necessarily found in the middle of the shunt in our data. The automatic shunt position tracking also provided an estimate of the diameter of the shunt, which is typically also documented during the clinical evaluation.

The speckle tracking estimates were validated toward PW Doppler and autocorrelation estimates in this work. The axial velocities match the PW spectra well in Figures 10 and 11. Other sample volumes were tested and gave similar results. Based on the current data, a statistical comparison between the axial velocity estimations from speckle tracking and autocorrelation cannot be made. The comparison was performed only as an initial validation of the axial speckle tracking. A general comparison of the accuracy and robustness of the two methods requires a separate study. The absolute velocity profiles for the speckle tracking and angle-corrected autocorrelation estimates in Figure 12 are reasonable and indicate that the tracking works in both the axial and lateral directions.

For near-transverse flow both the autocorrelation and speckle tracking estimates will suffer from clutter filter issues. In areas with a high beam-to-flow angle, the blood signal as well as the clutter signal will be attenuated by the clutter filter, and the image will suffer from signal dropouts. In addition, the autocorrelation estimates will be overestimated in the filter transition region, as seen to the right in Figure 11, where the autocorrelation estimates were filtered using the same FIR filter used for the speckle tracking estimates. It was observed that the speckle tracking provided more consistent estimates well below the filter cutoff velocity. The speckle tracking approach is also capable of providing velocity estimates beyond the Nyquist range and, thus, exhibits a wider range of measurable velocity compared with the autocorrelation technique. If no aliasing artifacts or clutter filter issues are present, the axial velocity estimates from the autocorrelation method are, however, quite robust. In low signal-to-noise conditions, the speckle tracking and autocorrelation estimates could therefore be combined to further improve the robustness of the velocity estimates (Swillens et al. 2010).

The limitation of speckle tracking is mainly speckle decorrelation leading to inaccurate tracking results. The speckle pattern decorrelates rapidly because of spatial and temporal velocity gradients, non-laminar flow and out-of-plane movement (Friemel et al. 1998). With ultrahigh frame rates equal to the PRF, where instantaneous images over a full field of view are acquired, the speckle decorrelation from frame to frame is reduced compared with what can be achieved based on a conventional imaging scheme. Out-of-plane movements were observed, but did not seem to influence the in-plane velocity estimates in our data. The ultrahigh frame rates are achieved with single plane wave emissions, and a loss in contrast and lateral resolution and a low signal-to-noise ratio is thus potentially a problem in our setup for flow imaging. Transducer surface heating constraints limited our transmission voltage and sequence (*e.g.*, coded excitation was no applicable). However, newborns often have good acoustic windows for cardiac imaging (you can often image through their ribs), and fairly good signal-to-noise ratios were achieved in the data examples in this work. The loss of contrast and lateral resolution was minimized by apodization and dynamic focusing (F-number = 1.1) on receive, and for the blood speckle tracking results, the ultrahigh frame rate achieved was probably more important than the resolution reduction. A larger patient study, however, is needed to map the clinical feasibility of this approach.

The robustness of the tissue speckle tracking was dependent on a visual septum during the cardiac cycle.

Out-of-plane movement made the tracking more difficult. The frame rate of the B-mode images in our setup was sufficient to track the septal defect movement in our limited data material. However, to conclude on this matter, the method must be tested on a broader set of patients to evaluate robustness and usability.

A linear probe was used in this work, because it can easily use plane transmit waves and parallel receive beamforming, and the depth and field of view needed for cardiac imaging in newborns were achievable. Further work should include an evaluation of high-frame-rate speckle tracking using phased arrays, as these probes are conventionally used in pediatric imaging. An imaging scheme in which diverging transmit beams are used together with parallel receive beamforming must then be implemented to achieve similar high-frame-rate flow images. Further work will also evaluate the potential clinical impact of the method for a larger patient population. In addition, methods for volume flow measurements will be included and potential solutions to the clutter filter issues will be investigated.

CONCLUSIONS

High-frame-rate speckle tracking based on plane wave imaging may improve the measurement of peak velocities for the evaluation of shunt flow in atrial and ventricular septal defects in newborns. The peak shunt velocity was more clearly visualized than in color flow imaging, and the need for manual angle correction was eliminated for quantitative measurements. Further, by adding spatial tracking of shunt position, the spatiotemporal peak velocity in the imaging plane could be found, which was shown to differ from that obtained based on Doppler estimates. The proposed technique may thus help increase diagnostic accuracy and decrease interobserver variability.

SUPPLEMENTARY DATA

Supplementary data related to this article can be found online at http://dx.doi.org/10.1016/j.ultrasmedbio.2014.03.029.

REFERENCES

Acar P, Abadir S, Paranon S, Latcu G, Grosjean J, Dulac Y. Live 3D echocardiography with the pediatric matrix probe. Echocardiography 2007;24:750–755.

Benavidez OJ, Gauvreau K, Jenkins KJ, Geva T. Diagnostic errors in pediatric echocardiography: Development of taxonomy and identification of risk factors. Circulation 2008;117:2995–3001.

Bercoff J, Montaldo G, Loupas T, Savery D, Mézière F, Fink M, Tanter M. Ultrafast compound Doppler imaging: Providing full blood flow characterization. IEEE Trans Ultrason Ferroelectr Freq Control 2011;58:134–147.

Bjaerum S, Torp H, Kristoffersen K. Clutter filter design for ultrasound color flow imaging. IEEE Trans Ultrason Ferroelectr Freq Control 2002;49:204–216.

Bohs L, Friemel B, Trahey G. Experimental velocity profiles and volumetric flow via two-dimensional speckle tracking. Ultrasound Med Biol 1995;21:885–898.

Bohs L, Gebhart S. 2-D motion estimation using two parallel receive beams. IEEE Trans Ultrason Ferroelectr Freq Control 2001;48:392–408.

Bohs LN, Geiman BJ, Anderson ME, Gebhart SC, Trahey GE. Speckle tracking for multi-dimensional flow estimation. Ultrasonics 2000;38:369–375.

Cespedes I, Huang Y, Ophir J, Spratt S. Methods for estimation of subsample time delays of digitized echo signals. Ultrason Imaging 1995;17:142–171.

Cheng TO, Xie MX, Wang XF, Wang Y, Lu Q. Real-time 3-dimensional echocardiography in assessing atrial and ventricular septal defects: An echocardiographic-surgical correlative study. Am Heart J 2004;148:1091–1095.

Driscoll D, Allen HD, Atkins DL, Brenner J, Dunnigan A, Franklin W, Gutgesell HP, Herndon P, Shaddy RE, Taubert K. Guidelines for evaluation and management of common congenital cardiac problems in infants, children, and adolescents. A statement for healthcare professionals from the Committee on Congenital Cardiac Defects of the Council on Cardiovascular Disease in the Young, American Heart Association. Circulation 1994;90:2180–2188.

Dunmire B, Beach KW, Labs K, Plett M, Strandness DE. Cross-beam vector Doppler ultrasound for angle-independent velocity measurements. Ultrasound Med Biol 2000;26:1213–1235.

Ekroll IK, Swillens A, Segers P, Dahl T, Torp H, Lovstakken L. Simultaneous quantification of flow and tissue velocities based on multi-angle plane wave imaging. IEEE Trans Ultrason Ferroelectr Freq Control 2013;60:727–738.

Forbus GA, Shirali GS. Anomalies of the ventricular septum. In: Lai WW, Mertens LL, Cohen MS, Geva T, (eds). Echocardiography in pediatric and congenital heart disease. Chichester: Wiley-Blackwell; 2009. p. 179.

Friemel BH, Bohs LN, Nightingale KR, Trahey GE. Speckle decorrelation due to two-dimensional flow gradients. IEEE Trans Ultrason Ferroelectr Freq Control 1998;45:317–327.

Hanslik A, Pospisil U, Salzer-Muhar U, Greber-Platzer S, Male C. Predictors of spontaneous closure of isolated secundum atrial septal defect in children: A longitudinal study. Pediatrics 2006;118:1560–1565.

Kasai C, Namekawa K, Koyano A, Omoto R. Real-time two-dimensional blood flow imaging using an autocorrelation technique. IEEE Trans Sonics Ultrason 1985;32:458–464.

Lovstakken L, Bjaerum S, Martens D, Torp H. Blood flow imaging—A new real-time, 2-D flow imaging technique. IEEE Trans Ultrason Ferroelectr Freq Control 2006;532:289–299.

Nyrnes SA, Lovstakken L, Torp H, Haugen BO. Blood flow imaging-a new angle-independent ultrasound modality for the visualization of flow in atrial septal defects in children. Echocardiography 2007;24:975–981.

Oliver-Ruiz JM, Bret-Zurita M. Magnetic resonance imaging in the evaluation of congenital intracardiac shunts. Rev Esp Cardiol 2007;60:895–898.

Pastorelli A, Torricelli G, Scabia M, Biagi E, Masotti L. A real-time 2-D vector Doppler system for clinical experimentation. IEEE Trans Med Imaging 2008;27:1515–1524.

Penny DJ, Vick GW. Ventricular septal defect. Lancet 2011;377:1103–1112.

Poelma C, Mari JM, Foin N, Tang MX, Krams R, Caro CG, Weinberg PD, Westerweel J. 3D flow reconstruction using ultrasound PIV. Exp Fluids 2009;50:777–785.

Ramnarine KV, Nassiri DK, Hoskins PR, Lubbers J. Validation of a new blood-mimicking fluid for use in Doppler flow test objects. Ultrasound Med Biol 1998;24:451–459.

Steel R, Ramnarine KV, Criton A, Davidson F, Allan PL, Humphries N, Routh HF, Fish PJ, Hoskins PR. Angle-dependence and reproducibility of dual-beam vector Doppler ultrasound in the common carotid arteries of normal volunteers. Ultrasound Med Biol 2004;30:271–276.

Swillens A, Segers P, Lovstakken L. Two-dimensional flow imaging in the carotid bifurcation using a combined speckle tracking and

phase-shift estimator: A study based on ultrasound simulations and in vivo analysis. Ultrasound Med Biol 2010;36:1722–1735.
Tanter M, Bercoff J, Sandrin L, Fink M. Ultrafast compound imaging for 2-D motion vector estimation: Application to transient elastography. IEEE Trans Ultrason Ferroelectr Freq Control 2002;49:1363–1374.
Thrush A. Spectral Doppler ultrasound. In: Hoskins PR, Martin K, Thrush A, (eds). Diagnostic ultrasound: Physics and equipment. 2nd ed. Cambridge: University Press; 2010. p. 105–120.
Tortoli P, Dallai A, Boni E, Francalanci L, Ricci S. An automatic angle tracking procedure for feasible vector Doppler blood velocity measurements. Ultrasound Med Biol 2010;36:488–496.
Udesen J, Gran F, Hansen KL, Jensen JA, Thomsen C, Nielsen MB. High frame-rate blood vector velocity imaging using plane waves: simulations and preliminary experiments. IEEE Trans Ultrason Ferroelectr Freq Control 2008;55:1729–1743.
Van der Linde D, Konings EEM, Slager MA, Witsenburg M, Helbing WA, Takkenberg JJM, Roos-Hesselink JW. Birth prevalence of congenital heart disease worldwide: a systematic review and meta-analysis. J Am Coll Cardiol 2011;58:2241–2247.
Zheng H, Liu L, Williams L, Hertzberg JR, Lanning C, Shandas R. Real time multicomponent echo particle image velocimetry technique for opaque flow imaging. Appl Phys Lett 2006;88:261915.